STUDY OF SOME ELASTODYNAMICAL PROBLEMS IN LAYERED MEDIA

A Thesis

Submitted in partial fulfillment of the requirements for the award of the degree of

DOCTOR OF PHILOSOPHY

in

Mathematics

By

Shikhadeep

(Registration No.: 41700245)

Supervised by

Dr. Vikas Sharma

LOVELY PROFESSIONAL UNIVERSITY

PUNJAB

JUNE, 2022

DECLARATION

I hereby declare that the research work which is being presented in the thesis entitled "**Study of some elastodynamical problems in layered media"** submitted for the award of the degree of **Doctor of Philosophy** in Department of Mathematics of Lovely Professional University, Phagwara (Punjab) is an authenticated record of my own research work has been carried out under the supervision of **Dr. Vikas Sharma**, Professor, School of Chemical Engineering and Physical Sciences, Lovely Professional University.

The work has not been submitted for the award of any other degree/diploma/certificate in this university or any other university of India or abroad.

This is to certify that the above statement is correct to the best of our knowledge.

Shikha

Date: 04-07-2022

Shikhadeep

Reg. No.: 41700245

Vikas Sharma

Dr. Vikas Sharma

(Supervisor)

Professor,

School of Chemical Engineering and Physical Sciences,

Lovely Professional University,

Phagwara, Punjab, India

CERTIFICATE

This is to certify that the work presented in the thesis entitled "**Study of some elastodynamical problems in layered media"** submitted by **Ms. Shikhadeep** (Reg. No.: 41700245) in the fulfillment of the requirement for the award of the degree of **Doctor of Philosophy** in Department of Mathematics, Lovely Professional University, Phagwara (Punjab) is a record of candidate's own work has been carried out under my supervision and guidance. The work has not been submitted for the award of any other degree/diploma/certificate in this university or any other university of India or abroad.

This is to certify that the above statement is correct to the best of my knowledge.

Date: 04-07-2022

Dr. Vikas Sharma

(Supervisor)

Professor,

School of Chemical Engineering and Physical Sciences,

Lovely Professional University,

Phagwara, Punjab

India

ACKNOWLEDGMENT

Foremost, I would like to express my sincere gratitude and acknowledgment to my revered supervisor **Dr. Vikas Sharma,** Professor, Department of Mathematics, School of Chemical Engineering and Physical Sciences, Lovely Professional University, Punjab for his guidance, patience, enthusiasm, motivation and continuous support throughout the period of my research work. He supported me in each aspect throughout my PhD study. I could not have been supposed to have had a better supervisor and mentor for my PhD work.

I also impart my thanks to the Head of the Department of Mathematics, Lovely Professional University, and other faculty members and staff, for availing me all necessary resources and co-operation to complete my research work.

Words cannot express my heartfelt gratitude to my adoring **parents**, **sister,** and **brother** who have so much faith and confidence in me and by whose blessings and efforts I have reached here. Their support and countless sacrifices are unwavering. Not to forget my wonderful nephew **Adhiraj Sharma** who has been my stress-buster during this whole period of my research work.

Above all, I express my greatest thanks to the **Almighty** for bestowing upon me his kindness and blessings. It is difficult for me to express my gratitude in words but I am very thankful to God that he provided me with this best opportunity of my life.

Finally, I am gratified to my friends and colleagues of Lovely Professional University for their inspiration, love, and support during my research work.

Shikha

Shikhadeep

TABLE OF CONTENTS

LIST OF SYMBOLS

ε_{ij}	Strain tensor
δ_{ij}	Kronecker's delta
$\Delta = \varepsilon_{ii}$	Volume dilatation
ϵ_{ijk}	Permutation tensor
ζ	Wave number
ω	Angular frequency
c	Phase velocity
τ_{ij}	Stress tensor of an elastic material
τ_{ji}^{C}	Stress tensor of couple stress theory
τ_{ij}^{F}	Stress tensor of fiber-reinforced material
τ_{ij}^{V}	Stress tensor of viscoelastic material
τ_{ij}^{D}	Stress tensor of dry sandy material
λ and μ	Lame's parameters of an elastic material
λ^{C} and μ^{C}	Lame's parameters of couple stress theory
λ^{F}	Lame's parameter of fiber-reinforced material
λ^{V} and μ^{V}	Lame's parameters of viscoelastic material
μ^{D}	Lame's parameter of dry sandy material
ρ	Density of an elastic material
ρ^{C}	Density of couple stress theory
ρ^{F}	Density of fiber-reinforced material
ρ^{V}	Density of viscoelastic material
ρ^{D}	Density of dry sandy material
μ_{ji}^{C}	Skew-symmetric couple stress tensor
η^{C}	Couple stress coefficient
l	Characteristic length parameter
(u, v, w)	Displacement components of an elastic material

(u^C, v^C, w^C)	Displacement components of couple stress theory
(u^F, v^F, w^F)	Displacement components of fiber-reinforced material
(u^V, v^V, w^V)	Displacement components of viscoelastic material
(u^D, v^D, w^D)	Displacement components of dry sandy material
η^D	Sandiness parameter of dry sandy material

LIST OF TABLES

LIST OF FIGURES

TABLE OF CONTENTS

ABSTRACT

The thesis entitled "***Study of some elastodynamical problems in layered media***" is carried out for the study of elastodynamical problems related to propagation of waves in layered structures. The thesis is divided into five chapters and the contribution of the chapters is as follows:

Chapter 1 contains basics of classical theory of elasticity and basics of consistent couple stress theory. Chapter further contains discussion about fiber-reinforced, viscoelastic and dry sandy materials. It also contains basics of different types of waves in elastic media such as Love waves, shear waves and Rayleigh waves etc.

Chapter 2 includes discussion about the Love waves propagation in a single layer attached to a substrate. The chapter has two parts. First section of chapter investigates dispersion of Love waves in a layer made of dry sandy material which is imperfectly bonded to an elastic half-space. The problem is solved by using a suitable mathematical treatment and dispersion equation is calculated for propagation of Love waves. Dispersion equations are further deduced in two special cases, firstly when layer and substrate are perfectly attached to each other and in second case, when dry sandy layer behaves as an isotropic elastic medium. The impacts of sandiness parameter, thickness of the layer and imperfectness parameter are manifested through graphical illustrations. The second section of chapter deals with the Love waves propagation in dry sandy layer imperfectly attached to the microstructural substrate which is modeled through consistent couple stress theory. An analysis has been done in two cases, first, when top surface of the layer is stress-free, and in second case, top surface of layer is considered as clamped. Dispersion relations are derived for both the cases separately, using effective boundary conditions. Under both the conditions, a special case is also derived by assuming layer is perfectly attached to the substrate. A detailed analysis has been done by studying the impacts of microstructural parameter of substrate, sandiness parameter, thickness of layer, imperfectness parameter on the propagation behavior of Love waves in the form of graphical illustrations.

Chapter 3 is an extension of work carried out in chapter-2 and it includes study of dispersion of Love waves in double layered structure attached to a substrate. This chapter also consists of two sections. First section of chapter, presents Love waves propagation in a layer modeled using homogeneous pre-stressed material which is lying between a layer modeled using dry sandy material and a microstructural substrate, depicted using consistent couple stress theory. Secular equation for the Love waves propagation is established by using the suitable mathematical approach. The impacts of microstructural parameter associated with substrate, sandiness parameter of upper layer, width ratio and initial stress of middle layer are manifested through graphical illustrations. In second section of chapter, Love waves propagation is studied in a geometrical configuration consisting a layer of finite width made of viscoelastic material, which lies between a layer of finite width made of fiber-reinforced material and a microstructural substrate. The substrate is modeled using size-dependent consistent couple stress theory. By using suitable mathematical approach, dispersion and damping relations are established. The impact of fiber reinforcement, heterogeneity, internal friction, thickness ratio of the layers, and microstructural parameter associated with substrate are presented on the phase velocity of Love waves through graphical representations.

Chapter 4 deals with the study of Rayleigh waves propagation in a finite thicker layer of an isotropic elastic material imperfectly attached to a microstructural substrate, depicted using consistent couple stress theory. Dispersion relation is obtained by using appropriate boundary conditions to depict imperfectness at the interfacial surface in the considered geometry. A mathematical relation depicting dispersion equation of Rayleigh waves in a layer which is perfectly attached to the substrate is also established, as a special case in the chapter. A dispersion relation is also obtained for Rayleigh waves propagation in a stress-free consistent couple stress substrate. The effect of thickness of the layer, imperfectness parameters and microstructural parameter of the substrate are manifested graphically on the propagation behavior of Rayleigh waves.

Chapter 5 includes discussion about the propagation of shear horizontal (SH) waves in a layer of finite width which is sandwiched between two substrates. The layer in the problem is presented using fiber-reinforced material and the two microstructural substrates are modeled using consistent couple stress theory. Analysis is done by considering two different conditions at the interfacial surfaces between fiber-reinforced layer and two substrates. Secular equation for the propagation of SH-waves is obtained by using appropriate boundary conditions which depict that layer is perfectly/imperfectly attached between the substrates. Some particular cases have also been investigated under different conditions. The impact of characteristic length parameter of substrates, inhomogeneity parameter, reinforcement, and imperfectness are manifested on the propagation of SH-waves through graphical illustrations.

CHAPTER-1

INTRODUCTION

1.1 PRELIMINARIES

Elasticity is the property of materials by the virtue of which materials regain their original size and shape, when external forces causing deformation are removed. On the basis of this property, materials can be classified as elastic, rigid, and plastic. Materials which do not deform, with the application of external forces, are classified as rigid materials and those materials which do not regain their original size and shape after removal of deforming forces are classified as plastic materials. Materials behave as elastic materials until forces causing deformation do not exceed certain limits called elastic limit. Theory of elasticity deals with study of response of elastic materials to the action of external forces. Theory of elasticity uses various laws of classical mechanics to build a mathematical model of a problem of deformation. These mathematical formulations are solved by employing various analytical/numerical techniques using appropriate boundary conditions. Theory of elasticity has many applications in multidisciplinary fields such as in civil engineering it helps in doing stress analysis, deflection analysis etc. in beams, plates, and shells. In mechanical engineering, theory of elasticity is used in designing of various machine elements by doing analysis about contact stresses, fatigue and fracture mechanics etc. Aerospace and aeronautical engineering uses it to find stresses, fatigue and fractures in large aerostructures. Theory of elasticity is used in various biomechanics engineering problems such as solid-fluid interactions, injury biomechanics etc.

Theory of elasticity has applications in the fields of seismology, geomechanics, and geology as well. The subject of seismology deals with theoretical/experimental study of propagation of earthquakes/seismic waves within the earth. These studies help in finding various ways to mitigate the devastating effects of earthquake on humanity. The reflection or refraction of seismic waves is used in geophysics to explore the internal structure of the earth. Theory of elasticity also has applications in non-destructive testing techniques (NDT), where elastic waves are used to detect corrosion, cracks, and other defects in materials.

1.2 CLASSICAL THEORY OF ELASTICITY

1.2.1 Stress and strain components

Theory of elasticity assumes a material to be uniformly distributed throughout its volume without any defects and all the particles possess same material properties, irrespective of their positions. Theory of elasticity studies the response of elastic materials under the action of external forces, using some fundamental equations and constitutive relations. Fundamental equations are developed using universal laws of physics such as conservation of mass, conservation of energy and momentum etc.

If relative position of the points is altered in a continuous medium then medium is said to be strained and deformation occurs, when the change in relative position of material points is accompanied by a change in distance between them. Strain is defined as measure of deformation and study of strain is referred to as strain analysis. Consider a continuous elastic medium with surface S and volume V' which undergoes deformation. When deformation occurs, let us assume that particle in continuous medium changes its position from $P^0(x_1^0, x_2^0, x_3^0)$ to $\bar{P}(\overline{x_1}, \overline{x_2}, \overline{x_3})$ as shown in Fig. (1.1). The displacement from P^0 to $\bar{P}$ is given as $u_i(x_1, x_2, x_3) = \overline{x_i} - x_i^0$, where $u_i; i = 1,2,3$ are displacement components. The infinitesimal strain tensor is defined as $\varepsilon_{ij} = \frac{1}{2}\left(\frac{\partial u_i}{\partial x_j} + \frac{\partial u_j}{\partial x_i}\right); i, j = 1,2,3$. The strain tensor ε_{ij} is symmetric and $\varepsilon_{11}, \varepsilon_{22}, \varepsilon_{33}$ are normal strain components and $\varepsilon_{12} = \varepsilon_{21}, \varepsilon_{13} = \varepsilon_{31}, \varepsilon_{23} = \varepsilon_{32}$ are shear strain components.

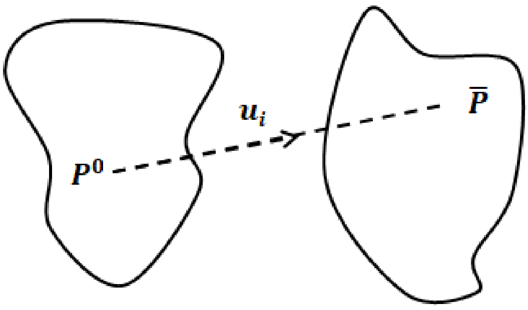

Figure 1.1 Deformation in an elastic body

Stress is the internal resistance developed within the material as a reaction to the application of external forces. Stress is measured as force per unit area. Consider an arbitrary element having area ΔA in the continuum within normal n_i and $T_i^n \Delta A$ is the stress vector on the elementary area. $T_i^n$is a force-traction vector and it is related to symmetric stress tensor τ_{ij} as $T_i^n = \tau_{ij} n_j;\, i, j = 1, 2, 3$. Components of stress tensor (τ_{ij}), completely determine the state of stress at any point. Components $\tau_{11}, \tau_{22}, \tau_{33}$ are called as normal stress components and $\tau_{12} = \tau_{21}, \tau_{13} = \tau_{31}, \tau_{23} = \tau_{32}$ are shear stresses.

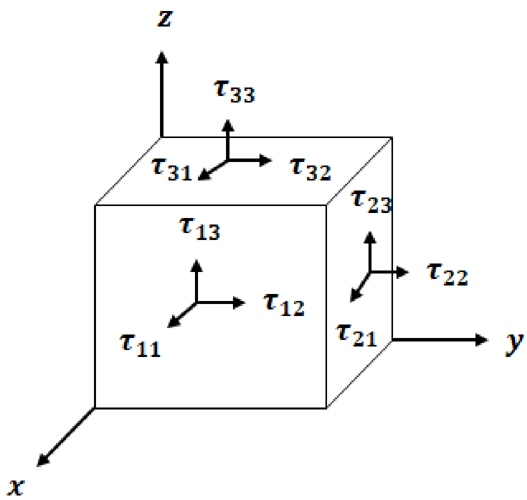

Figure 1.2 Stress components

1.2.2 Generalized Hooke's law

In 1660, Robert Hooke gave the relationship between stress and strain for elastic materials which says that the stress is directly proportional to the strain upto elastic limit of material and it is known as *Hooke's law*. The mathematical expression for generalized Hooke's law is given as $\tau_{ij} = C_{ijkl}\varepsilon_{kl}$; $i, j, k, l = 1, 2, 3$, where ε_{kl} are the infinitesimal strain components, τ_{ij} are the stress components and C_{ijkl} are elastic constants. In generalised Hooke's law the count of elastic constants C_{ijkl} is 81. By imposing the condition of symmetry of strain and stress tensors, the count of elastic constants reduces to 36. These elastic constants are reduced to 21 by imposing the condition $C_{ijkl} = C_{klij}$ which comes by assuming the system to be isothermal or adiabatic in nature. Further by assuming symmetries of axes, planes, and by assuming that material is isotropic, having same properties in all the directions, these elastic coefficients are reduced to 2. Therefore, the Hooke's law for a homogeneous isotropic material becomes [109]

$$\tau_{ij} = \lambda\Delta\delta_{ij} + 2\mu\varepsilon_{ij} \tag{1.1}$$

where λ and μ are Lame's constants, $\Delta = \varepsilon_{ii} = \varepsilon_{11} + \varepsilon_{22} + \varepsilon_{33}$ is volume dilatation and δ_{ij} is called Kronecker's delta which is defined as

$$\delta_{ij} = \begin{cases} 1, & if \quad i = j \\ 0, & if \quad i \neq j \end{cases}$$

The coefficient μ can be identified as shear modulus or modulus of rigidity.

Let a closed surface S, having volume V' be in equilibrium. For equilibrium, resultant of all the forces should vanish and it leads to the condition of equilibrium which is given as

$$\tau_{ij,j} = -F_i \tag{1.2}$$

Eq. (1.2) represents equation of motion for the classical mechanics. Here F_i are the components of forces and $\tau_{ij,j} = \frac{\partial \tau_{ij}}{\partial x_j}$

Eq. (1.2) is written out in full notations as

$$\frac{\partial\tau_{11}}{\partial x}+\frac{\partial\tau_{12}}{\partial y}+\frac{\partial\tau_{13}}{\partial z}=-F_1$$

$$\frac{\partial\tau_{21}}{\partial x}+\frac{\partial\tau_{22}}{\partial y}+\frac{\partial\tau_{23}}{\partial z}=-F_2$$

$$\frac{\partial\tau_{31}}{\partial x}+\frac{\partial\tau_{32}}{\partial y}+\frac{\partial\tau_{33}}{\partial z}=-F_3$$

By using $\tau_{ij}=\lambda\Delta\delta_{ij}+2\mu\varepsilon_{ij}$ in Eq. (1.2), we get

$$(\lambda+\mu)u_{j,ji}+\mu u_{i,jj}+F_i=0 \tag{1.3}$$

where u_i are the displacement components and $i=1,2,3.$

The vector form of Eq. (1.3) is given as

$$(\lambda+\mu)\nabla(\nabla.\vec{u})+\mu\nabla^2\vec{u}+\vec{F}=0 \tag{1.4}$$

where $\nabla=\hat{\imath}\frac{\partial}{\partial x}+\hat{\jmath}\frac{\partial}{\partial y}+\hat{k}\frac{\partial}{\partial z}$ and $\nabla^2=\frac{\partial^2}{\partial x^2}+\frac{\partial^2}{\partial y^2}+\frac{\partial^2}{\partial z^2}$

The equation of motion is derived from condition of equilibrium by adding components of inertial force per unit volume. Hence, equation of motion of an isotropic elastic medium can be written as [109]

$$(\lambda+\mu)u_{j,ji}+\mu u_{i,jj}+F_i=\rho\frac{\partial^2 u_i}{\partial t^2} \tag{1.5}$$

In vector form, Eq. (1.5) is given as

$$(\lambda+\mu)\nabla(\nabla.\vec{u})+\mu\nabla^2\vec{u}+\vec{F}=\rho\frac{\partial^2\vec{u}}{\partial t^2} \tag{1.6}$$

1.3 CONSISTENT COUPLE STRESS THEORY

As already stated, that classical theory of elasticity [109, 113], assumes the material to be homogeneous and isotropic in nature and it does not take into consideration the molecular or atomic structure of material. There are many materials such as cellular solids, fibrous, asphalts, polymers, granular media, crystals which possess internal structures and they do not satisfy the assumptions taken in classical theory of elasticity. The behavior of materials at macroscale depends upon the structure of material at microscale, which is not considered in classical mechanics. These shortcomings of classical mechanics have resulted in the evolution of new theories for solids which take care of internal structure of material and these are known as microcontinuum theories.

Voigt [121] initiated the idea of couple stresses in materials by suggesting that interaction of material particles depends on the force stress vector as well as on couple stress vector. Later, Cosserat and Cosserat [24], proposed mathematical formulations involving couple stresses by assuming that deformation depends upon displacement components as well as on an independent rotation vector. Rotations and displacements are linked to couple stresses and non-symmetric stresses through constitutive equations. This was in contrast to classical mechanics, that explained stress as a symmetric tensor and there was no couple stresses involved in the mathematical formulations. Later on, the idea was followed by various investigators such as Mindlin and Tiersten [69], Toupin [116], Koiter [52], Nowacki [74]. Many researchers have worked on microcontinuum theories to remove their inconsistencies such as Toupin [115], Mindlin and Eshel [68], Nowacki [74]. Many researchers employed microcontinuum theories such as Ottosen $et\ al.$ [76], Chen and Wang [20], Yang $et\ al.$ [127], Sharma and Kumar [95], Guven [36], Akgoz and Civalek [7], Ke $et\ al.$ [50] and Xu and Fan [126].

Hadjesfandiari and Dargush [37] have introduced the consistent couple stress theory. They showed that mathematical formulations of elastic materials, consist two Lame's constants, ($\lambda^C,\ \mu^C$) and an additional third constant called as couple stress coefficient (η^C). The couple stress coefficient is associated with shear modulus (μ^C) through a relation $\eta^C = \mu^C l^2$, where l is characteristic length material parameter and it is considered to be of the size of internal microstructures of material. Many investigators worked on consistent couple stress theory to solve different problems such as Sharma and Kumar [97] analysed dispersion of Lamb waves in a microstructural plate and they derived dispersion equation using suitable mathematical treatment. Ajri $et\ al.$ [5] used consistent couple stress theory for viscoelastic materials to study vibrations in nano-plates. Goyal and Kumar [32] analysed dispersion of Love waves in a layer made of piezoelectric material which is bounded between a viscoelastic layer and a microstructural substrate. They obtained dispersion equation and impacts of internal friction parameter, heterogeneity parameter and microstructural parameter are demonstrated through graphical illustration. Singh $et\ al.$ [105] analysed the G-type waves propagation in a couple stress layer followed by a functionally graded transversely isotropic half-space. They obtained secular equation by using suitable analytical approach and they studied the impacts of anisotropy, microstructural parameter and functional gradedness on the wave. Singhal $et\ al.$ [107] analysed Love waves propagation in a layer made of initially stressed orthotropic material which is imperfectly attached to a couple stress half-space. They obtained the dispersion relation for imperfect/perfect interface and showed the effects of microstructural parameter, initial stresses, thickness of the layer and imperfectness parameter through graphical illustrations on Love waves propagation.

The constitutive equations of Consistent couple stress theory are written [37] as

$$\tau_{ji}^{C} = \lambda^{C} u_{k,k}^{C} \delta_{ij} + \mu^{C}\left(u_{i,j}^{C} + u_{j,i}^{C}\right) - \eta^{C}\nabla^{2}\left(u_{i,j}^{C} - u_{j,i}^{C}\right) \quad (1.7)$$

$$\mu_{ji}^{C} = 4\eta^{C}\left(\omega_{i,j} - \omega_{j,i}\right)\ ;\ \omega_{i} = \frac{1}{2}\epsilon_{ijk} u_{k,j}^{C} \quad (1.8)$$

where μ_{ji}^{C} is skew-symmetric couple stress tensor, (λ^{C}, μ^{C}) are Lame's parameters, u_{i}^{C} are displacement components, ω_{i} is the rotation vector, τ_{ji}^{C} is non-symmetric stress tensor; $i, j, k = 1, 2, 3$. η^{C} is couple stress coefficient which depends upon an intrinsic characteristic length parameter (l), through the relation $\eta^{C} = \mu^{C} l^{2}$. The characteristic length material parameter (l), is comparable with cell size in composites or average spacing in fibrous composites.

The equation of motion without body forces is [37]

$$(\lambda^{C} + \mu^{C} + \eta^{C}\nabla^{2})\nabla(\nabla.\vec{u}) + (\mu^{C} - \eta^{C}\nabla^{2})\nabla^{2}\vec{u} = \rho^{C}\frac{\partial^{2}\vec{u}}{\partial t^{2}} \quad (1.9)$$

where ρ^{C} is density and $\vec{u} = (u^{C}, v^{C}, w^{C})$ is displacement vector.

1.4 FIBER-REINFORCED MATERIALS

Fiber-reinforced composites are anisotropic materials that possess stiffness, high strength, low weight and flexibility. The fiber-reinforced composite materials behave as a single anisotropic unit as long as these composite materials stay in their elastic limits. Belfield [12] presented the explicit constitutive relation for fiber-reinforced composite material as

$$\tau_{ij}^{F} = \lambda^{F}\varepsilon_{kk}\delta_{ij} + 2\mu_{T}\varepsilon_{ij} + \alpha^{F}\left(a_k a_m \varepsilon_{km}\delta_{ij} + a_i a_j \varepsilon_{kk}\right) + 2(\mu_L - \mu_T)\left(a_i a_k \varepsilon_{kj} + a_j a_k \varepsilon_{ki}\right) + \beta^{F} a_k a_m \varepsilon_{km} a_i a_j \; ; \; i,j,k,m = 1,2,3 \qquad (1.10)$$

where τ_{ij}^{F} are stress components, δ_{ij} is Kronecker's delta and ε_{ij} are infinitesimal strain components, that is, $\varepsilon_{ij} = \frac{1}{2}\left(\frac{\partial u_i^F}{\partial x_j} + \frac{\partial u_j^F}{\partial x_i}\right)$. The preferred direction of reinforcement is along $\vec{a} = (a_1, a_2, a_3)$, where $a_1^2 + a_2^2 + a_3^2 = 1$. The vector $\vec{a}$ is a function of the position. λ^F is the Lame's constant. The coefficients α^F and β^F are material constants. μ_T and μ_L are transverse and longitudinal shear moduli respectively.

The equation of motion without body forces is

$$\tau_{ij,j}^{F} = \rho^{F}\frac{\partial^2 u_i^F}{\partial t^2} \qquad (1.11)$$

where ρ^F is density of the fiber-reinforced material, u_i^F are displacement components and $i, j = 1, 2, 3$.

Cheng *et al.* [21], Ardanuy *et al.* [10], Zagho *et al.* [130], Rajak *et al.* [85] have discussed various applications of fiber-reinforced materials. Many researchers have studied problems of wave propagation using fiber-reinforced materials under different conditions, such as Chattopadhyay and Choudhury [16] analysed propagation, transmission and reflection of magnetoelastic waves in a self-reinforced layer attached to a substrate. Sengupta and Nath [92] studied dispersion of surface waves in an anisotropic fiber-reinforced solid medium. They discussed particular cases of Love, Rayleigh and Stoneley waves. They noticed that velocity of Rayleigh waves in fiber-reinforced material is higher as compared to the velocity of Rayleigh waves in elastic solids. Chattopadhyay *et al.* [17] analysed Torsional waves propagation in self-reinforced medium and noticed that in self-reinforced medium, reinforcement parameters affect propagation behavior of Torsional waves. Abbas *et al.* [1] investigated dispersion of plane waves in an anisotropic fiber-reinforced thermoelastic substrate under the effects of magnetic field. They obtained dispersion relation by using boundary conditions and demonstrated the impacts of time parameter on displacement distribution, thermal stresses and temperature distribution through graphical illustration. Alla *et al.* [3] studied surface waves in fiber-reinforced medium in the presence of gravity field. The results are compared in the presence and absence of gravity. Kaur $et\ al.$ [49] investigated Rayleigh waves propagation in an inviscid liquid medium bonded to a self-reinforced substrate in the presence of gravity. Kumari $et\ al.$ [55] studied behavior of SH-waves in a self-reinforced layer lying between a piezoelectric layer and an isotropic gravitational substrate. They obtained the dispersion relation and showed the impacts of width ratio of layers, reinforced parameter, dielectric constant and piezoelectric constant on SH-waves. Hussain and Bayones [41] studied Rayleigh waves propagation in an anisotropic fiber-reinforced magneto thermo viscoelastic layer which is attached to an initially stressed homogeneous elastic substrate. They obtained dispersion relation of Rayleigh waves and graphically depicted the impacts of magnetic field and rotation on phase velocity. Sharma and Sharma [102] studied Love waves in fiber-reinforced layer which is not perfectly attached to microcontinuum half-space. They derived the dispersion and damping equations and presented the effects of various parameters through graphical illustrations.

1.5 VISCOELASTIC MATERIALS

The behavior of elastic materials is characterised by stress-strain relationship which states that the strain is directly proportional to an applied load, with an instantaneous response of the elastic materials to an applied stress. In case of viscous materials, stress is proportional to rate of strain with resultant displacement depends upon history of loading. Viscoelastic materials exhibit the properties of both elastic and viscous materials. The behavior of these types of materials is time dependent and the stress-strain relation is depends on time or on frequency. These materials are good absorbers of impact, so, they are used in the manufacturing of shockers, shoe insoles, helmets, etc. There are many applications of viscoelastic materials in various fields such as soil dynamics, seismology and fluid dynamics. Researchers have studied various problems of propagation of waves using viscoelastic materials such as Carcione [14] analysed propagation behavior of seismic wave in viscoelastic media. Simonetti and Cawley [104] studied shear horizontal (SH) waves propagation in elastic plates covered with viscoelastic materials. Meral *et al.* [67] studied Rayleigh-Lamb waves propagation in viscoelastic materials. Sahu *et al.* [90] analysed SH-waves in a viscoelastic medium followed by a substrate under the effect of gravity. They obtained the dispersion and damped equations and showed impacts of gravity, heterogeneity and internal friction through graphical illustrations. Liu [63] studied about Love waves sensors in a multi-layered model containing multiple number of viscoelastic layers which are lying over a piezoelectric half-space. He concluded that Love waves sensors in two layers structure gives better performance than single viscoelastic guiding layer. Moradi and Innanen [70] investigated homogeneous and inhomogeneous waves propagation in viscoelastic media. Alam *et al.* [8] investigated Torsional waves in viscoelastic medium lying between inhomogeneous dry sandy medium and inhomogeneous dry sandy substrate. They obtained dispersion and damping equations of Torsional waves and graphically depicted the effects of sandiness, attenuation coefficient, thickness ratio, and heterogeneity. Sharma and Kumar [99] studied dispersion of shear horizontal waves in a layer made of viscoelastic material which is imperfectly attached to a microstructural substrate. They obtained the dispersion relation and impacts of heterogeneity, characteristic length, thickness, imperfectness and friction parameter are demonstrated through graphical illustrations. Yuan *et al.* [129] investigated Rayleigh waves propagation in viscoelastic media. They analysed dispersion and attenuation of Rayleigh waves.

The constitutive relation for viscoelastic materials is given [31]

$$\tau_{ij}^V = \left(\lambda^V + \lambda_1' \frac{\partial}{\partial t}\right)\delta_{ij} v_{k,k}^V + \left(\mu^V + \eta^V \frac{\partial}{\partial t}\right)\left(v_{i,j}^V + v_{j,i}^V\right) \tag{1.12}$$

where λ_1' and η^V are internal friction parameters, τ_{ij}^V is the stress vector, λ^V, μ^V are Lame's parameters and v_i^V are displacement components; $i, j, k = 1, 2, 3$.

Equation of motion for viscoelastic materials without body forces [86] is

$$\tau_{ij,j}^V = \rho^V \frac{\partial^2 v_i^V}{\partial t^2} \tag{1.13}$$

where ρ^V is density of the medium.

1.6 DRY SANDY MATERIALS

A dry sandy material is composed of sandy particles that do not contain any water vapours or moisture. The layers of soil inside the earth are sandy in nature. According to the classical mechanics, relation between poisson's ratio (σ^D), modulus of rigidity (μ^D) and young's modulus (E^D) is given as $\frac{E^D}{\mu^D} = 2(1 + \sigma^D)$ which is not true for sandy materials. Weiskopf [124] stated that due to slippage of grains, the resistance to shear stress in dry sandy soil is lower than in elastic materials, and thus the shearing deflection is higher and for such materials, $\frac{E^D}{\mu^D} > 2(1 + \sigma^D)$. Weiskopf defined the mechanics of dry sandy material and presented a modified relationship between poisson's ratio (σ^D), modulus of rigidity (μ^D) and young's modulus (E^D) as $\frac{E^D}{\mu^D} = 2\eta^D(1 + \sigma^D)$ where η^D is called sandiness parameter. For dry sandy medium, the value of η^D should be greater than one, if $\eta^D = 1$ then above relation corresponds to the case of an elastic medium. Researchers have solved many problems by using sandy material such as Sethi et al. [93] investigated Torsional waves propagation in an inhomogeneous layer which is attached to a viscoelastic substrate. They obtained dispersion relation by using appropriate boundary conditions and graphically represented the impacts of internal friction, rigidity and inhomogeneity parameters. Pal and Mandal [78] investigated shear horizontal waves in a layer made of dry sandy material followed by an isotropic substrate and they discussed shear stress discontinuities for different values of sandiness parameters. Pal *et al.* [79] analysed propagation of Rayleigh waves in an anisotropic layer followed by a substrate. Kundu and Maity [56] investigated Edge waves propagation in a pre-stressed plate. Gupta *et al.* [35] analysed Love waves propagation in an initially stressed anisotropic layer bounded between two substrates. The upper substrate is considered as heterogeneous sandy substrate and lower substrate is modeled as pre-stressed porous substrate. They derived dispersion relation with the help of suitable mathematical treatment and also derived some special cases of classical elasticity. Bayones [11] analysed the dispersion of shear waves in an inhomogeneous dry sandy layer followed by an elastic substrate. He graphically represented the impact of gravity, initial stress and inhomogeneity parameters. Kuznetsov [59] analysed Rayleigh and Lamb waves propagation in a dry sandy layer followed by an isotropic substrate.

1.7 WAVE PROPAGATION IN AN ELASTIC MEDIA

1.7.1 Wave equations in an elastic media

For an isotropic elastic medium, equation of motion given in Eq. (1.6) without body forces is

$$(\lambda + \mu)\nabla(\nabla.\vec{u}) + \mu\nabla^2\vec{u} = \rho\frac{\partial^2\vec{u}}{\partial t^2} \tag{1.14}$$

By using formula, $\nabla \times (\nabla \times \vec{u}) = \nabla(\nabla.\vec{u}) - \nabla^2\vec{u}$, Eq. (1.14) can be reduced to

$$(\lambda + 2\mu)\nabla(\nabla.\vec{u}) - \mu\nabla \times (\nabla \times \vec{u}) = \rho\frac{\partial^2\vec{u}}{\partial t^2} \tag{1.15}$$

$$\beta_1^2\nabla(\nabla.\vec{u}) - \beta_2^2\nabla \times (\nabla \times \vec{u}) = \frac{\partial^2\vec{u}}{\partial t^2} \tag{1.16}$$

where $\beta_1 = \sqrt{\frac{\lambda+2\mu}{\rho}}$ and $\beta_2 = \sqrt{\frac{\mu}{\rho}}$

Now, by employing Helmholtz decomposition theorem, displacement vector $(\vec{u})$ is expressed as

$$\vec{u} = \nabla\phi + \nabla \times \vec{\psi} \text{ and } \nabla \cdot \vec{\psi} = 0 \tag{1.17}$$

Now, $\nabla\phi = \hat{\imath}\frac{\partial\phi}{\partial x} + \hat{\jmath}\frac{\partial\phi}{\partial y} + \hat{k}\frac{\partial\phi}{\partial z}$ and

$$\nabla \times \vec{\psi} = \hat{\imath}\left(\frac{\partial \psi_z}{\partial y} - \frac{\partial \psi_y}{\partial z}\right) - \hat{\jmath}\left(\frac{\partial \psi_z}{\partial x} - \frac{\partial \psi_x}{\partial z}\right) + \hat{k}\left(\frac{\partial \psi_y}{\partial x} - \frac{\partial \psi_x}{\partial y}\right)$$

Using above two expressions in Eq. (1.17), we get displacement components as

$$u = \frac{\partial \phi}{\partial x} + \frac{\partial \psi_z}{\partial y} - \frac{\partial \psi_y}{\partial z},$$

$$v = \frac{\partial \phi}{\partial y} - \frac{\partial \psi_z}{\partial x} + \frac{\partial \psi_x}{\partial z},$$

$$w = \frac{\partial \phi}{\partial z} + \frac{\partial \psi_y}{\partial x} - \frac{\partial \psi_x}{\partial y}$$

where $\vec{u} = (u, v, w)$ is the displacement vector, ϕ and $\vec{\psi} = \left(\psi_x, \psi_y, \psi_z\right)$ are scalar and vector potential functions, respectively.

Using these expressions in Eq. (1.16), we get

$$grad\left(\beta_1^2 \nabla^2 \phi - \frac{\partial^2 \phi}{\partial t^2}\right) + curl\left(\beta_2^2 \nabla^2 \vec{\psi} - \frac{\partial^2 \vec{\psi}}{\partial t^2}\right) = 0 \tag{1.18}$$

This equation will be satisfied, if

$$\nabla^2 \phi = \frac{1}{\beta_1^2} \frac{\partial^2 \phi}{\partial t^2} \tag{1.19}$$

$$\nabla^2 \vec{\psi} = \frac{1}{\beta_2^2} \frac{\partial^2 \vec{\psi}}{\partial t^2} \tag{1.20}$$

The Eqs. (1.19) and (1.20) are standard wave equations travelling with velocities β_1 and β_2, respectively. As $curl\ (grad\phi) = 0$, so movement ϕ is purely irrotational, longitudinal, or dilatational, and since, $div\ \left(curl\vec{\psi}\right) = 0$, so the movement $\vec{\psi}$ is purely distortional, equivoluminal, or transverse.

1.7.2 Waves in an elastic media

Elastic waves are classified as Surface and Body waves.

Body waves:

Body waves are the waves that travel into interior of the medium. Body waves have shorter wavelengths and smaller amplitudes than surface waves and they travel at a faster rate. These can be classified as Longitudinal and Transverse waves.

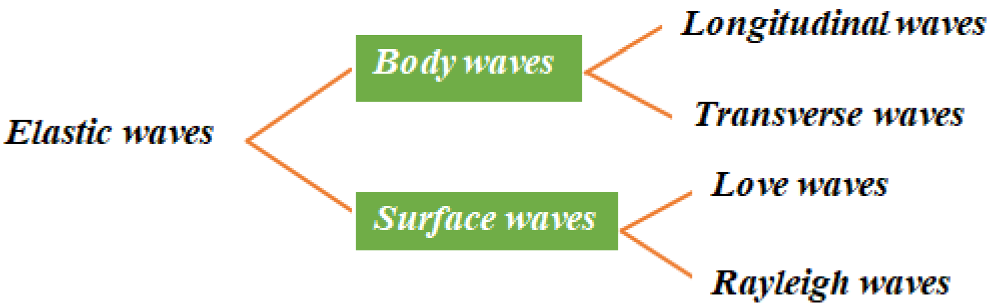

Figure 1.3 Elastic waves

(a) Longitudinal waves: Longitudinal waves are also known as dilatational/irrotational/compressional waves. In seismology, these waves are termed as P-waves or primary waves. These waves are associated with rarefaction and compression of the particles as wave travels through medium. In primary waves, the particles vibrate about their equilibrium position along the direction of wave propagation. These are the fastest waves and are the first to appear on seismograms.

(b) Transverse waves: Transverse waves are also known as equivoluminal/shear/rotational waves. In seismology, these waves are termed as S-waves or secondary waves. Transverse waves are associated with rotational and shearing motion of the particles as wave travels through medium without any change in volume. In these waves, particles vibrate in a direction which is perpendicular to the direction of wave propagation and these waves are classified as SH-waves and SV-waves. When the motion of the particles is polarized in horizontal plane, these waves are called as horizontally polarized shear (SH) waves. When motion of the particles is polarized in vertical plane, these waves are known as vertically polarized shear (SV) waves. Transverse and longitudinal waves both can travel in solid medium.

Surface waves:

Those waves which can travel along free surface of a bounded medium are called as surface waves. Surface waves propagate at a lower velocity than body waves, so during seismic activity these are detected on seismogram after body waves. Surface waves can be classified as Love and Rayleigh waves.

(a) Love waves: Love waves can travel in layered structures which consists a layer of finite thickness attached to a substrate. Love waves can propagate, if the velocity of layer is lower than velocity of half-space. In these waves, motion of the particles is transverse and parallel to surface. Love waves were studied by A.E.H Love, in 1911 [65]. These are shear horizontal (SH) type waves. Love waves are used in sensors and in non-destructive testing techniques to detect cracks, corrosion and flaws in the materials (Tamarin *et al.* [112], Papadakis *et al.* [82], Kuznetsov S.V. [58], Qingzeng *et al.* [66]). Many researchers have investigated Love waves propagation in different types of layered structures such as Hudson [40] studied about Love waves in heterogeneous medium. Wolf [125] discussed about the behavior of shear horizontal waves in an irregular layer attached to an elastic substrate. Kończak *et al.* [53] analysed Love waves propagation in a porous medium attached to an elastic inhomogeneous substrate. They developed dispersion relation and showed effects of heterogeneity and anisotropy parameters. Vardoulakis and Georgiadis [117], have shown the existence of horizontally polarised shear (SH) waves in a homogeneous half-space using continuum theory of gradient elasticity with surface energy. They presented that if the problem is investigated through generalized microcontinuum theory, then these waves could exist in a homogeneous substrate. Liu *et al.* [62] analysed dispersion of Love waves in a piezoelectric layered model under initial stresses. They showed impacts of various parameters including initial stress parameter on behavior of Love waves. Chaudhary *et al.* [19] analysed transmission and reflection of shear waves in a self-reinforced layer lying between viscoelastic substrates. Eskandari and Shodja [29] analysed behavior of Love waves in piezoelectric layered model and obtained dispersion equation by using appropriate mathematical treatment. Wang and Zhang [123] investigated behavior of Love waves in a layer attached to transversely isotropic fluid-saturated porous substrate. They discussed two situations in this problem, firstly they showed the result for an elastic layer which is attached to a poroelastic substrate. Secondly, they showed the result for poroelastic layer which is lying over an elastic substrate. They obtained the dispersion equations for these two cases and plotted the attenuation and dispersion curves of Love waves. Zhu *et al.* [132] investigated Love waves in a functionally graded layer followed by an isotropic half-space. They established secular equation by using suitable mathematical conditions. Saha *et al.* [89] investigated Love waves in a pre-stressed orthotropic medium followed by a porous substrate. They obtained dispersion equation by suitable mathematical treatment and discussed the impacts of porosity, gravity, initial stress and inhomogeneity parameters. Goyal and Kumar [31] studied behavior of Love waves in a heterogeneous viscoelastic layer bounded between a piezoelectric layer and a microstructural substrate modeled by consistent couple stress theory. They obtained the dispersion and damping relations and have presented the effects of various parameters such as internal friction parameter, heterogeneity parameter and length scale parameter through graphical illustrations. Sharma and Kumar [101] studied dispersion of Love waves in a piezomagnetic layer lying between a viscous liquid layer and a micropolar substrate and they showed the impacts of characteristic length parameter, liquid mass density, thickness of the layers and coefficient of viscosity on phase velocity of Love waves.

(b) Rayleigh waves: Lord Rayleigh in 1887, studied about Rayleigh waves which propagate along the free surface of a homogeneous half-space [64]. These waves cannot penetrate far beneath the surface of half-space as their amplitude decrease exponentially going into the half-space. In these waves the motion of the particle is elliptical, retrograde and polarized in a vertical plane. Rayleigh surface waves have many applications, they are broadly used in sensors, SAW devices and non-destructive testing techniques for damage characterization of materials (Isobe [44], Shin *et al.* [103], Ono [75]). Many researchers studied about propagation of Rayleigh waves in various elastodynamical problems. Scholte [91] analysed Rayleigh waves propagation in a viscoelastic medium. Deresiewicz [25] studied Rayleigh waves propagation on the surface of thermally elastic medium. Smith and Dahlen [108] investigated Love and Rayleigh waves propagation in an anisotropic medium and showed impacts of anisotropy on Love and Rayleigh waves propagation. Chimenti *et al.* [22] investigated Leaky Rayleigh waves in a layered substrate. Ottosen *et al.* [76] analysed propagation behaviour of Rayleigh waves in couple-stress medium and showed impacts of couple stresses on Rayleigh waves. Tolipov [114] theoretically investigated Rayleigh waves propagation in an elastic wedge. Vashisth and Khurana [119] analysed Rayleigh waves in a multi-layered model, consisting of an anisotropic poroelastic solid layers stack beneath a fluid layer and lying over an elastic substrate. They obtained dispersion equation and showed the impacts of anisotropy and heterogeneity through graphical illustration. Pang *et al.* [81] investigated Rayleigh waves in a piezoelectric layer followed by a piezomagnetic substrate and obtained the dispersion relation of Rayleigh waves. Pasternak [83] studied Rayleigh waves in a viscoelastic layer attached to a substrate. Sharma *et al.* [96] investigated Rayleigh waves in a homogeneous, thermally conducting solid substrate. They derived secular equations and computed temperature change, amplitude ratios of surface displacements, micro-rotation and microstretch on the surface of solid substrate. Vinh [120] analysed the dispersion of Rayleigh waves in an initially stressed orthotropic elastic medium in the presence of gravity field. Chiriţă [23] investigated surface waves propagation in an anisotropic homogeneous thermoelastic half-space. He obtained dispersion equation of Rayleigh waves and discussed the impact of temperature and strain on the propagation of Rayleigh waves. He also derived a special case where thermoelastic half-space is considered as isotropic and homogeneous in nature. Zhang *et al.* [131] analysed Rayleigh waves propagation in an initially stressed magnetoelectroelastic medium. They showed the impact of initial stress and also discussed electric, magnetic and mechanical responses in detail. Ozisik [77] investigated Rayleigh waves in an initially stressed half-plane covered with two layers under complete contact conditions. Kaur and Singh [47] analysed Rayleigh waves in isotropic substrate and concluded impacts of nonlocality and mass diffusion parameters on the speed of Rayleigh waves and also concluded a special case of classical Rayleigh wave. Gupta *et al.* [34] investigated Rayleigh waves in an isotropic thermoelastic dry sandy substrate. They obtained dispersion relation for propagation of Rayleigh waves. Propagation of surface waves and phenomena associated with these waves are also described in detail such as Love [65], Landau and Lifšic [60], Novotny [73], Müller [71], Rushchitsky [88].

CHAPTER- 2

PROPAGATION OF LOVE WAVES IN A LAYER LYING OVER A SUBSTRATE[1]

2.1 INTRODUCTION

Earth is considered as one of the most complex structured bodies, as it contains various rocks, oils, gases, minerals and many materials in different strata of the earth. The theoretical study of Love waves can reveal various facts and information about the interior of earth. These waves have been detected during earthquakes and underground explosions. This chapter aims to study the dispersion of Love waves in a layer attached to a half-space. In a layered structure, the nature of bonding at the joining surface of two media is an important factor while studying propagation behavior of waves. It is difficult to achieve perfect bonding between different materials due to various reasons such as properties of the materials, environment conditions, cracks, and damages during the manufacturing process etc. The bonding between two media is mathematically modeled as perfect across the interface by assuming continuity of field variables such as displacement and stress components. In case of imperfect bonding, stresses are considered as continuous across the interface and the difference between displacement components is considered to be linearly proportional to the stress vector.

There are two sections in this chapter. The section 2.2 deals with investigation of the Love waves propagation in a dry sandy layer imperfectly attached to an elastic substrate. Dispersion equation is obtained by using suitable mathematical treatment and impacts of various parameters such as imperfect interface, thickness of the layer and

---

[1]Details of the contents of this chapter are given as follows

1. The contents of section (2.2) are published in *Journal of Physics-Conference Series-IOP* Science, 1531, 012069, (Scopus, SJR-0.22).
2. The contents of section (2.3) are published in (Book Chapter) *Recent Advances in Applied Mechanics,* Part of Lecture notes in Mechanical Engineering, Springer, Singapore, 697-710, 2022, (Scopus, SJR-0.15).

sandiness parameter are presented through graphical illustrations. Many researchers have used the condition of imperfectness at the interfacial surfaces to study various problems of wave propagation [39, 106, 122, 18, 6, 99].

Section 2.3 of chapter presents the analysis of Love waves in a layer made of dry sandy material which is not in perfect contact with a substrate described by consistent couple stress theory. The role of microstructures of the material is brought into consideration by modeling the half-space using microcontinuum theory. Further, propagation of Love waves is investigated in two scenarios, one when the top surface of attached layer is stress-free and in other case, attached layer is assumed as clamped in nature. For stress-free conditions at surface, stress components must vanish and for achieving clamped conditions, displacement components should be zero at the surface. Kaplunov *et al.* [46] have investigated Love waves propagation in layered substrate with the clamped surface. They stated that Love waves can exist in a clamped layered structure, provided shear waves velocity of half-space exceeds velocity of layer.

2.2 LOVE WAVES IN A DRY SANDY LAYER IMPERFECTLY ATTACHED TO AN ISOTROPIC SUBSTRATE

2.2.1 Formulation and solution of the problem

A dry sandy layer of finite thickness (H) is attached with an elastic substrate as shown in Fig. (2.1). It is considered that layer is imperfectly attached to the substrate, origin (O) of cartesian coordinate system is at the joining surfaces of two media, $z-$axis is going downwards into the isotropic substrate, and $x-$ axis is pointing along the direction of wave propagation. The displacement components for dry sandy layer are taken as (u^D, v^D, w^D) and displacement components for isotropic half-space are taken as (u, v, w). For the propagation of Love waves, all field variables are assumed as independent of y-coordinates, that is $\frac{\partial}{\partial y} \equiv 0$ and the displacement components are considered as, $u^D = w^D = 0,\ u = w = 0,\ v^D = v^D(x, z, t),\ v = v(x, z, t)$.

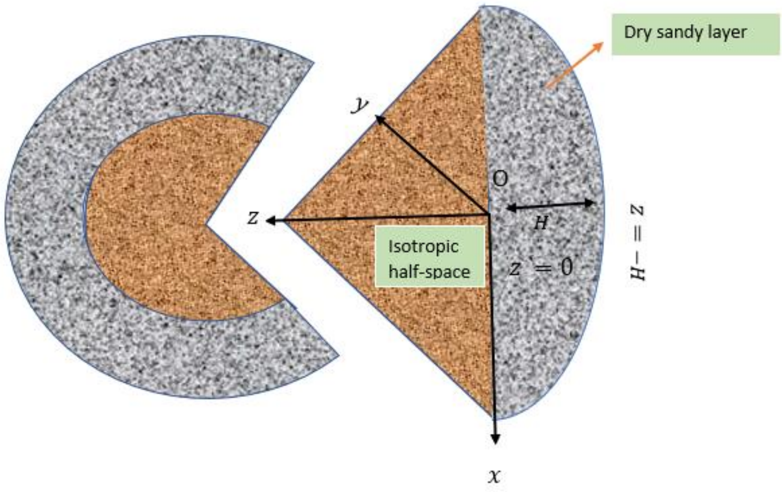

Figure 2.1 Geometry of the problem

2.2.1.1 Solution of dry sandy layer

By using the conditions, which are stated above for propagation of Love waves, the equation of motion for dry sandy material is [78]

$$\frac{\mu^D}{\eta^D}\left(\frac{\partial^2 v^D}{\partial x^2} + \frac{\partial^2 v^D}{\partial z^2}\right) = \rho^D \frac{\partial^2 v^D}{\partial t^2} \tag{2.1}$$

where μ^D is Lame's constant, ρ^D is the density of material and η^D is sandiness parameter.

Assume solution of Eq. (2.1) as

$$v^D(x, z, t) = g(z)e^{-i(\omega t - \zeta x)} \tag{2.2}$$

where c is phase velocity, ζ is wave number and $\omega = \zeta c$ is angular velocity.

Eq. (2.1) becomes

$$\frac{d^2 g}{dz^2} + \zeta^2 s^2 g(z) = 0 \tag{2.3}$$

The solution of Eq. (2.3) is

$$g(z) = A_1 e^{i\zeta s z} + A_2 e^{-i\zeta s z} \tag{2.4}$$

The displacement component for the layer becomes

$$v^D(x,z,t) = \left(A_1 e^{i\zeta sz} + A_2 e^{-i\zeta sz}\right) e^{-i(\omega t - \zeta x)} \tag{2.5}$$

where $s = \sqrt{\frac{c^2\eta^D}{\beta_1^2} - 1}$, $\beta_1^2 = \frac{\mu^D}{\rho^D}$

The non-vanishing stress component is

$$\tau_{32}^D = \frac{\mu^D}{\eta^D}\frac{\partial v^D}{\partial z} = \frac{i\zeta s\mu^D}{\eta^D}\left(e^{i\zeta sz}A_1 - e^{-i\zeta sz}A_2\right)e^{-i(\omega t - \zeta x)} \tag{2.6}$$

2.2.1.2 Solution of isotropic elastic half-space

Equation of motion for an isotropic material is

$$\frac{\mu}{\rho}\left(\frac{\partial^2 v}{\partial x^2} + \frac{\partial^2 v}{\partial z^2}\right) = \frac{\partial^2 v}{\partial t^2} \tag{2.7}$$

where ρ is density of the material and μ is Lame's parameter.

Let assume solution of Eq. (2.7) as

$$v(x,z,t) = h(z)e^{-i(\omega t - \zeta x)} \tag{2.8}$$

Eq. (2.7) becomes

$$\frac{d^2h}{dz^2} - \zeta^2 d^2 h(z) = 0 \tag{2.9}$$

Solution of Eq. (2.9) is

$$h(z) = B_1 e^{d\zeta z} + B_2 e^{-d\zeta z} \tag{2.10}$$

As $z \to \infty$, $h(z)$ must vanish, so to make this happen, we take $B_1 = 0$, so, solution given in Eq. (2.10) becomes

$$h(z) = B_2 e^{-d\zeta z} \tag{2.11}$$

Hence, the displacement component for an isotropic elastic substrate is

$$v(x,z,t) = B_2 e^{-d\zeta z} e^{-i(\omega t - \zeta x)} \tag{2.12}$$

where $d = \sqrt{1 - \frac{c^2}{\beta_2^2}}$, $\beta_2^2 = \frac{\mu}{\rho}$.

The non-vanishing stress component becomes

$$\tau_{32} = \mu \frac{\partial v}{\partial z} = -\mu\zeta d\left(e^{-d\zeta z} B_2\right) e^{-i(\omega t - \zeta x)} \tag{2.13}$$

2.2.2 Boundary conditions

(i) The upper surface of dry sandy layer must be stress-free, so,
$\tau_{32}^{D} = 0$, at $z = -H$.

(ii) Since the interface between two media is imperfect in nature, so difference in displacement fields must be proportional to stress component, that is,
$\tau_{32}^{D} = G(v - v^{D})$, at $z = 0$
where G measures the degree of imperfectness at joining surface of layer and substrate.

(iii) The stress components must be continuous at joining surface of dry sandy layer and an isotropic substrate, that is,
$\tau_{32}^{D} = \tau_{32}$ at $z = 0$.

2.2.3 Derivation of secular equation

By using boundary conditions, we obtain three equations as

$$e^{-i\zeta sH} A_1 - e^{i\zeta sH} A_2 = 0 \tag{2.14}$$

$$\left(\frac{i\zeta s\mu^{D}}{\eta^{D}} + G\right) A_1 + \left(\frac{-i\zeta s\mu^{D}}{\eta^{D}} + G\right) A_2 - GB_2 = 0 \tag{2.15}$$

$$\frac{is\mu^{D}}{\eta^{D}} A_1 + \frac{-is\mu^{D}}{\eta^{D}} A_2 + \mu d B_2 = 0 \tag{2.16}$$

For the non-trivial solution of Eqs. (2.14)-(2.16), determinant of arbitrary constants must vanish.

$$\begin{vmatrix} e^{-i\zeta sH} & -e^{i\zeta sH} & 0 \\ \frac{i\zeta s\mu^{D}}{\eta^{D}} + G & \frac{-i\zeta s\mu^{D}}{\eta^{D}} + G & -G \\ \frac{is\mu^{D}}{\eta^{D}} & \frac{-is\mu^{D}}{\eta^{D}} & \mu d \end{vmatrix} = 0 \tag{2.17}$$

By solving Eq. (2.17), we get secular equation for propagation of Love waves as

$$tan\left(\frac{\omega}{c}H\sqrt{\frac{c^2\eta^D}{\beta_1^2}-1}\right)=\frac{\mu\sqrt{1-\frac{c^2}{\beta_2^2}}}{\frac{\mu^D}{\eta^D}\sqrt{\frac{c^2\eta^D}{\beta_1^2}-1}\left(1+\frac{\mu\omega}{Gc}\sqrt{1-\frac{c^2}{\beta_2^2}}\right)} \tag{2.18}$$

2.2.4 Particular cases

Case 1: If the value of sandiness parameter, $\eta^D=1$, then dry sandy material behaves as an isotropic elastic material and in that case, Eq. (2.18) becomes

$$tan\left(\frac{\omega}{c}H\sqrt{\frac{c^2}{\beta_1^2}-1}\right)=\frac{\mu\sqrt{1-\frac{c^2}{\beta_2^2}}}{\mu^D\sqrt{\frac{c^2}{\beta_1^2}-1}\left(1+\frac{\mu\omega}{Gc}\sqrt{1-\frac{c^2}{\beta_2^2}}\right)} \tag{2.19}$$

Eq. (2.19) shows dispersion relation for Love waves propagation, when isotropic layer and substrate are imperfectly attached to each other.

Case 2: If $G\to\infty$, the dry sandy layer and isotropic substrate are perfectly bonded to each other and, in that case, dispersion relation in Eq. (2.18) becomes

$$tan\left(\frac{\omega}{c}H\sqrt{\frac{c^2\eta^D}{\beta_1^2}-1}\right)=\frac{\mu\sqrt{1-\frac{c^2}{\beta_2^2}}}{\frac{\mu^D}{\eta^D}\sqrt{\frac{c^2\eta^D}{\beta_1^2}-1}} \tag{2.20}$$

Eq. (2.20) gives frequency equation for Love waves propagation, when layer and half-space are perfectly attached.

Case 3: If $G\to\infty$ and $\eta^D=1$, then Eq. (2.18) reduces to

$$tan\left(\frac{\omega}{c}H\sqrt{\frac{c^2}{\beta_1^2}-1}\right)=\frac{\mu\sqrt{1-\frac{c^2}{\beta_2^2}}}{\mu^D\sqrt{\frac{c^2}{\beta_1^2}-1}} \tag{2.21}$$

Eq. (2.21) represents dispersion equation of isotropic layer which is perfectly attached to the isotropic half-space [73].

2.2.5 Graphical results and discussion

To manifest impacts of various parameters involved in the problem, we have taken following material constants [33] and the results are depicted through graphical illustrations.

Dry Sandy Layer	$\mu^D = 6.54 \times 10^{10}\ N/m^2$	$\rho^D = 3409\ Kg/m^3$
Isotropic Half-space	$\mu = 7.10 \times 10^{10}\ N/m^2$	$\rho = 3321\ Kg/m^3$

Table 2.1 Material parameters

In Figs. (2.2)-(2.6), vertical axis represents normalized phase velocity (c/β_1) and horizontal axis represents normalized wave number (ζH).

2.2.5.1 The influence of sandiness parameter $(\boldsymbol{\eta^D})$

The effects of sandiness parameter (η^D) is elucidated by assuming five values of the sandiness parameter as $\eta^D = 1, 1.6, 2.1, 2.6, 3.1$. The value of thickness of layer is taken as $H = 0.04\ m$. Figure (2.2) shows the impact of the sandiness parameter, when dry sandy layer and isotropic substrate are imperfectly $(G = 30.5 \times 10^9)$ attached to each other. Figure (2.3) is again plotted for five values of sandiness parameter as mentioned above, when both media are perfectly attached to each other $(G \to \infty)$. From both the figures, it is found that velocity decreases, when sandiness parameter (η^D) increases. From both figures it can be seen that the sandiness parameter works against phase velocity of Love waves.

2.2.5.2 The influence of imperfectness parameter $(\boldsymbol{G})$

The role of degree of imperfectness parameter (G) on phase velocity is presented by taking five values of imperfectness parameter as $G = 30.5 \times 10^9, 10 \times 30.5 \times 10^9, 40 \times 30.5 \times 10^9, 100 \times 30.5 \times 10^9$ and $G \to \infty$. Other parameters are taken as $H = 0.04\ m$ and $\eta^D = 1.2$. In Fig. (2.4), phase velocity increases, with increase in imperfectness parameter G. As G is increasing the bonding among layer and half space is getting better and as $G \to \infty$, dry sandy layer and isotropic substrate are perfectly bonded to each other. Phase velocity is maximum, when both media are perfectly attached. Figure (2.5) is again plotted for showing the results of imperfectness parameter by taking five values of G as mentioned above, but herein value of sandiness parameter is kept as $\eta^D = 1$ which corresponds that layer is isotropic in nature. Results found in Fig. (2.5) are similar to the results found in Fig. (2.4).

2.2.5.3 The influence of thickness parameter $(\boldsymbol{H})$

To elucidate the impacts of thickness (H) of layer on the behavior of Love waves, graph is plotted by taking five values of thickness parameter as $H = 0.04\ m, 0.08\ m, 0.15\ m, 0.21\ m, 0.26\ m$. The value of sandiness parameter is taken as $\eta^D = 1.2$. Figure (2.6) shows the impacts of thickness of layer, when the joining surface of the dry sandy medium and an elastic substrate is imperfect $(G = 30.5 \times 10^9)$. It is seen that velocity increases with increase in thickness.

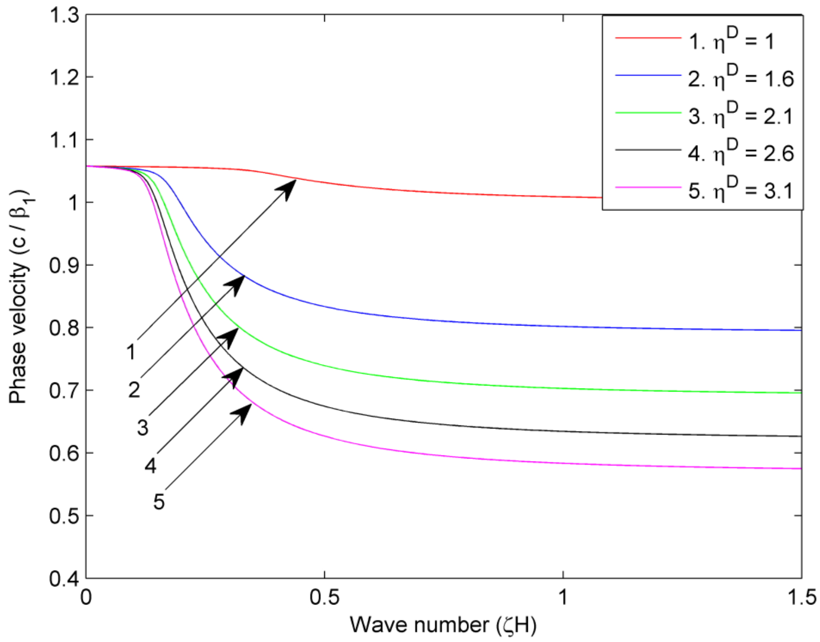

Figure 2.2 Plots for showing impacts of sandiness parameter (η^D) with imperfect interface

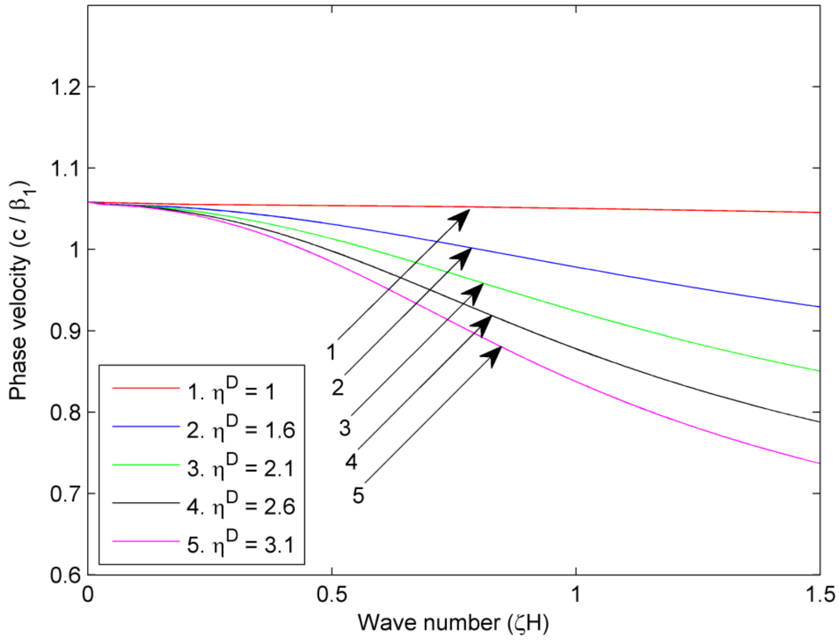

Figure 2.3 Plots for showing impacts of sandiness parameter (η^D) with perfect interface

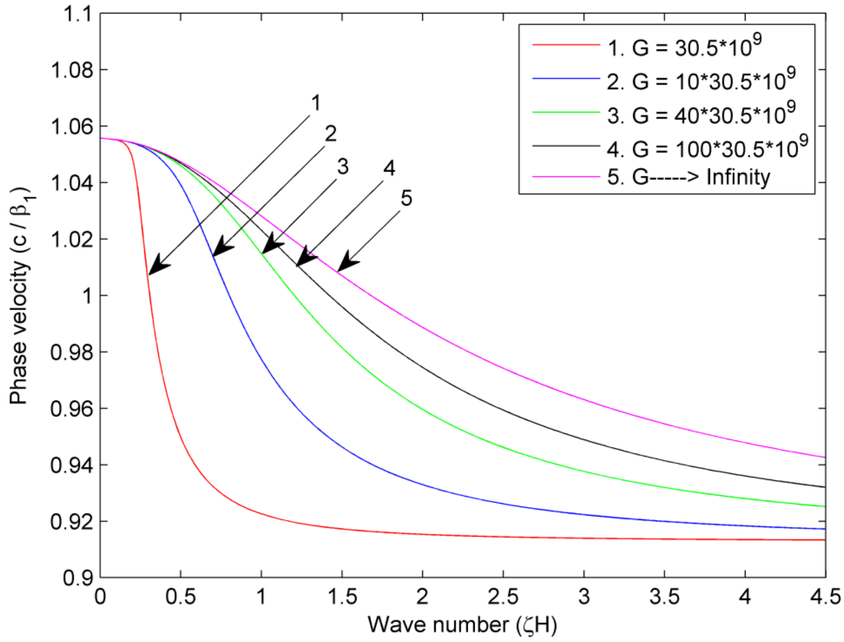

Figure 2.4 Plots for showing impacts of imperfectness parameter (G), when $\eta^D = 1.2$

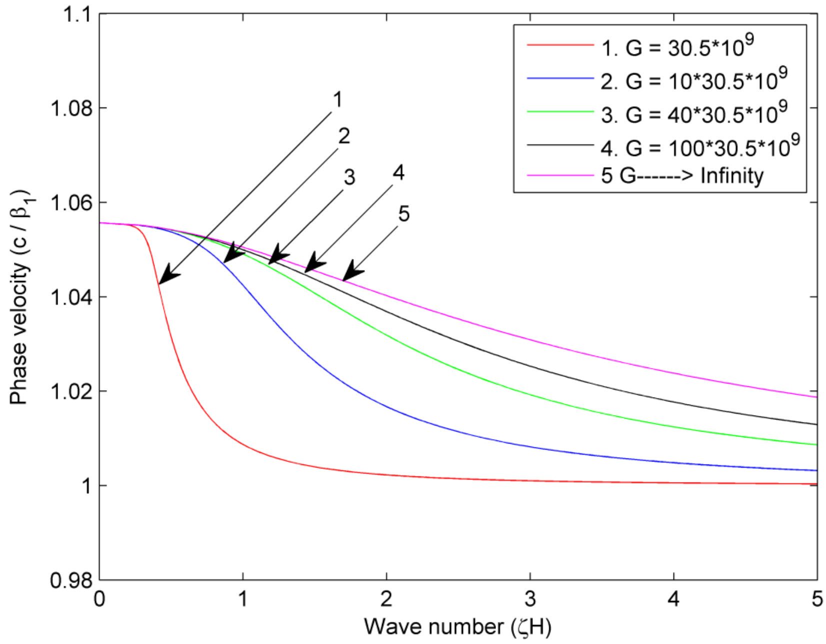

Figure 2.5 Plots for showing impacts of imperfectness parameter (G), when $\eta^{D} = 1$

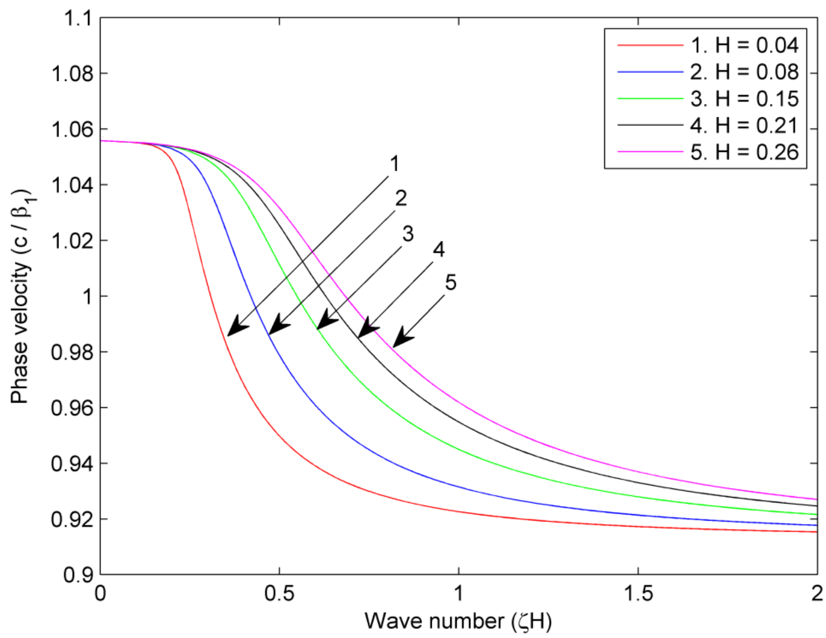

Figure 2.6 Plots for showing impacts of thickness (H) of layer with imperfect interface

2.2.6 Conclusion

The problem deals with Love waves propagation in a dry sandy layer attached to an isotropic half-space. Both the media are assumed to be imperfectly attached to each other. The dispersion equation is calculated by using the appropriate boundary conditions. Conclusions drawn from the analysis are:

- The impacts of sandiness parameter (η^D) of dry sandy layer are quite interesting and phase velocity decreases with increase in sandiness parameter. Similar results are found in both the cases, whether two media are perfectly/imperfectly attached to each other.
- The imperfectness parameter (G), affects the velocity of Love waves. It is seen that velocity increases, when the value of G increases. Phase velocity is highest when two media are perfectly attached to each other.
- Propagation of Love waves gets affected by thickness (H) of layer and thickness favors phase velocity.

2.3 LOVE WAVES IN A DRY SANDY LAYER IMPERFECTLY ATTACHED TO A MICROSTRUCTURAL SUBSTRATE: AN ANALYSIS USING STRESS-FREE AND CLAMPED BOUNDARY CONDITIONS AT THE TOP SURFACE OF LAYER

2.3.1 Formulation and solution of the problem

It is assumed that a dry sandy layer is imperfectly attached with a microstructural substrate (Fig. 2.7). The thickness of dry sandy layer is H, origin (O) of coordinate system is assumed between two media. Further, x-axis is going vertically downward into the substrate and wave is propagating along y-axis. The displacement components for dry sandy layer are (u^D, v^D, w^D) and for couple stress substrate are (u^C, v^C, w^C). The propagation of Love waves is causing displacement in z-direction, so, field variables are independent of z-coordinate, that is $\frac{\partial}{\partial z} \equiv 0$. For Love waves propagation, displacement components are assumed as $u^D = 0, v^D = 0, u^C = 0,\ v^C = 0, w^D = w^D(x, y, t)$ and $w^C = w^C(x, y, t)$.

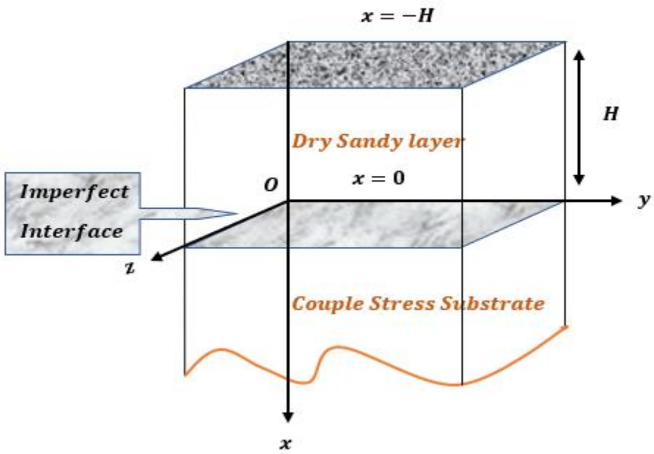

Figure 2.7 Geometry of the problem

2.3.1.1 **Solution of dry sandy layer**

Equation of motion is given as [78]

$$\frac{\mu^D}{\eta^D}\left(\frac{\partial^2 w^D}{\partial x^2} + \frac{\partial^2 w^D}{\partial y^2}\right) = \rho^D \frac{\partial^2 w^D}{\partial\, t^2} \tag{2.22}$$

where ρ^D is density of material, μ^D is Lame's constant and η^D is sandiness parameter.

Let the solution of Eq. (2.22) is

$$w^D(x, y, t) = f(x)e^{-i(\omega t - \zeta y)} \tag{2.23}$$

Eq. (2.22) becomes

$$\frac{d^2 f}{dx^2} + \zeta^2 s^2 f(x) = 0 \tag{2.24}$$

where $s = \sqrt{\frac{\eta^D c^2}{\beta_1^2} - 1}$ and $\beta_1 = \sqrt{\frac{\mu^D}{\rho^D}}$

Eq. (2.24) becomes

$$f(x) = A_1 cos(\zeta s x) + B_1 sin(\zeta s x) \tag{2.25}$$

A_1 and $B_1$are arbitrary constants.

Therefore, the displacement component of dry sandy material becomes

$$w^D(x,y,t) = \{A_1 cos(\zeta sx) + B_1 sin(\zeta sx)\}e^{-i(\omega t-\zeta y)} \tag{2.26}$$

The non-vanishing stress component is

$$\tau_{13}^D = \frac{\mu^D}{\eta^D}\frac{\partial w^D}{\partial x} = \frac{\mu^D}{\eta^D}(\zeta s)\{-A_1 \sin(\zeta sx) + B_1 \cos(\zeta sx)\}e^{-i(\omega t-\zeta y)} \tag{2.27}$$

2.3.1.2 Solution of consistent couple stress substrate

Equation of motion of substrate is given as [37]

$$(\lambda^C + \mu^C + \eta^C\nabla^2)\nabla(\nabla.\vec{w}) + (\mu^C - \eta^C\nabla^2)\nabla^2\vec{w} = \rho^C \frac{\partial^2\vec{w}}{\partial t^2} \tag{2.28}$$

The justification of parameters λ^C, μ^C, ρ^C and η^C is given in section (1.3) of chapter-1 and $\vec{w} = (u^C, v^C, w^C)$ is displacement vector.

By imposing the conditions of Love waves propagation, Eq. (2.28) reduces to

$$\left(\frac{\partial^2 w^C}{\partial x^2} + \frac{\partial^2 w^C}{\partial y^2}\right) - l^2\left(\frac{\partial^4 w^C}{\partial x^4} + \frac{\partial^4 w^C}{\partial y^4} + 2\frac{\partial^4 w^C}{\partial x^2\partial y^2}\right) = \frac{1}{\beta_2^2}\frac{\partial^2 w^C}{\partial t^2} \tag{2.29}$$

where $\beta_2 = \sqrt{\frac{\mu^C}{\rho^C}}$

Assume solution of Eq. (2.29) as

$$w^C(x,y,t) = g(x)e^{-i(\omega t-\zeta y)} \tag{2.30}$$

Eq. (2.29) by using Eq. (2.30) becomes

$$\frac{d^4 g}{dx^4} - L_1\frac{d^2 g}{dx^2} + L_2 g(x) = 0 \tag{2.31}$$

where $L_1 = 2\zeta^2 + \frac{1}{l^2}$ and $L_2 = \zeta^4 + \frac{\zeta^2}{l^2} - \frac{(\zeta c)^2}{l^2\beta_2^2}$

As $x \to \infty$, $g(x)$ must vanish, hence, solution of Eq. (2.31) becomes

$$g(x) = A_2 e^{-px} + B_2 e^{-qx} \tag{2.32}$$

where A_2 and B_2 are arbitrary constants and $p = \sqrt{\frac{L_1 + \sqrt{L_1^2 - 4L_2}}{2}}$ and $q = \sqrt{\frac{L_1 - \sqrt{L_1^2 - 4L_2}}{2}}$

The displacement component of microstructural substrate becomes

$$w^C(x, y, t) = (A_2 e^{-px} + B_2 e^{-qx})\, e^{-i(\omega t - \zeta y)} \tag{2.33}$$

The constitutive equations are

$$\tau_{ji}^C = \lambda^C w_{k,k}^C \delta_{ij} + \mu^C\left(w_{i,j}^C + w_{j,i}^C\right) - \eta^C \nabla^2 (w_{i,j}^C - w_{j,i}^C) \tag{2.34}$$

$$\mu_{ji}^C = 4\eta^C (\omega_{i,j} - \omega_{j,i}) \tag{2.35}$$

where $\omega_i = \frac{1}{2}\epsilon_{ijk} w_{k,j}^C$ is rotation vector. The parameters τ_{ji}^C and μ_{ji}^C are given in section (1.3) of chapter-1.

The force stress and couple stress components become

$$\tau_{13}^C = \mu^C[p(l^2p^2 - l^2\zeta^2 - 1)e^{-px}A_2 + q(l^2q^2 - l^2\zeta^2 - 1)e^{-qx}B_2]e^{-i(\omega t - \zeta y)} \tag{2.36}$$

$$\mu_{12}^C = -2\mu^C l^2[(p^2 - \zeta^2)e^{-px}A_2 + (q^2 - \zeta^2)e^{-qx}B_2]e^{-i(\omega t - \zeta y)} \tag{2.37}$$

2.3.2 Boundary conditions

2.3.2.1 Stress-free boundary conditions

(i) All the stresses at the top surface of the layer vanish, so,

$\tau_{13}^D = 0$ at $x = -H$

(ii) Layer and microstructural substrate are not perfectly attached, so, the difference in displacement components is proportional to stress component, so,

$\tau_{13}^D = G(w^C - w^D)$ at $x = 0$

where G defines the degree of imperfectness

(iii) Stress components must be equal at the interface, so,

$\tau_{13}^D = \tau_{13}^C$ at $x = 0$

(iv) Couple stress coefficient vanishes at the interface, so,

$\mu_{12}^C = 0$ at $x = 0$

2.3.2.2 Clamped boundary conditions

(i) Upper surface of layer is assumed as clamped, and for achieving this condition, displacement component must vanish at top surface of layer, that is,
$w^D(x,y,t) = 0$ at $x = -H$.

(ii) Layer and microstructural substrate are not perfectly attached, so, the difference in displacement components is proportional to stress component, that is,
$\tau_{13}^D = G(w^C - w^D)$ at $x = 0$
where G defines the degree of imperfectness

(iii) Stress components must balance at the interface, so,
$\tau_{13}^D = \tau_{13}^C$ at $x = 0$

(iv) Couple stress coefficient vanishes at the interface, that is
$\mu_{12}^C = 0$ at $x = 0$

2.3.3 Derivation of secular equations

2.3.3.1 Secular equation with stress-free conditions

By implementing the stress-free boundary conditions, we obtain the following equations

$$A_1 sin(\zeta sH) + B_1 cos(\zeta sH) = 0 \tag{2.38}$$

$$GA_1 + \frac{\mu^D \zeta s}{\eta^D} B_1 - GA_2 - GB_2 = 0 \tag{2.39}$$

$$\frac{\mu^D \zeta s}{\eta^D} B_1 + (\mu^C p - \mu^C l^2 p^3 + \mu^C l^2 p \zeta^2) A_2 + (\mu^C q - \mu^C l^2 q^3 + \mu^C l^2 q \zeta^2) B_2 = 0 \tag{2.40}$$

$$(p^2 - \zeta^2) A_2 + (q^2 - \zeta^2) B_2 = 0 \tag{2.41}$$

For the non-trivial solution of the Eqs. (2.38)-(2.41), determinant of the arbitrary coefficients must vanish.

$$\begin{vmatrix} sin(\zeta sH) & cos(\zeta sH) & 0 & 0 \\ G & \varphi & -G & -G \\ 0 & \varphi & T_1 & T_2 \\ 0 & 0 & \varphi_1 & \varphi_2 \end{vmatrix} = 0 \tag{2.42}$$

where $\varphi = \frac{\mu^D \zeta s}{\eta^D}$, $\varphi_1 = p^2 - \zeta^2$, $\varphi_2 = q^2 - \zeta^2$, $T_1 = \mu^C p - \mu^C l^2 p^3 + \mu^C l^2 p \zeta^2$ and $T_2 = \mu^C q - \mu^C l^2 q^3 + \mu^C l^2 q \zeta^2$

By solving Eq. (2.42), we obtain following dispersion relation for Love waves propagation, when layer is imperfectly attached to the substrate by taking stress-free boundary conditions at top surface of layer.

$$tan(\zeta sH) = \frac{G(\varphi_2 T_1 - \varphi_1 T_2)}{\left(\frac{\mu^D \zeta s}{\eta^D}\right)\left(\varphi_2(T_1 + G) - \varphi_1(T_2 + G)\right)} \tag{2.43}$$

2.3.3.2 Secular equation with clamped conditions

By imposing clamped boundary conditions, we get following equations

$$A_1 cos(\zeta sH) - B_1 sin(\zeta sH) = 0 \tag{2.44}$$

$$GA_1 + \frac{\mu^D \zeta s}{\eta^D} B_1 - GA_2 - GB_2 = 0 \tag{2.45}$$

$$\frac{\mu^D \zeta s}{\eta^D} B_1 + (\mu^C p - \mu^C l^2 p^3 + \mu^C l^2 p \zeta^2) A_2 + (\mu^C q - \mu^C l^2 q^3 + \mu^C l^2 q \zeta^2) B_2 = 0 \tag{2.46}$$

$$(p^2 - \zeta^2) A_2 + (q^2 - \zeta^2) B_2 = 0 \tag{2.47}$$

For the non-trivial solution of the Eqs. (2.44)-(2.47), determinant of the arbitrary coefficients must vanish.

$$\begin{vmatrix} cos(\zeta sH) & -sin(\zeta sH) & 0 & 0 \\ G & \varphi & -G & -G \\ 0 & \varphi & T_1 & T_2 \\ 0 & 0 & \varphi_1 & \varphi_2 \end{vmatrix} = 0 \tag{2.48}$$

By solving Eq. (2.48), we get following dispersion relation of Love waves propagation with clamped boundary conditions, when two materials are imperfectly attached.

$$tan(\zeta sH) = \frac{\left(\frac{\mu^D \zeta s}{\eta^D}\right)\left(\varphi_2(T_1 + G) - \varphi_1(T_2 + G)\right)}{G(\varphi_1 T_2 - \varphi_2 T_1)} \tag{2.49}$$

2.3.4 Particular cases

2.3.4.1 Particular cases for stress-free conditions

Case 1: If the value of sandiness parameter, $\eta^D = 1$, then dry sandy material behaves as an isotropic elastic material and in that case, Eq. (2.43) becomes

$$tan(\zeta sH) = \frac{G(\varphi_2 T_1 - \varphi_1 T_2)}{(\mu^D \zeta s)\big(\varphi_2(T_1+G) - \varphi_1(T_2+G)\big)} \tag{2.50}$$

Eq. (2.50) shows dispersion relation for Love waves propagation under stress-free conditions when isotropic layer and half-space are imperfectly attached to each other.

Case 2: If $G \to \infty$, the interface between dry sandy layer and microstructural substrate becomes perfect in nature under stress-free conditions, so dispersion relation given in Eq. (2.43) reduces to

$$tan(\zeta sH) = \frac{\varphi_2 T_1 - \varphi_1 T_2}{\left(\frac{\mu^D \zeta s}{\eta^D}\right)(q^2 - p^2)} \tag{2.51}$$

Case 3: If $G \to \infty$ and $\eta^D = 1$, then Eq. (2.43) reduces to

$$tan(\zeta sH) = \frac{\varphi_2 T_1 - \varphi_1 T_2}{(\mu^D \zeta s)(q^2 - p^2)} \tag{2.52}$$

Eq. (2.52) represents secular equation of Love waves in an isotropic elastic layer perfectly attached to the microstructural substrate.

2.3.4.2 Particular cases for clamped conditions

Case 1: If the value of sandiness parameter, $\eta^D = 1$, then dry sandy material behaves as an isotropic elastic material and in that case, Eq. (2.49) becomes

$$tan(\zeta sH) = \frac{(\mu^D \zeta s)\big(\varphi_2(T_1+G) - \varphi_1(T_2+G)\big)}{G(\varphi_1 T_2 - \varphi_2 T_1)} \tag{2.53}$$

Eq. (2.54) shows dispersion relation for Love waves propagation under clamped conditions when isotropic layer and half-space are imperfectly attached to each other.

Case 2: If $G \rightarrow \infty$, the interface between dry sandy layer and microstructural substrate becomes perfect in nature under clamped conditions, so dispersion relation given in Eq. (2.49) reduces to

$$tan(\zeta sH) = \frac{\left(\frac{\mu^D \zeta s}{\eta^D}\right)(q^2 - p^2)}{\varphi_1 T_2 - \varphi_2 T_1} \tag{2.54}$$

Case 3: If $G \rightarrow \infty$ and $\eta^D = 1$, then Eq. (2.49) reduces to

$$tan(\zeta sH) = \frac{(\mu^D \zeta s)(q^2 - p^2)}{\varphi_1 T_2 - \varphi_2 T_1} \tag{2.55}$$

Eq. (2.55) represents secular equation of Love waves in an isotropic elastic layer perfectly attached to the couple stress substrate.

2.3.5 Graphical results and discussion

To manifest impacts of various parameters involved in the problem, we have taken material constants which are mentioned in Table 2.2 and the results are presented through graphical illustrations.

Dry Sandy Layer [80]	$\mu^D = 6 \times 10^9\ N/m^2$	$\rho^D = 2300\ Kg/m^3$
Couple Stress Substrate [117]	$\mu^C = 30.5 \times 10^9\ N/m^2$	$\rho^C = 2717\ Kg/m^3$

Table 2.2 Material parameters

The impacts of various parameters are shown on the phase velocity of Love waves, by considering the initial mode $(n = 0)$ of Love waves, when top surface of layer is stress-free. It is further found that initial mode $(n = 0)$ of Love waves is not conclusive, when the top surface of layer is clamped, so for this case, graphical results are depicted by considering the first mode $(n = 1)$ of Love waves. For Figs. (2.8)-(2.13), the value of the imperfectness parameter is considered as $G = 30.5 \times 10^9$. In Figs. (2.8), (2.9), (2.10), (2.11), (2.14) and (2.15), vertical axis represents non-dimensional phase velocity (c/β_1) and horizontal axis represents non-dimensional wave number (ζH). In

Figs. (2.12) and (2.13), vertical axis represents dimensionless phase velocity (c/β_1) and horizontal axis represents non-dimensional wave number (ζl).

2.3.5.1 *The influence of microstructural parameter* $(\boldsymbol{l})$

The effect of microstructural parameter is elucidated by assuming three values of the parameter as $l = 0.0001\,m, 0.0004\,m,\ 0.0006\,m$. For graphical illustrations, other parameters are considered as $H = 1.9\ m$ and $\eta^D = 1.2$. Figure (2.8) is plotted for stress-free boundary conditions and Fig. (2.9) is plotted using clamped boundary conditions. It is noticed in the Figs. (2.8) and (2.9), that characteristic length favors phase velocity. The velocity increases, when value of characteristic length parameter increases. Impacts of this parameter are meager and it was expected, as it is a microstructural parameter. Results are depicted by considering two cases, firstly, when two media are mechanically in perfect contact and secondly when they are imperfectly attached. Although the pattern is same in both cases, but phase velocity is higher when layer and substrate are perfectly attached.

2.3.5.2 The influence of sandiness parameter $(\boldsymbol{\eta^D})$

Impacts of sandiness parameter are presented on phase velocity by considering three values as $\eta^D = 1, 1.4, 1.6$. Other parameters are kept as $l = 0.0004\,m,\ H = 1.9\,m$. Figure (2.10) is plotted by taking stress-free conditions, and for Fig. (2.11) layer is clamped. It is noticed from the graphs that velocity decreases, when sandiness parameter increases, and behavior is same, whether two media are perfectly or imperfectly attached. Therefore, the sandiness parameter opposes phase velocity. For any given value of sandiness parameter, the phase velocity is higher, when two media are attached perfectly as compared to when they are attached imperfectly.

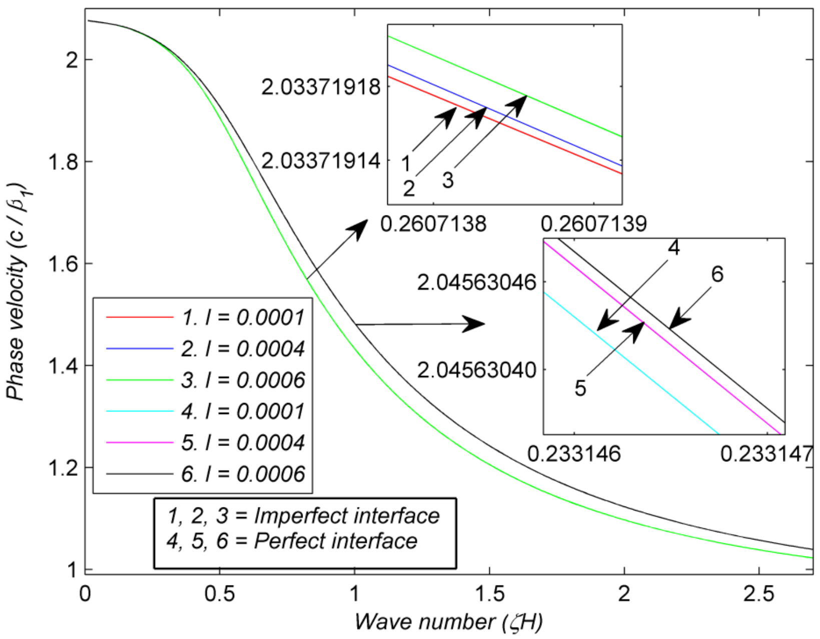

Figure 2.8 Plots for showing impacts of characteristic length (l) under stress-free conditions

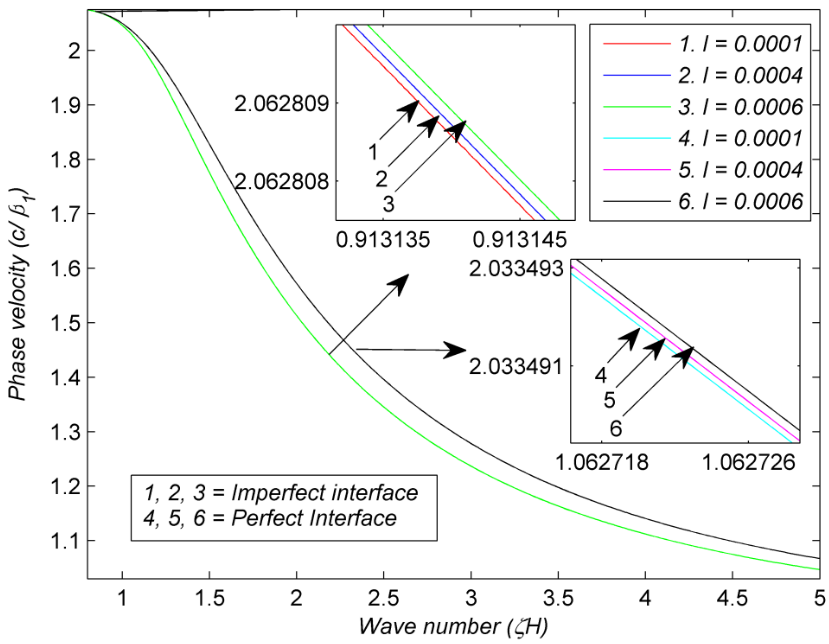

Figure 2.9 Plots for showing impacts of characteristic length (l) under clamped conditions

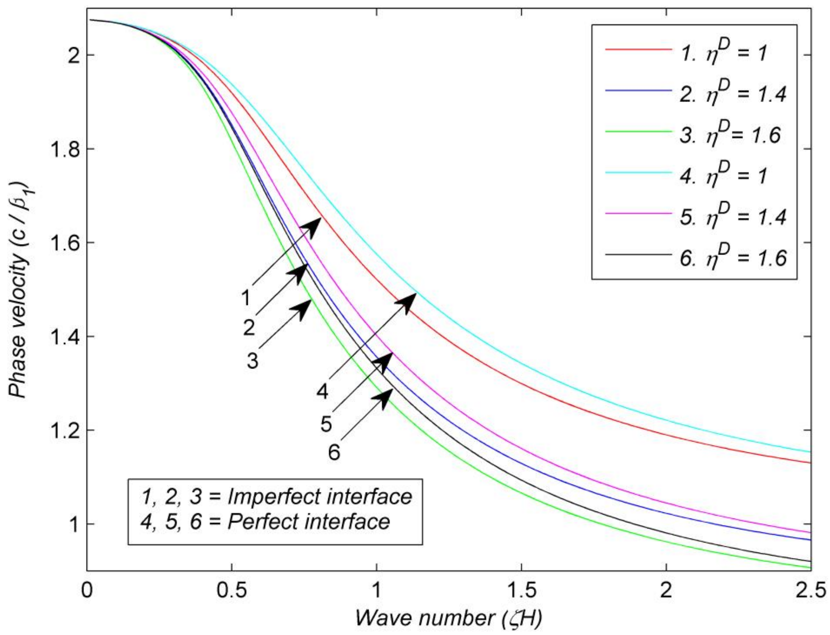

Figure 2.10 Plots for showing impacts of sandiness parameter (η^D) under stress-free conditions

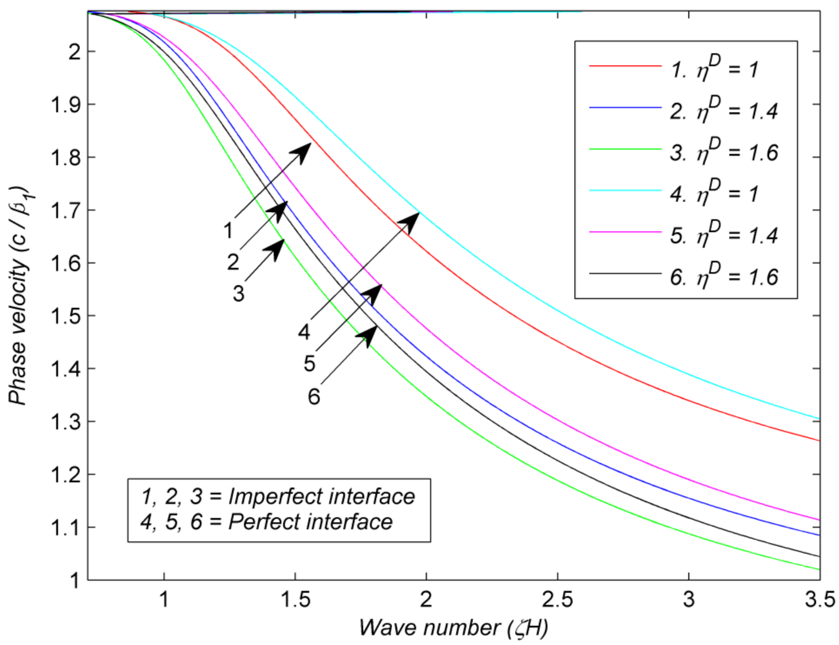

Figure 2.11 Plots for showing impacts of sandiness parameter (η^D) under clamped conditions

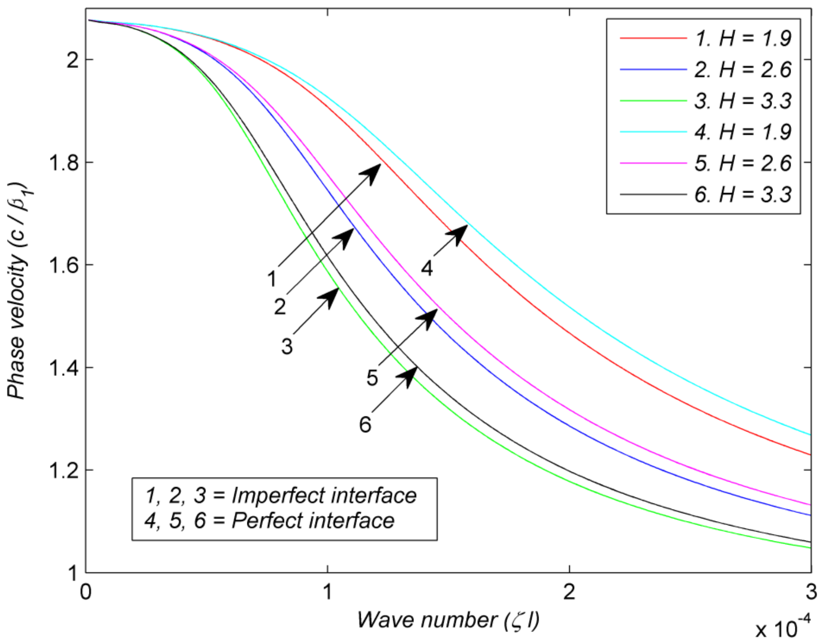

Figure 2.12 Plots for showing impacts of thickness (H) of layer under stress-free conditions

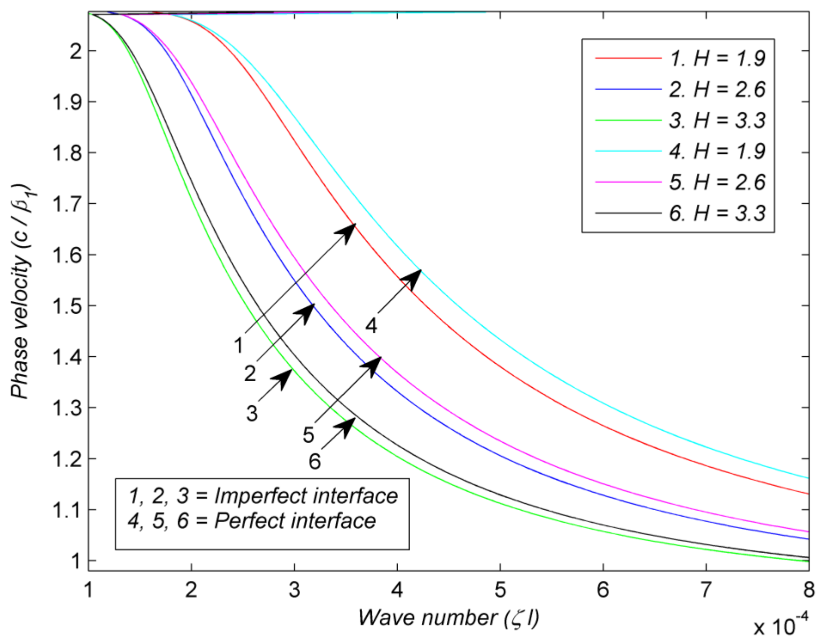

Figure 2.13 Plots for showing impacts of thickness (H) of layer under clamped conditions

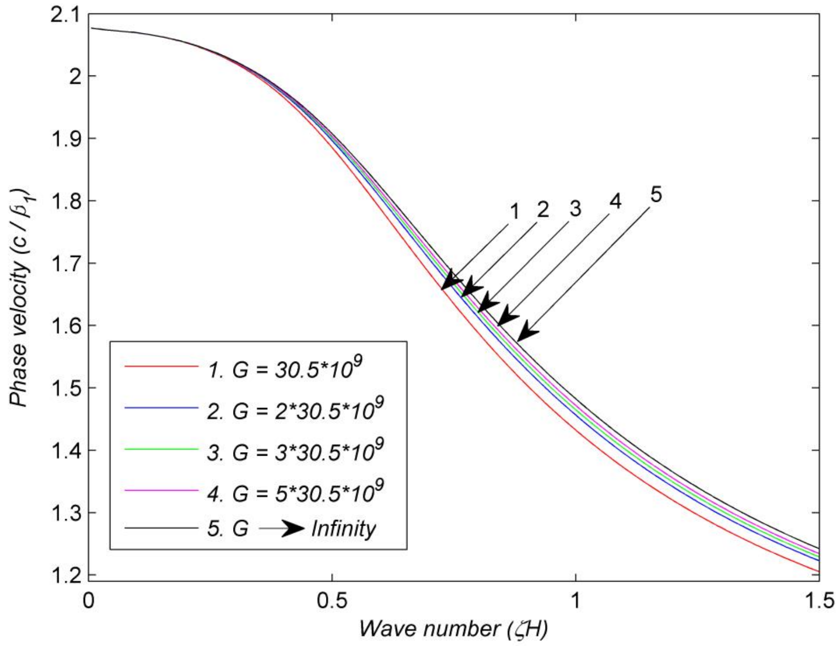

Figure 2.14 Plots for showing impacts of imperfectness parameter (G) under stress-free conditions

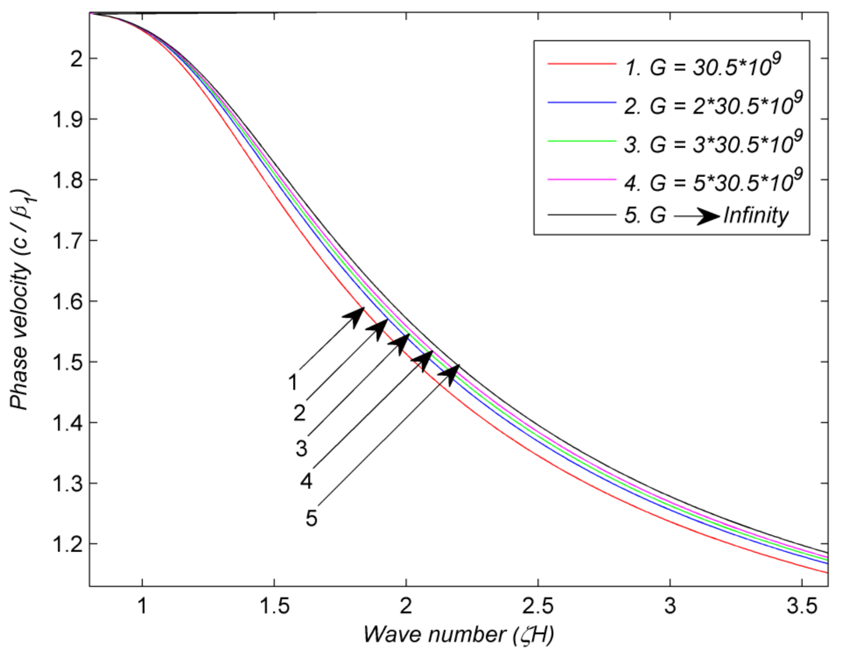

Figure 2.15 Plots for showing impacts of imperfectness parameter (G) under clamped conditions

2.3.5.3 The influence of thickness (H) of layer

To elucidate the impacts of thickness parameter (H) on Love waves propagation, graphs are plotted by considering three values of thickness as $H = 1.9\,m, 2.6\,m, 3.3\,m$. The values of other parameters are $l = 0.0004\,m$ and $\eta^D = 1.2$. Figure (2.12) is drawn by taking stress-free conditions and for Fig. (2.13) layer is clamped. From both figures, it can be noticed that phase velocity decreases, when thickness of layer increases. This pattern remains same whether layer and half-space are perfectly or imperfectly attached.

2.3.5.4 The impacts of imperfectness parameter $(\boldsymbol{G})$

The impacts of imperfectness parameter (G) on phase velocity are shown in Figs. (2.14) and (2.15) by considering five values as $G = 30.5 \times 10^9, 2 \times 30.5 \times 10^9, 3 \times 30.5 \times 10^9, 5 \times 30.5 \times 10^9$, $G \to \infty$. Other parameters are kept as $H = 1.9\,m, \eta^D = 1.2$ and $l = 0.0004\,m$. When $G \to \infty$, dry sandy layer and microstructural couple stress substrate are perfectly attached. Figure (2.14) is plotted using stress-free conditions at the top surface of layer, and for Fig. (2.15) layer is clamped. Since the degree of imperfectness and parameter G are inversely proportional, so from the trends, it is found that velocity increases, when degree of imperfectness (increasing value of G) decreases. Phase velocity is maximum, when degree of imperfectness is least $(G \to \infty)$ and two media are in perfect contact with each other.

2.3.6 Conclusion

This problem investigates the existence of Love waves in a dry sandy layer followed by a substrate which is described using consistent couple stress theory under two different sets of boundary conditions. In one case, top surface of attached layer is assumed as stress-free, and in second case, the free surface of attached layer is considered as clamped. It is found that the initial mode of Love waves is not conclusive when the top surface of layer is clamped, but higher modes are found clearly and hence all the graphical illustrations are given in this case by using the first mode $(n = 1)$ of

Love waves. In case of stress-free conditions at the top surface of layer, initial as well as higher modes are clearly visible, so in this case, graphical results are given using an initial mode ($n = 0$). In general, it can be found that phase velocity is higher when two media are in perfect contact as compared to the case when they are imperfectly attached.

- Impacts of characteristic length (l) parameter associated with the substrate, are shown on velocity and it can be noticed that this parameter favors phase velocity.
- Sandiness parameter (η^D) and thickness (H) of dry sandy layer works against phase velocity.
- The bonding between two media tends to become stronger, when value of imperfectness parameter (G) increases. It can be noticed that phase velocity increases, when imperfectness parameter increases and velocity of wave is maximum when both the media are perfectly attached ($G \to \infty$).

This problem covers two major aspects, first the study of Love waves propagation, when top surface of layer is clamped, secondly the role of bonding between layer and substrate on Love waves propagation. Further half-space is modeled using size-dependent consistent couple stress theory, so it highlights impacts of microstructural parameter on phase velocity of Love waves.

CHAPTER- 3

PROPAGATION OF LOVE WAVES IN DOUBLE LAYERED STRUCTURE[2]

3.1 INTRODUCTION

The chapter deals with the study of Love waves propagation in double layered structure attached to a microstructural substrate. This chapter has two sections and the first section (section 3.2) of chapter deals with study of Love waves in a pre-stressed layer which is sandwiched between a dry sandy layer and a couple stress substrate. Both layers are of finite widths. Initial stresses may develop in the materials due to various reasons, such as certain faults in manufacturing process or during assembly of different parts of a structure. Due to presence of various types of internal forces, these initial stresses do exist in the interior of earth. Existence of initial stresses in interior of the earth can have an impact on propagation of seismic waves. Many researchers have studied problems of wave propagation using different types of materials in the presence of initial stresses [26, 2, 4, 57, 128, 38, 28]. In this problem, dispersion equation is derived by using an appropriate mathematical treatment. Impacts of various parameters which are involved in the problem, such as characteristic length parameter of substrate, sandiness parameter, initial stresses and width ratio are manifested graphically on behavior of Love waves.

The second section (section 3.3) of chapter deals with the study of Love waves in a viscoelastic layer which is bounded between a fiber-reinforced layer and a microstructural couple stress substrate. Both layers are of finite widths. Dispersion and damping relations are obtained by using boundary conditions and an appropriate

---

[2]The contents of this chapter are published in following journals:

1. The contents of section (3.2) are published in *Mechanics of Solids*, 56(5), 807-818, 2021, (Both SCI and Scopus indexed journal, Impact factor- 0.452, SJR- 0.283).
2. The contents of section (3.3) are published in *Iranian Journal of Science and Technology , Transactions of Mechanical Engineering*, 46(1), 225-235, 2021, (Both SCI and Scopus indexed journal, Impact factor- 1.596, SJR- 0.328).

analytical approach. The impact of fiber reinforcement, heterogeneity, thickness ratio, internal friction and microstructural parameter are presented graphically.

3.2 LOVE WAVES IN A PRE-STRESSED LAYER LYING BETWEEN A DRY SANDY LAYER AND CONSISTENT COUPLE STRESS HALF-SPACE

3.2.1 Formulation and solution of the problem

It is assumed that a pre-stressed (P') elastic layer is bounded between a dry sandy layer and a microstructural substrate described by consistent couple stress theory. The thicknesses of homogeneous pre-stressed layer and dry sandy layer are taken as H and H_1 respectively. The origin (O) is assumed at the joining surface of pre-stressed elastic layer and the substrate, z-axis is pointing vertically downward into substrate and x-axis is pointing in direction of wave propagation (Fig. 3.1).

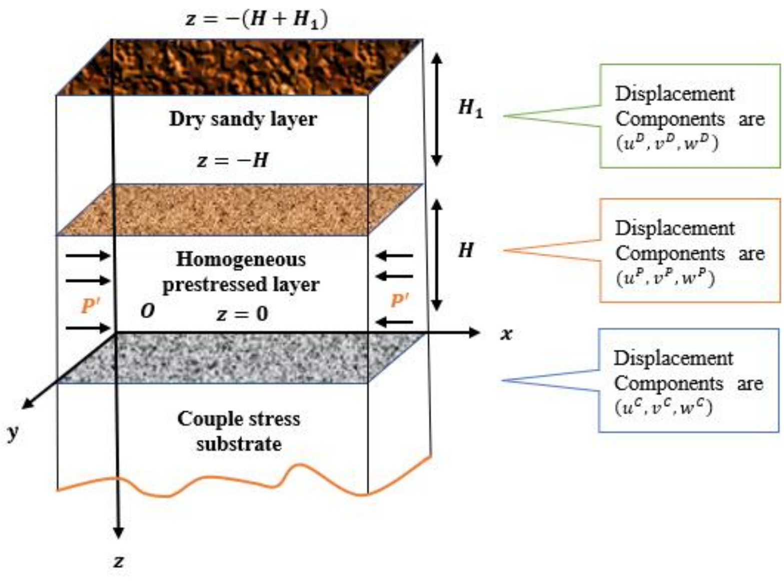

Figure 3.1 Geometrical configuration of the problem

The displacement components for couple stress substrate, pre-stressed layer and dry sandy layer are taken as (u^C, v^C, w^C), (u^P, v^P, w^P) and (u^D, v^D, w^D) respectively. For

Love waves propagation, field variables are independent of y-axis, that is $\frac{\partial}{\partial y} \equiv 0$ and displacement components are $u^D = w^D = 0,\ v^D = v^D(x,z,t),\ u^P = w^P = 0,\ v^P = v^P(x,z,t)$ and $u^C = w^C = 0,\ v^C = v^C(x,z,t)$.

3.2.1.1 Solution of dry sandy layer $\{-(\boldsymbol{H}+\boldsymbol{H_1}) < z < -H\}$

Equation of motion and detailed solution are given in section (2.2.1.1) of chapter- 2 from Eq. (2.1) to (2.6).

3.2.1.2 Solution of pre-stressed layer $\{-\boldsymbol{H} < z < 0\}$

Equations of motion for homogeneous pre-stressed material are given as [57]

$$\left.\begin{aligned} \frac{\partial \tau_{11}^P}{\partial x} + \frac{\partial \tau_{12}^P}{\partial y} + \frac{\partial \tau_{13}^P}{\partial z} - P'\left(\frac{\partial \omega_3^P}{\partial y} - \frac{\partial \omega_2^P}{\partial z}\right) = \rho^P \frac{\partial^2 u^P}{\partial t^2} \\ \frac{\partial \tau_{21}^P}{\partial x} + \frac{\partial \tau_{22}^P}{\partial y} + \frac{\partial \tau_{23}^P}{\partial z} - P'\left(\frac{\partial \omega_3^P}{\partial x}\right) = \rho^P \frac{\partial^2 v^P}{\partial t^2} \\ \frac{\partial \tau_{31}^P}{\partial x} + \frac{\partial \tau_{32}^P}{\partial y} + \frac{\partial \tau_{33}^P}{\partial z} - P'\left(\frac{\partial \omega_2^P}{\partial x}\right) = \rho^P \frac{\partial^2 w^P}{\partial t^2} \end{aligned}\right\} \tag{3.1}$$

where ρ^P is density of material and P' is initial stress parameter. The rotation components are $\omega_1^P = \frac{1}{2}\left(\frac{\partial w^P}{\partial y} - \frac{\partial v^P}{\partial z}\right)$, $\omega_2^P = \frac{1}{2}\left(\frac{\partial u^P}{\partial z} - \frac{\partial w^P}{\partial x}\right)$ and $\omega_3^P = \frac{1}{2}\left(\frac{\partial v^P}{\partial x} - \frac{\partial u^P}{\partial y}\right)$.

By using the conditions stated above for Love waves propagation, the equations of motion in Eq. (3.1) become

$$\frac{\mu^P}{\rho^P}\left[\left(1 - \frac{P\prime}{2\mu^P}\right)\frac{\partial^2 v^P}{\partial x^2} + \frac{\partial^2 v^P}{\partial z^2}\right] = \frac{\partial^2 v^P}{\partial t^2} \tag{3.2}$$

μ^P is Lame's constant.

Assume solution of Eq. (3.2) as

$$v^P(x,z,t) = h(z)e^{-i(\omega t - \zeta x)} \tag{3.3}$$

Eq. (3.2) becomes

$$\frac{d^2 h}{dz^2} + \zeta^2 J^2 h(z) = 0 \tag{3.4}$$

where $J^2 = \left[\frac{c^2}{\beta_2^2} + \xi - 1\right]$, $\beta_2^2 = \frac{\mu^P}{\rho^P}$ and $\xi = \frac{P\prime}{2\mu^P}$

Solution of Eq. (3.4) is

$$h(z) = A_3 e^{i\zeta J z} + A_4 e^{-i\zeta J z} \tag{3.5}$$

The displacement component of the pre-stressed homogeneous medium becomes

$$v^P(x,z,t) = (A_3 e^{i\zeta J z} + A_4 e^{-i\zeta J z}) e^{-i(\omega t - \zeta x)} \tag{3.6}$$

A_3 and A_4 are the arbitrary constants.

The non-vanishing stress component becomes

$$\tau_{32}^P = \mu^P \frac{\partial v^P}{\partial z} = \mu^P (i\zeta J)(A_3 e^{i\zeta J z} - A_4 e^{-i\zeta J z}) e^{-i(\omega t - \zeta x)} \tag{3.7}$$

3.2.1.3 Solution of couple stress substrate $\{\boldsymbol{z} > 0\}$

Equation of motion is given as [37]

$$(\lambda^C + \mu^C + \eta^C \nabla^2)\nabla(\nabla.\vec{v}) + (\mu^C - \eta^C \nabla^2)\nabla^2 \vec{v} = \rho^C \frac{\partial^2 \vec{v}}{\partial t^2} \tag{3.8}$$

The justification of parameters λ^C, μ^C, ρ^C and η^C is given in section (1.3) of chapter-1 and $\vec{v} = (u^C, v^C, w^C)$ is displacement vector.

By imposing conditions for Love waves propagation, equation of motion in Eq. (3.8) reduces to

$$\left(\frac{\partial^2 v^C}{\partial x^2} + \frac{\partial^2 v^C}{\partial z^2}\right) - l^2 \left(\frac{\partial^4 v^C}{\partial x^4} + \frac{\partial^4 v^C}{\partial z^4} + 2\frac{\partial^4 v^C}{\partial x^2 \partial z^2}\right) = \frac{1}{\beta_3^2}\frac{\partial^2 v^C}{\partial t^2} \tag{3.9}$$

where $\beta_3^2 = \frac{\mu^C}{\rho^C}$

Assume solution of Eq. (3.9) as

$$v^C(x,z,t) = f(z) e^{-i(\omega t - \zeta x)} \tag{3.10}$$

Eq. (3.9) becomes

$$\frac{d^4 f}{dz^4} - L_1 \frac{d^2 f}{dz^2} + L_2 f = 0 \tag{3.11}$$

where $L_1 = \frac{1}{l^2} + 2\zeta^2$ and $L_2 = \zeta^4 + \frac{\zeta^2}{l^2} - \frac{\zeta^2 c^2}{l^2 \beta_3^2}$

As $z \to \infty$, $f(z)$ must vanish, so, the solution of Eq. (3.11) becomes

$$f(z) = A_5 e^{-pz} + A_6 e^{-qz} \tag{3.12}$$

where A_5 and A_6 are arbitrary constants and $p = \sqrt{\frac{L_1+\sqrt{L_1^2-4L_2}}{2}}$ and $q = \sqrt{\frac{L_1-\sqrt{L_1^2-4L_2}}{2}}$

The displacement component of substrate becomes

$$v^C(x,z,t) = (A_5 e^{-pz} + A_6 e^{-qz}) e^{-i(\omega t-\zeta x)} \tag{3.13}$$

The constitutive equations are

$$\tau_{ji}^C = \lambda^C v_{k,k}^C \delta_{ij} + \mu^C \left(v_{i,j}^C + v_{j,i}^C\right) - \eta^C \nabla^2 (v_{i,j}^C - v_{j,i}^C) \tag{3.14}$$

$$\mu_{ji}^C = \ 4\eta^C (\omega_{i,j} - \omega_{j,i}) \tag{3.15}$$

where $\omega_i = \frac{1}{2} \epsilon_{ijk} v_{k,j}^C$ is a rotation vector. The parameters τ_{ji}^C and μ_{ji}^C are discussed in section (1.3) of chapter 1.

The force stress and couple stress components become

$$\tau_{32}^C = \mu^C \frac{\partial v^C}{\partial z} - \mu^C l^2 \left[\frac{\partial^3 v^C}{\partial z^3} + \frac{\partial^3 v^C}{\partial z \partial x^2}\right] = \begin{bmatrix} \mu^C(-pA_5 e^{-pz} - qA_6 e^{-qz}) - \\ \mu^C l^2 (p\zeta^2 A_5 e^{-pz} + q\zeta^2 A_6 e^{-qz} \\ -p^3 A_5 e^{-pz} - q^3 A_6 e^{-b_1 z}) \end{bmatrix} e^{-i(\omega t-\zeta x)} \tag{3.16}$$

$$\mu_{31}^C = -2\mu^C l^2 [(p^2 A_5 e^{-pz} + q^2 A_6 e^{-qz}) - (A_5 \zeta^2 e^{-pz} + A_6 \zeta^2 e^{-qz})] e^{-i(\omega t-\zeta x)} \tag{3.17}$$

3.2.2 Boundary conditions

(i) The upper surface of dry sandy layer must be stress free, so,

$\frac{\mu^D}{\eta^D} \frac{\partial v^D}{\partial z} = 0$ at $z = -(H + H_1)$.

(ii) The displacement and stress components must be continuous at joining surface of upper and intermediate layer, that is,

a. $\frac{\mu^D}{\eta^D}\frac{\partial v^D}{\partial z} = \mu^P \frac{\partial v^P}{\partial z}$ at $z = -H$

b. $v^D(x,z,t) = v^P(x,z,t)$ at $z = -H$

(iii) The displacement and stress components must be continuous at joining surface of pre-stressed layer and couple stress half-space, that is,

a. $\mu^P \frac{\partial v^P}{\partial z} = \mu^C \frac{\partial v^C}{\partial z} - \mu^C l^2 \left[\frac{\partial^3 v^C}{\partial z^3} + \frac{\partial^3 v^C}{\partial z \partial x^2}\right]$ at $z = 0$

b. $v^P(x,z,t) = v^C(x,z,t)$ at $z = 0$

c. The couple stresses should vanish at interfacial surface, so, $\mu_{31}^C = 0$ at $z = 0$

3.2.3 Derivation of secular equation

By employing boundary conditions, we obtain six equations as

$$e^{-i\zeta s(H+H_1)}A_1 - e^{i\zeta s(H+H_1)}A_2 = 0 \tag{3.18}$$

$$\frac{\mu^D s}{\eta^D}e^{-i\zeta sH}A_1 - \frac{\mu^D s}{\eta^D}e^{i\zeta sH}A_2 - \mu^P J e^{-i\zeta JH}A_3 + \mu^P J e^{i\zeta JH}A_4 = 0 \tag{3.19}$$

$$e^{-i\zeta sH}A_1 + e^{i\zeta sH}A_2 - e^{-i\zeta JH}A_3 - e^{i\zeta JH}A_4 = 0 \tag{3.20}$$

$$i\zeta\mu^P J A_3 - i\zeta\mu^P J A_4 + T_1 A_5 + T_2 A_6 = 0 \tag{3.21}$$

$$A_3 + A_4 - A_5 - A_6 = 0 \tag{3.22}$$

$$(p^2 - \zeta^2)A_5 + (q^2 - \zeta^2)A_6 = 0 \tag{3.23}$$

For the non-trivial solution of homogeneous linear equations from Eqs (3.18)-(3.23), determinant of arbitrary coefficients must vanish.

$$\begin{vmatrix} e^{-i\zeta s(H+H_1)} & -e^{i\zeta s(H+H_1)} & 0 & 0 & 0 & 0 \\ \mu^D s e^{-i\zeta sH}/\eta^D & -\mu^D s e^{i\zeta sH}/\eta^D & -\mu^P J e^{-i\zeta JH} & \mu^P J e^{i\zeta JH} & 0 & 0 \\ e^{-i\zeta sH} & e^{i\zeta sH} & -e^{-i\zeta JH} & -e^{i\zeta JH} & 0 & 0 \\ 0 & 0 & i\zeta\mu^P J & -i\zeta\mu^P J & T_1 & T_2 \\ 0 & 0 & 1 & 1 & -1 & -1 \\ 0 & 0 & 0 & 0 & \varphi_1 & \varphi_2 \end{vmatrix} = 0 \tag{3.24}$$

$T_1 = \mu^C(p - l^2p^3 + l^2p\zeta^2)$, $T_2 = \mu^C(q - l^2q^3 + l^2q\zeta^2)$, $\varphi_1 = (p^2 - \zeta^2)$

$\varphi_2 = (q^2 - \zeta^2)$

By solving Eq. (3.24), we get following secular equation of Love waves in an initially stressed homogeneous elastic layer bounded between a dry sandy layer and a microstructural substrate.

$$Q_1 cos\big(\zeta(JH - sH_1)\big) + Q_2 cos\big(\zeta(JH + sH_1)\big) + Q_3 sin\big(\zeta(JH - sH_1)\big) - Q_4 sin\big(\zeta(JH + sH_1)\big) = 0 \quad (3.25)$$

where

$$Q_1 = -\frac{s\mu^D T_2(p^2-\zeta^2)}{\eta^D} + \mu^P J T_2(p^2 - \zeta^2) + \frac{s\mu^D T_1(q^2-\zeta^2)}{\eta^D} - \mu^P J T_1(q^2 - \zeta^2)$$

$$Q_2 = \frac{s\mu^D T_2(p^2-\zeta^2)}{\eta^D} + \mu^P J T_2(p^2 - \zeta^2) - \frac{s\mu^D T_1(q^2-\zeta^2)}{\eta^D} - \mu^P J T_1(q^2 - \zeta^2)$$

$$Q_3 = \frac{\zeta s J \mu^D \mu^P(p^2-\zeta^2)}{\eta^D} - \zeta(\mu^P)^2 J^2(p^2 - \zeta^2) - \frac{\zeta s J \mu^D \mu^P(q^2-\zeta^2)}{\eta^D} + \zeta(\mu^P)^2 J^2(q^2 - \zeta^2)$$

$$Q_4 = \frac{\zeta s J \mu^D \mu^P(p^2-\zeta^2)}{\eta^D} + \zeta(\mu^P)^2 J^2(p^2 - \zeta^2) - \frac{\zeta s J \mu^D \mu^P(q^2-\zeta^2)}{\eta^D} - \zeta(\mu^P)^2 J^2(q^2 - \zeta^2)$$

Case: If the value of sandiness parameter, $\eta^D = 1$, then dry sandy material behaves as an isotropic elastic material and in that case, Eq. (3.25) becomes

$$Q_1' cos\big(\zeta(JH - sH_1)\big) + Q_2' cos\big(\zeta(JH + sH_1)\big) + Q_3' sin\big(\zeta(JH - sH_1)\big) - Q_4' sin\big(\zeta(JH + sH_1)\big) = 0$$

where

$$Q_1' = -s\mu^D T_2(p^2 - \zeta^2) + \mu^P J T_2(p^2 - \zeta^2) + s\mu^D T_1(q^2 - \zeta^2) - \mu^P J T_1(q^2 - \zeta^2)$$

$$Q_2' = s\mu^D T_2(p^2 - \zeta^2) + \mu^P J T_2(p^2 - \zeta^2) - s\mu^D T_1(q^2 - \zeta^2) - \mu^P J T_1(q^2 - \zeta^2)$$

$$Q_3' = \zeta s J \mu^D \mu^P(p^2 - \zeta^2) - \zeta(\mu^P)^2 J^2(p^2 - \zeta^2) - \zeta s J \mu^D \mu^P(q^2 - \zeta^2) + \zeta(\mu^p)^2 J^2(q^2 - \zeta^2)$$

$Q'_4 = \zeta s J \mu^D \mu^P (p^2 - \zeta^2) + \zeta(\mu^P)^2 J^2 (p^2 - \zeta^2) - \zeta s J \mu^D \mu^P (q^2 - \zeta^2) -$
$\zeta(\mu^P)^2 J^2 (q^2 - \zeta^2)$

3.2.4 Graphical results and discussion

The material constants taken for graphical results are mentioned in Table 3.2.

Dry sandy layer [80]	$\mu^D = 6 \times 10^9 N/m^2$	$\rho^D = 2300\ kg/m^3$
Pre-stressed layer [9]	$\mu^P = 6.82 \times 10^9 N/m^2$	$\rho^P = 3380\ kg/m^3$
Couple stress substrate [117]	$\mu^C = 30.5 \times 10^9\ N/m^2$	$\rho^C = 2717\ Kg/m^3$

Table 3.1 Material parameters

Above mentioned parameters of couple stress substrate are of Dionysos marble and the average internal cell size of Dionysos marble is of the order $O(10^{-4})$. In all the figures, impacts of different parameters are shown by considering initial mode of Love waves. In Figs. (3.2)-(3.8), vertical axis represents dimensionless phase velocity (c/β_2) and horizontal axis represents non-dimensional wave number (ζH). In Figs. (3.9)-(3.11), vertical axis represents dimensionless phase velocity (c/β_2) and horizontal axis represents dimensionless wave number (ζl).

3.2.4.1 The influence of microstructural parameter $(\boldsymbol{l})$

In Figs. (3.2)-(3.4) phase velocity $(c/\beta_2)$is plotted against wave number (ζH), to depict the impacts of microstructural parameter (l) associated with substrate. Figure (3.2) is plotted by taking four values of microstructural parameter as $l = 0.0001\ m, 0.0004\ m, 0.0006\ m,$ and $0.0008\ m$. The values of other parameters are taken as $\xi = 0.2, \eta^D = 1.2$ and $H_1/H = 1$. From Fig. (3.2), it can be observed that results are very meager and it was quite expected, as characteristic length is a microstructural parameter. To depict these results, graph has been zoomed and it is observed that this parameter favors phase velocity and with the increase of microstructural parameter velocity increases. Figure (3.3) again shows the impacts of microstructural parameter, values of all parameters are kept same, except $\eta^D = 1$, which depicts that dry sandy layer behaves as an isotropic material. Figure (3.4) also shows the impacts of microstructural parameter on phase velocity, when $\xi = 0$, that is, there are no pre-existing stresses in the intermediate layer and other parameters are taken as $\eta^D = 1.2$ and $H_1/H = 1$. Figures (3.3) and (3.4) are special cases, and results found in both these figures are also similar to the results obtained in Fig. (3.2).

3.2.4.2 The influence of initial stress ($\boldsymbol{\xi}$)

The effects of initial stress parameter of intermediate layer are shown in Figs. (3.5) and (3.6), by taking five values of initial stress (ξ) parameter as $\xi = \frac{P\prime}{2\mu^P} = 0.0, 0.2, 0.4, 0.6, 0.8$. For plotting Fig. (3.5), the values of other parameters are kept as $l = 0.0004m$, $\eta^D = 1.2$ and $H_1/H = 1$. It can be noticed that the initial stress parameter goes against phase velocity of Love waves as with the increase in initial stress parameter velocity decreases. Velocity is maximum, when value of initial stress parameter is zero ($\xi = 0$), that is, there are no pre-existing stresses in the intermediate layer. Figure (3.6) depicts the impacts of initial stress parameter, when $\eta^D = 1$, that is, when dry sandy layer behaves as isotropic and the value of other parameters are $l = 0.0004\ m$ and $H_1/H = 1$. Results found in Fig. (3.6) are similar to the results found in Fig. (3.5).

3.2.4.3 The influence of sandiness parameter ($\boldsymbol{\eta^D}$)

The effects of sandiness (η^D) parameter on the behavior of Love waves are shown in Figs. (3.7) and (3.8), by taking five values of sandiness parameter as $\eta^D = 1, 1.2, 1.4, 1.6$ and 1.8. The values of other parameters are considered for plotting the Fig. (3.7) are $l = 0.0004m, \xi = 0.2, H_1/H = 1$. From Fig. (3.7), it is observed that sandiness parameter goes against phase velocity of Love waves. The phase velocity is maximum, when dry sandy medium behaves as an isotropic elastic material ($\eta^D = 1$). Figure (3.8) also depicts the effects of sandiness parameter, when $\xi = 0$, that is, there are no initial stresses in intermediate layer and values of other parameters are $l = 0.0004\ m$ and $H_1/H = 1$. Results found in Fig. (3.8) are similar to the results found in Fig. (3.7).

3.2.4.4 The influence of width ratio (H_1/H)

As two layers are of finite widths, so effects of width ratio (H_1/H) are elucidated on propagation of Love waves in Figs. (3.9)-(3.11). These figures are plotted by taking five values of width ratio as $H_1/H = 0.6, 0.8, 1.0, 1.2$ and 1.4. For Fig. (3.9) values for other parameters are $l = 0.0004\, m$, $\eta^D = 1.2$, $\xi = 0.2$. The results found for width ratio are quite interesting, as for lower wave numbers the velocity decreases with increase in width ratio and pattern reverses after a particular value of wave number. The trend found for width ratio is quite visible for lower wave numbers, but these effects curtail with the increase in wave number. Figure (3.10) shows the effects of width ratio (H_1/H) when $\eta^D = 1$, that is, dry sandy layer is isotropic and the values of other parameters are $\xi = 0.2$ and $l = 0.0004\, m$. Fig. (3.11) shows the impacts of width ratio (H_1/H) when $\xi = 0$, that is, there are no initial stresses in the medium and values of other parameters are $\eta^D = 1.2$ and $l = 0.0004\, m$. Both these figures showed similar types of effects as were found in Fig. (3.9).

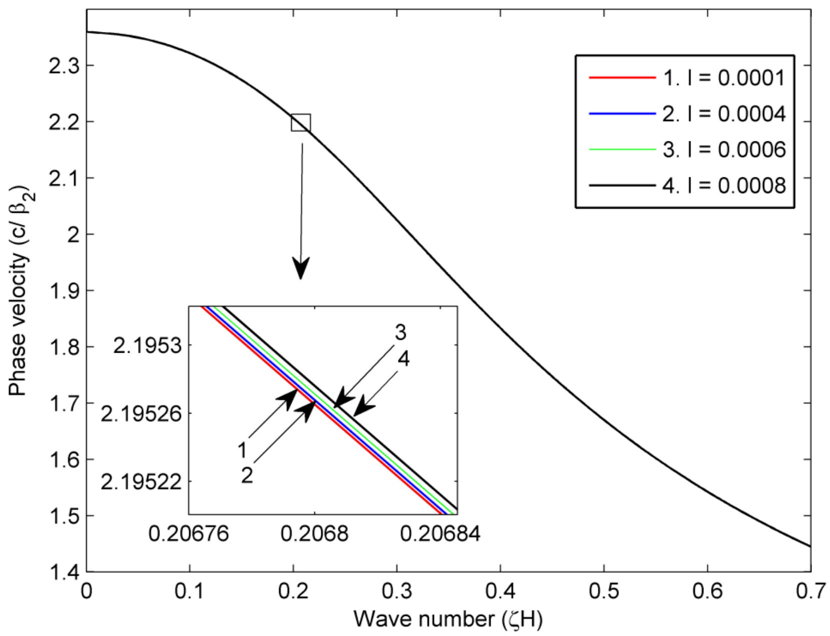

Figure 3.2 Plots for showing impacts of characteristic length (l), when $\eta^D = 1.2$ & $\xi = 0.2$

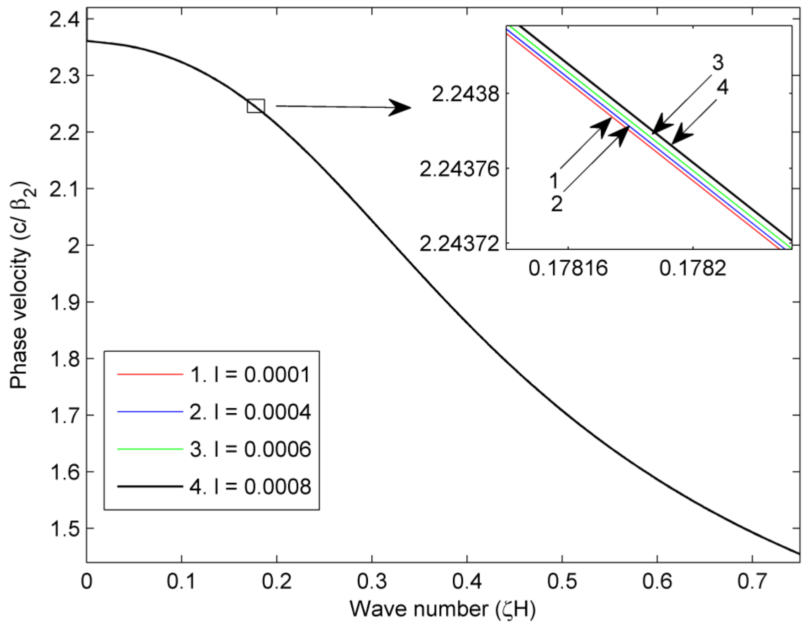

Figure 3.3 Plots for showing impacts of characteristic length (l), when $\eta^D = 1$ & $\xi = 0.2$

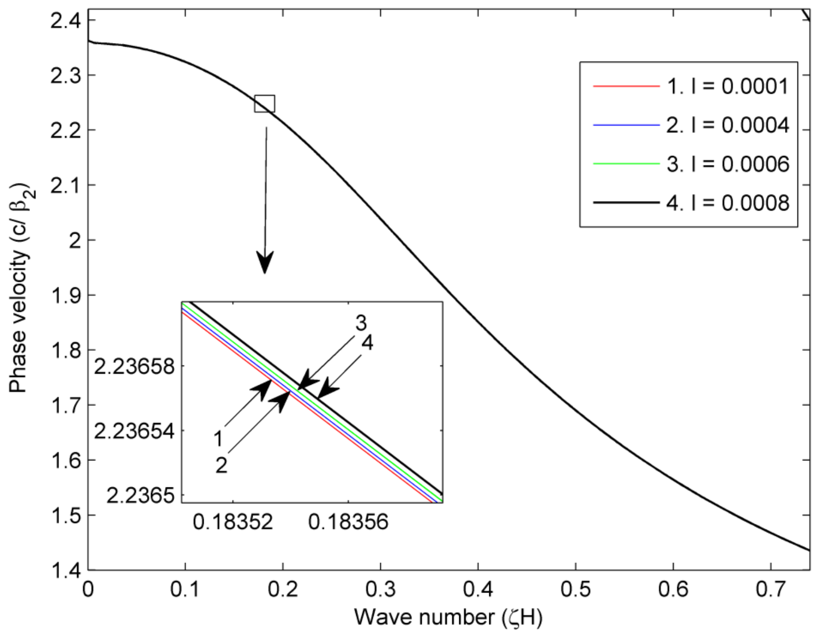

Figure 3.4 Plots for showing impacts of characteristic length (l), when $\eta^D = 1.2$ & $\xi = 0$

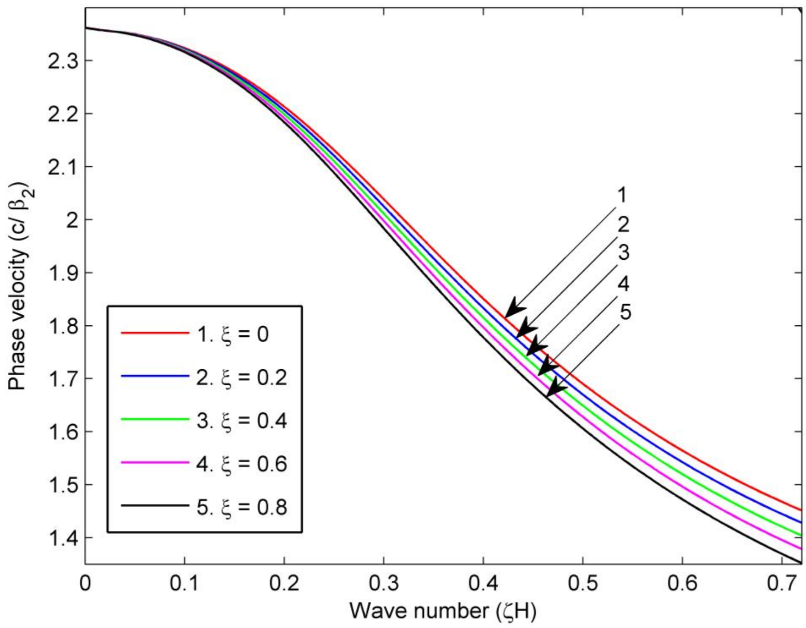

Figure 3.5 Plots for showing impacts of initial stress parameter (ξ), when $\eta^D = 1.2$

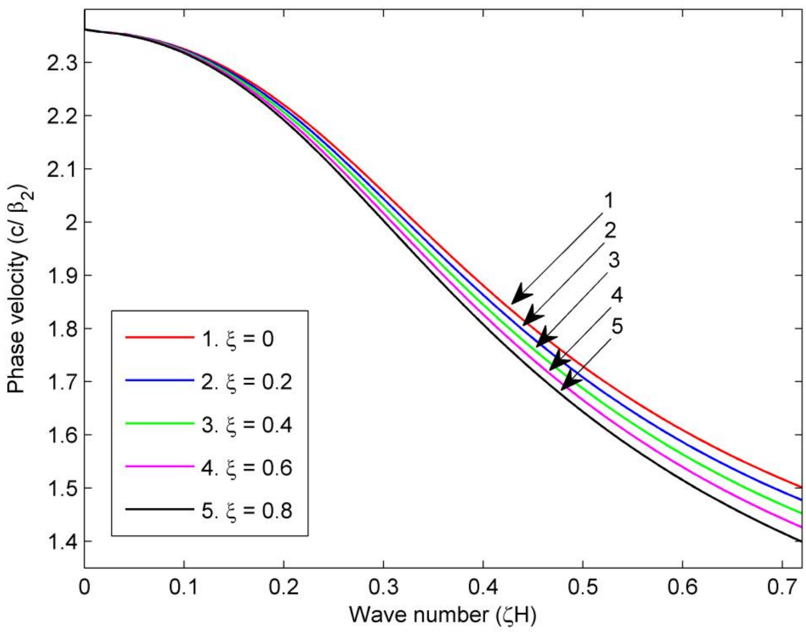

Figure 3.6 Plots for showing impacts of initial stress parameter (ξ), when $\eta^D = 1$

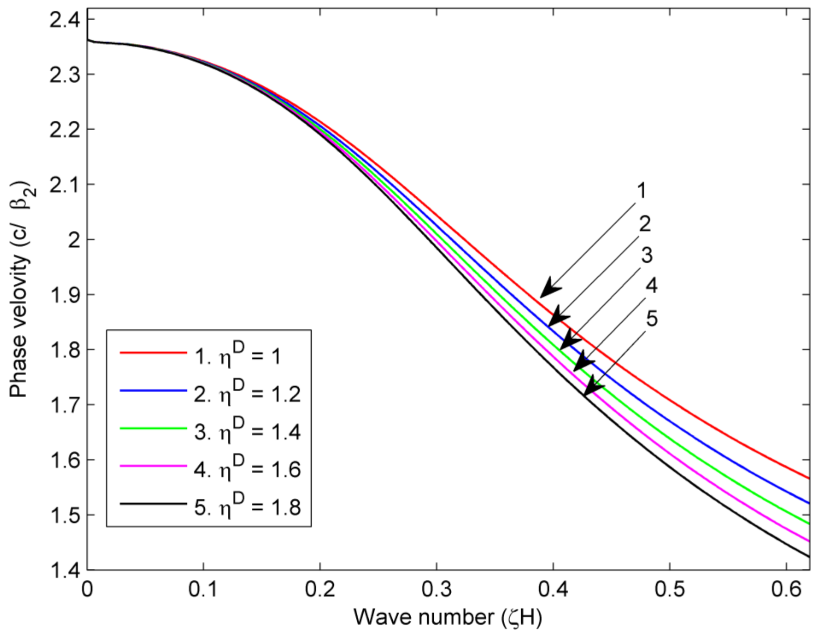

Figure 3.7 Plots for showing impacts of sandiness parameter (η^D), when $\xi = 0.2$

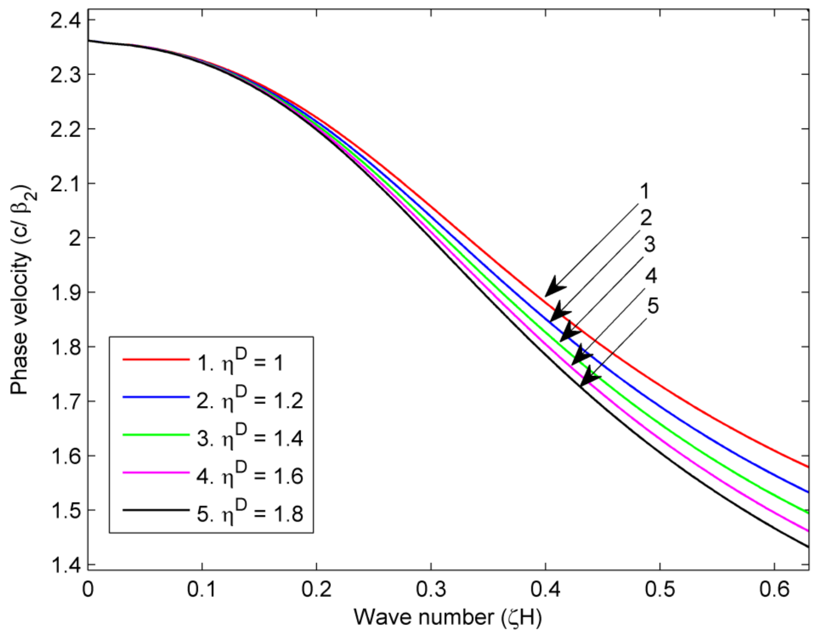

Figure 3.8 Plots for showing impacts of sandiness parameter (η^D), when $\xi = 0$

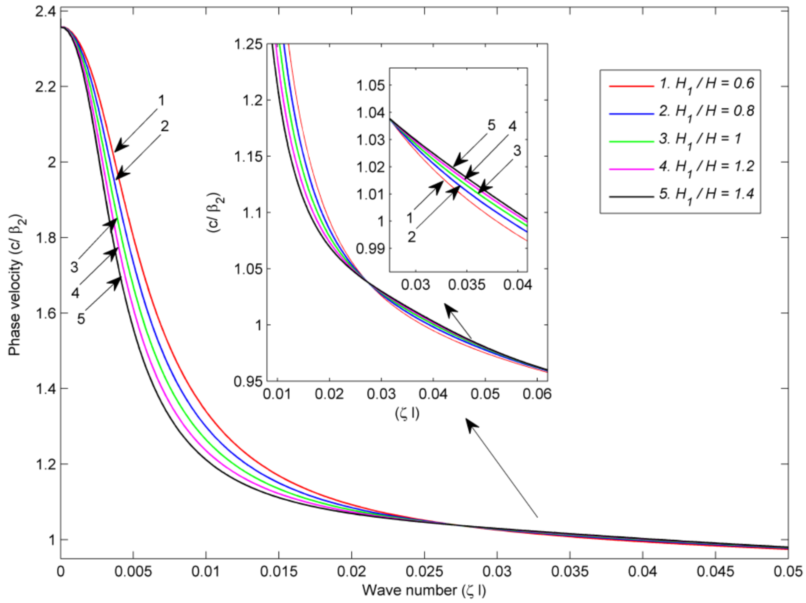

Figure 3.9 Plots for showing impacts of width ratio (H_1/H), when $\eta^D = 1.2$ & $\xi = 0.2$

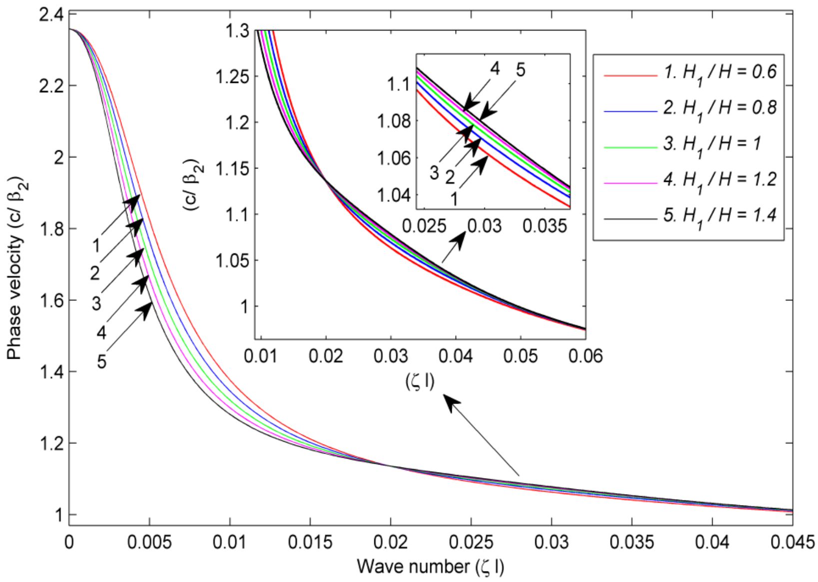

Figure 3.10 Plots for showing impacts of width ratio (H_1/H), when $\eta^D = 1$ & $\xi = 0.2$

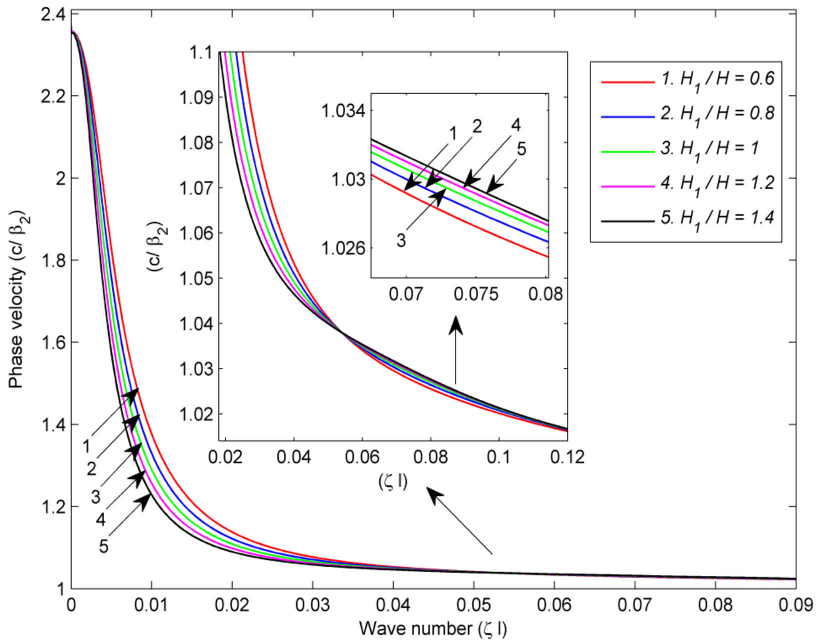

Figure 3.11 Plots for showing impacts of width ratio (H_1/H), when $\eta^D = 1.2$ & $\xi = 0$

3.2.5 Conclusion

The study presents an analysis of Love waves propagation in a pre-stressed homogeneous layer lying between a dry sandy layer and couple stress substrate. The outcomes drawn from the analysis are given below.

- It is observed that microstructural parameter (l) associated with substrate favors phase velocity. The results for the parameter are quite meager, yet these effects have highlighted the role of size effects into the problem.
- The presence of initial stresses in the middle layer is adversely affecting the velocity of Love waves. Phase velocity is highest when there are no initial stresses in the medium.
- Sandiness parameter works against the velocity of Love waves. Phase velocity is maximum, when material behaves as an isotropic elastic material.

- The width ratio of the dry sandy layer and pre-stressed layer has shown very interesting results. For the lower wave numbers phase velocity decreases, when value of width ratio increases but pattern tends to reverse after a particular wave number. The trends found for width ratio diminishes with the increasing wave number.

3.3 LOVE WAVES IN A VISCOELASTIC LAYER LYING BETWEEN A FIBER-REINFORCED LAYER AND CONSISTENT COUPLE STRESS SUBSTRATE

3.3.1 Formulation and solution of the problem

It is assumed that a viscoelastic layer of finite thickness H_1 is bounded between a fiber-reinforced layer of finite thickness H_0 and a couple stress substrate. The substrate is mathematically modeled by using consistent couple stress theory. The origin (O) is considered at joining surface of viscoelastic layer and microstructural substrate, x-axis is going downward into the substrate, and wave is propagating along y-axis (Fig. 3.12).

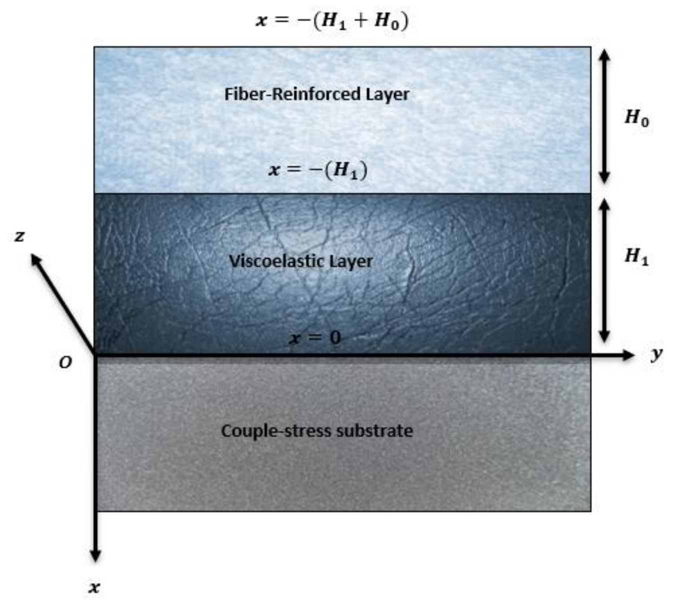

Figure 3.12 Geometrical configuration of the problem

For propagation of Love waves, displacement components of fiber-reinforced layer are taken as (u^F, v^F, w^F), viscoelastic layer are (u^V, v^V, w^V) and couple stress substrate are (u^C, v^C, w^C). All field variables are independent of z-coordinate, that is, $\frac{\partial}{\partial z} \equiv 0$ and $u^F = v^F = 0$, $w^F = w^F(x, y, t)$; $u^V = v^V = 0$, $w^V = w^V(x, y, t)$ and $u^C = v^C = 0$, $w^C = w^C(x, y, t)$.

3.3.1.1 Solution of fiber-reinforced layer

Equation of motion for fiber-reinforced layer is given as

$$\frac{\partial \tau_{31}^F}{\partial x} + \frac{\partial \tau_{32}^F}{\partial y} + \frac{\partial \tau_{33}^F}{\partial z} = \rho^F \frac{\partial^2 w^F}{\partial t^2} \tag{3.26}$$

ρ^F is the density of material.

Constitutive relation is given in section (1.4) of chapter 1. According to the geometry of the problem, direction of reinforcement is considered as $(a_1, a_2, 0)$.

By using constitutive relation, the equation of motion in Eq. (3.26) becomes

$$L\frac{\partial^2 w^F}{\partial x^2} + 2M\frac{\partial^2 w^F}{\partial x \partial y} + N\frac{\partial^2 w^F}{\partial y^2} = \frac{\rho^F}{\mu_T}\frac{\partial^2 w^F}{\partial t^2} \tag{3.27}$$

where $L = 1 + \left(\frac{\mu_L}{\mu_T} - 1\right)a_1^2$, $M = \left(\frac{\mu_L}{\mu_T} - 1\right)a_1 a_2$ and $N = 1 + \left(\frac{\mu_L}{\mu_T} - 1\right)a_2^2$

Assume solution of Eq. (3.27) as

$$w^F(x, y, t) = f(x)e^{-i(\omega t - \zeta y)} \tag{3.28}$$

Eq. (3.28) becomes

$$L\frac{d^2 f}{dx^2} + 2iM\zeta\frac{df}{dx} + \left(\frac{\rho^F c^2}{\mu_T} - N\right)\zeta^2 f(x) = 0 \tag{3.29}$$

The solution of Eq. (3.29) is

$$f(x) = \left(A_0 e^{-i\zeta p_0 x} + B_0 e^{-i\zeta q_0 x}\right) \tag{3.30}$$

A_0, B_0 are arbitrary constants and $p_0 = \frac{M + \sqrt{M^2 + L\left(\frac{\rho^F c^2}{\mu_T} - N\right)}}{L}$, $q_0 = \frac{M - \sqrt{M^2 + L\left(\frac{\rho^F c^2}{\mu_T} - N\right)}}{L}$

The displacement component becomes

$$w^F(x,y,t) = \left(A_0 e^{-i\zeta p_0 x} + B_0 e^{-i\zeta q_0 x}\right) e^{-i(\omega t - \zeta y)} \tag{3.31}$$

The non-vanishing stress component becomes

$$\tau_{13}^F = \mu_T \frac{\partial w^F}{\partial x} + (\mu_L - \mu_T)\left[a_1^2 \frac{\partial w^F}{\partial x} + a_1 a_2 \frac{\partial w^F}{\partial y}\right] = \mu_T i\zeta \begin{bmatrix} \left(R_1 e^{-i\zeta p_0 x}\right) A_0 \\ +\left(R_2 e^{-i\zeta q_0 x}\right) B_0 \end{bmatrix} e^{-i(\omega t - \zeta y)} \tag{3.32}$$

where$R_1 = -Lp_0 + M$ and $R_2 = -Lq_0 + M$.

3.3.1.2 Solution of viscoelastic layer

Equation of motion for viscoelastic material is given as

$$\frac{\partial \tau_{31}^V}{\partial x} + \frac{\partial \tau_{32}^V}{\partial y} + \frac{\partial \tau_{33}^V}{\partial z} = \rho^V \frac{\partial^2 w^V}{\partial t^2} \tag{3.33}$$

The constitutive relation is given as [31]

$$\tau_{ij}^V = \left(\lambda^V + \lambda_1' \frac{\partial}{\partial t}\right) \delta_{ij} w_{k,k}^V + \left(\mu^V + \eta^V \frac{\partial}{\partial t}\right)\left(w_{i,j}^V + w_{j,i}^V\right) \tag{3.34}$$

The parameters τ_{ij}^V, λ^V, μ^V, λ_1', $\eta^V$and $\rho^V$are explained in section (1.5) of chapter 1.

By using constitutive relation, the equation of motion in Eq. (3.33) becomes

$$\frac{\partial}{\partial x}\left[\left(\mu^V + \eta^V \frac{\partial}{\partial t}\right)\frac{\partial w^V}{\partial x}\right] + \left[\left(\mu^V + \eta^V \frac{\partial}{\partial t}\right)\frac{\partial^2 w^V}{\partial y^2}\right] = \rho^V \frac{\partial^2 w^V}{\partial t^2} \tag{3.35}$$

Assume solution of Eq. (3.35) as

$$w^V(x,y,t) = g(x) e^{-i(\omega t - \zeta y)} \tag{3.36}$$

By using Eq. (3.36), equation of motion in Eq. (3.35) becomes

$$\frac{d^2 g}{dx^2} + \frac{\left(\overline{\mu^V}\right)'}{\overline{\mu^V}} \frac{dg}{dx} + \left[\frac{\rho^V \omega^2}{\overline{\mu^V}} - \zeta^2\right] g(x) = 0 \tag{3.37}$$

where $\overline{\mu^V} = \mu^V - i\omega\eta^V$and $\left(\overline{\mu^V}\right)' = \frac{d\overline{\mu^V}}{dx}$

To solve Eq. (3.37), let assume $g(x) = \frac{Y_1(x)}{\sqrt{\overline{\mu^V}}}$, Eq. (3.37) becomes

$$\frac{d^2Y_1}{dx^2} + \left[\frac{1}{4\left(\overline{\mu^V}\right)^2}\left(\frac{d\overline{\mu^V}}{dx}\right)^2 - \frac{1}{2\overline{\mu^V}}\frac{d^2\overline{\mu^V}}{dx^2} + \left(\frac{\rho^V\omega^2}{\overline{\mu^V}} - \zeta^2\right)\right]Y_1 = 0 \tag{3.38}$$

The viscoelastic layer is assumed as heterogeneous, so, the parameters μ^V, η^V and ρ^V are taken as the function of depth as

$$\left.\begin{array}{l}\mu^V = \mu'(1 - \sin\alpha\, x)\\ \eta^V = \eta'(1 - \sin\alpha\, x)\\ \rho^V = \rho'(1 - \sin\alpha\, x)\end{array}\right\} \tag{3.39}$$

where μ', η' and ρ' are fixed values of μ^V, η^V and ρ^V respectively, and α has dimensions of inverse of length.

Eq. (3.38) by using Eq. (3.39) becomes

$$\frac{d^2Y_1}{dx^2} + m_1^2 Y_1 = 0 \tag{3.40}$$

where $m_1^2 = \frac{\alpha^2}{4} + \frac{\rho'\omega^2}{\overline{\mu'}} - \zeta^2$ and $\overline{\mu'} = \mu' - i\omega\eta'$

The solution of Eq. (3.40) is

$$Y_1(x) = (A_1\cos(m_1x) + B_1\sin(m_1x)) \tag{3.41}$$

A_1 and B_1 are arbitrary constants.

The displacement component becomes

$$w^V(x,y,t) = \frac{1}{\sqrt{\overline{\mu'}(1-\sin\alpha x)}}[A_1\cos(m_1x) + B_1\sin(m_1x)]e^{-i(\omega t-\zeta y)} \tag{3.42}$$

The non-vanishing stress component becomes

$$\tau_{13}^V = \left(\mu^V + \eta^V\frac{\partial}{\partial t}\right)\frac{\partial w^V}{\partial x}$$

$$= \frac{\sqrt{\overline{\mu'}}}{2\sqrt{(1-\sin\alpha\, x)}}\left\{\begin{array}{l}[\alpha\cos(\alpha x)\cos(m_1x) - 2m_1(1-\sin(\alpha x))\sin(m_1x)]A_1\\ +[\alpha\cos(\alpha x)\sin(m_1x) + 2m_1(1-\sin(\alpha x))\cos(m_1x)]B_1\end{array}\right\}e^{-i(\omega t-\zeta y)}$$

(3.43)

3.3.1.3 Solution of couple stress substrate

Equation of motion for consistent couple stress substrate is given as [37]

$$(\lambda^C + \mu^C + \eta^C \nabla^2)\nabla(\nabla.\vec{w}) + (\mu^C - \eta^C \nabla^2)\nabla^2 \vec{w} = \rho^C \frac{\partial^2 \vec{w}}{\partial t^2} \tag{3.44}$$

The justification of parameters λ^C, μ^C, ρ^C and η^C is given in section (1.3) of chapter-1 and $\vec{w} = (u^C, v^C, w^C)$ is displacement vector.

By imposing the conditions of Love waves propagation, Eq. (3.44) reduces to

$$\left(\frac{\partial^2 w^C}{\partial x^2} + \frac{\partial^2 w^C}{\partial y^2}\right) - l^2 \left(\frac{\partial^4 w^C}{\partial x^4} + \frac{\partial^4 w^C}{\partial y^4} + 2\frac{\partial^4 w^C}{\partial x^2 \partial y^2}\right) = \frac{1}{\beta_2^2}\frac{\partial^2 w^C}{\partial t^2} \tag{3.45}$$

where $\beta_2 = \sqrt{\frac{\mu^C}{\rho^C}}$

Assume solution of Eq. (3.45) as

$$w^C(x, y, t) = h(x)e^{-i(\omega t - \zeta y)} \tag{3.46}$$

Eq. (3.45), by employing Eq. (3.46) becomes

$$\frac{d^4 h}{dx^4} - L_1 \frac{d^2 h}{dx^2} + L_2 h(x) = 0 \tag{3.47}$$

where $L_1 = 2\zeta^2 + \frac{1}{l^2}$ and $L_2 = \zeta^4 + \frac{\zeta^2}{l^2} - \frac{(\zeta c)^2}{l^2 \beta_2^2}$

As $x \to \infty$, $h(x)$ must vanish, hence, solution of Eq. (3.47) becomes

$$h(x) = A_2 e^{-px} + B_2 e^{-qx} \tag{3.48}$$

A_2 and B_2 are arbitrary constants and $p = \sqrt{\frac{L_1 + \sqrt{L_1^2 - 4L_2}}{2}}$ and $q = \sqrt{\frac{L_1 - \sqrt{L_1^2 - 4L_2}}{2}}$

The displacement component of microstructural substrate becomes

$$w^C(x, y, t) = (A_2 e^{-px} + B_2 e^{-qx})\, e^{-i(\omega t - \zeta y)} \tag{3.49}$$

The constitutive equations are

$$\tau_{ji}^C = \lambda^C w_{k,k}^C \delta_{ij} + \mu^C\left(w_{i,j}^C + w_{j,i}^C\right) - \eta^C \nabla^2 (w_{i,j}^C - w_{j,i}^C) \tag{3.50}$$

$$\mu_{ji}^C = 4\eta^C (\omega_{i,j} - \omega_{j,i}) \tag{3.51}$$

where, $\omega_i = \frac{1}{2}\epsilon_{ijk} w_{k,j}^C$ is rotation vector. The parameters τ_{ji}^C and μ_{ji}^C are given in section (1.3) of chapter-1.

The non-vanishing force stress and couple stress components become

$$\tau_{13}^C = \mu^C \frac{\partial w^C}{\partial x} + \mu^C l^2 \left[\frac{\partial^3 w^C}{\partial x^3} + \frac{\partial^3 w^C}{\partial x \partial y^2}\right] = \mu^C [p(l^2\zeta^2 - p^2 l^2 - 1)e^{-px} A_2 + q(l^2\zeta^2 - q^2 l^2 - 1)e^{-qx} B_2] e^{-i(\omega t - \zeta y)} \tag{3.52}$$

$$\mu_{21}^C = 2\mu^C l^2 [(p^2 - \zeta^2)e^{-px} A_2 + (q^2 - \zeta^2)e^{-qx} B_2] e^{-i(\omega t - \zeta y)} \tag{3.53}$$

3.3.2 Boundary Conditions

(i) Upper surface of fiber-reinforced layer must be stress free, so,

$$\mu_T \frac{\partial w^F}{\partial x} + (\mu_L - \mu_T)\left[a_1^2 \frac{\partial w^F}{\partial x} + a_1 a_2 \frac{\partial w^F}{\partial y}\right] = 0 \text{ at } x = -(H_0 + H_1)$$

(ii) Stress and displacement components must be continuous at $x = -H_1$, that is,

a. $\mu_T \frac{\partial w^F}{\partial x} + (\mu_L - \mu_T)\left[a_1^2 \frac{\partial w^F}{\partial x} + a_1 a_2 \frac{\partial w^F}{\partial y}\right] = \left(\mu^V + \eta^V \frac{\partial}{\partial t}\right)\frac{\partial w^V}{\partial x}$

b. $w^F(x, y, t) = w^V(x, y, t)$

(iii) Stress and displacement components must be continuous, at $x = 0$, that is,

a. $\left(\mu^V + \eta^V \frac{\partial}{\partial t}\right)\frac{\partial w^V}{\partial x} = \mu^C \frac{\partial w^C}{\partial x} + \mu^C l^2 \left[\frac{\partial^3 w^C}{\partial x^3} + \frac{\partial^3 w^C}{\partial x \partial y^2}\right]$

b. $w^V(x, y, t) = w^C(x, y, t)$

(iv) The couple stresses should vanish at joining surface between intermediate layer and substrate, that is,

$$\mu_{21}^C = 0 \text{ at } x = 0$$

3.3.3 Derivation of secular equation

By employing boundary conditions, we obtain six equations as

$$R_1 e^{i\zeta(H_0+H_1)p_0} A_0 + R_2 e^{i\zeta(H_0+H_1)q_0} B_0 = 0 \tag{3.54}$$

$$i\zeta\mu_T R_1 e^{i\zeta p_0 H_1} A_0 + i\zeta\mu_T R_2 e^{i\zeta q_0 H_1} B_0 + \frac{-\sqrt{\overline{\mu}'}T_1 A_1}{2\sqrt{(1+\sin\alpha H_1)}} + \frac{-\sqrt{\overline{\mu}'}T_2 B_1}{2\sqrt{(1+\sin\alpha H_1)}} = 0 \tag{3.55}$$

$$e^{i\zeta p_0 H_1} A_0 + e^{i\zeta q_0 H_1} B_0 + \frac{-\cos(m_1 H_1)}{\sqrt{\overline{\mu}'}\sqrt{(1+\sin\alpha H_1)}} A_1 + \frac{\sin(m_1 H_1)}{\sqrt{\overline{\mu}'}\sqrt{(1+\sin\alpha H_1)}} B_1 = 0 \tag{3.56}$$

$$\frac{\alpha\sqrt{\overline{\mu}'}A_1}{2} + m_1\sqrt{\overline{\mu}'}B_1 + T_3 A_2 + T_4 B_2 = 0 \tag{3.57}$$

$$\frac{1}{\sqrt{\overline{\mu}'}} A_1 - A_2 - B_2 = 0 \tag{3.58}$$

$$(p^2 - \zeta^2)A_2 + (q^2 - \zeta^2)B_2 = 0 \tag{3.59}$$

where $T_1 = \alpha\cos(\alpha H_1)\cos(m_1 H_1) + 2m_1\big(1 + \sin(\alpha H_1)\big)\sin(m_1 H_1)$

$T_2 = -\alpha\cos(\alpha H_1)\sin(m_1 H_1) + 2m_1\big(1 + \sin(\alpha H_1)\big)\cos(m_1 H_1)$

$T_3 = \mu^C p[1 + l^2(p^2 - \zeta^2)]$

$T_4 = \mu^C q[1 + l^2(q^2 - \zeta^2)]$

To find non-trivial solution of Eqs. (3.54)-(3.59), determinant of arbitrary constants must vanish, so,

$$\begin{vmatrix} R_1 e^{i\zeta(H_0+H_1)p_0} & R_2 e^{i\zeta(H_0+H_1)q_0} & 0 & 0 & 0 & 0 \\ i\zeta\mu_T R_1 e^{i\zeta p_0 H_1} & i\zeta\mu_T R_2 e^{i\zeta q_0 H_1} & R_3 T_1 & R_3 T_2 & 0 & 0 \\ e^{i\zeta p_0 H_1} & e^{i\zeta q_0 H_1} & R_4 & R_5 & 0 & 0 \\ 0 & 0 & R_6 & \varphi & T_3 & T_4 \\ 0 & 0 & \varphi^* & 0 & -1 & -1 \\ 0 & 0 & 0 & 0 & \varphi_1 & \varphi_2 \end{vmatrix} = 0 \tag{3.60}$$

where

$$\varphi = m_1\sqrt{\mu'}\ , \varphi^* = \frac{1}{\sqrt{\mu'}}\ , \varphi_1 = p^2 - \zeta^2, \varphi_2 = q^2 - \zeta^2, R_3 = \frac{-\sqrt{\mu'}}{2\sqrt{(1+\sin\alpha H_1)}}\ ,$$

$$R_4 = \frac{-\cos(m_1 H_1)}{\sqrt{\mu'}\sqrt{(1+\sin\alpha H_1)}}\ , R_5 = \frac{\sin(m_1 H_1)}{\sqrt{\mu'}\sqrt{(1+\sin\alpha H_1)}}, R_6 = \frac{\alpha\sqrt{\mu'}}{2}$$

By solving Eq. (3.60), we get following equation

$$\left[\left(Q\left(P_1' - \frac{R_1 J_2'}{2}\right) + (p^2 - q^2)R_1 N_1'\right) + i\left(Q\left(-P_2' - \frac{R_1 I_2'}{2}\right) - (p^2 - q^2)R_1 N_2'\right)\right]\frac{e^{i\theta_1}}{\sqrt{1+\sin(\alpha H_1)}} + \left[\left(Q\left(-P_1' + \frac{R_2 J_2'}{2}\right) - (p^2 - q^2)R_2 N_3'\right) + i\left(Q\left(P_2' + \frac{R_2 I_2'}{2}\right) + (p^2 - q^2)R_2 N_4'\right)\right]\frac{e^{i\theta_2}}{\sqrt{1+\sin(\alpha H_1)}} = 0 \qquad (3.61)$$

From real part of Eq. (3.61), we get dispersion relation as

$$F_1'\cos\theta_1 - F_2'\sin\theta_1 + G_1'\cos\theta_2 - G_2'\sin\theta_2 = 0 \qquad (3.62)$$

and from imaginary part of Eq. (3.61), we get damping relation as

$$F_1'\sin\theta_1 + F_2'\cos\theta_1 + G_1'\sin\theta_2 + G_2'\cos\theta_2 = 0 \qquad (3.63)$$

where

$$F_1' = \frac{1}{\sqrt{(1+\sin\alpha H_1)}}\left(Q\left(P_1' - \frac{R_1 J_2'}{2}\right) + (p^2 - q^2)R_1 N_1'\right)$$

$$F_2' = \frac{1}{\sqrt{(1+\sin\alpha H_1)}}\left(Q\left(-P_2' - \frac{R_1 I_2'}{2}\right) - (p^2 - q^2)R_1 N_2'\right)$$

$$G_1' = \frac{1}{\sqrt{(1+\sin\alpha H_1)}}\left(Q\left(-P_1' + \frac{R_2 J_2'}{2}\right) - (p^2 - q^2)R_2 N_3'\right)$$

$$G_2' = \frac{1}{\sqrt{(1+\sin\alpha H_1)}}\left(Q\left(P_2' + \frac{R_2 I_2'}{2}\right) + (p^2 - q^2)R_2 N_4'\right)$$

$$\theta_1 = \zeta\big((H_0 + H_1)p_0 + H_1 q_0\big), \theta_2 = \zeta\big((H_0 + H_1)q_0 + H_1 p_0\big)$$

$$Q = T_4(p^2 - \zeta^2) - T_3(q^2 - \zeta^2)$$

$P'_1 = \frac{R_1 R_2 \mu_T \zeta(S'_1 \omega\eta' + S'_2 \mu')}{((\mu')^2 + (\omega\eta')^2)}$, $P'_2 = \frac{R_1 R_2 \mu_T \zeta(S'_1 \mu' - S'_2 \omega\eta')}{((\mu')^2 + (\omega\eta')^2)}$

$N'_1 = \frac{\alpha R_2 \zeta \mu_T S'_2}{2} - \frac{\alpha(\omega\eta' I'_2 + \mu' J'_2)}{4} + \zeta R_2 \mu_T (m'_2 E'_1 - m'_1 E'_2) + \frac{M'_1}{2}$

$N'_2 = \frac{\alpha R_2 \zeta \mu_T S'_1}{2} + \frac{\alpha(\mu' I'_2 - \omega\eta' J'_2)}{4} + \zeta R_2 \mu_T (m'_1 E'_1 + m'_2 E'_2) - \frac{M'_2}{2}$

$N'_3 = \frac{\alpha R_1 \zeta \mu_T S'_2}{2} - \frac{\alpha(\omega\eta' I'_2 + \mu' J'_2)}{4} + \zeta R_1 \mu_T (m'_2 E'_1 - m'_1 E'_2) + \frac{M'_1}{2}$

$N'_4 = \frac{\alpha R_1 \zeta \mu_T S'_1}{2} + \frac{\alpha(\mu' I'_2 - \omega\eta' J'_2)}{4} + \zeta R_1 \mu_T (m'_1 E'_1 + m'_2 E'_2) - \frac{M'_2}{2}$

$J'_1 = 2(1 + \sin(\alpha H_1))(m'_1 S'_1 - m'_2 S'_2) + \alpha \cos(\alpha H_1) E'_1$

$I'_1 = 2(1 + \sin(\alpha H_1))(m'_1 S'_2 + m'_2 S'_1) - \alpha \cos(\alpha H_1) E'_2$

$J'_2 = 2(1 + \sin(\alpha H_1))(m'_1 E'_1 + m'_2 E'_2) - \alpha \cos(\alpha H_1) S'_1$

$I'_2 = 2(1 + \sin(\alpha H_1))(m'_2 E'_1 - m'_1 E'_2) - \alpha \cos(\alpha H_1) S'_2$

$S'_1 = \sin(m'_1 H_1)\cosh(m'_2 H_1)$, $S'_2 = \cos(m'_1 H_1)\sinh(m'_2 H_1)$

$E'_1 = \cos(m'_1 H_1)\cosh(m'_2 H_1)$, $E'_2 = \sin(m'_1 H_1)\sinh(m'_2 H_1)$

$M'_1 = m'_1 \mu' J'_1 + m'_1 \omega\eta' I'_1 - m'_2 \mu' I'_1 + m'_2 \omega\eta' J'_1$

$M'_2 = m'_1 \mu' I'_1 - m'_1 \omega\eta' J'_1 + m'_2 \mu' J'_1 + m'_2 \omega\eta' I'_1$

$m'_1 = r^{\frac{1}{2}} \cos\left(\frac{\theta}{2}\right)$, $m'_2 = r^{\frac{1}{2}} \sin\left(\frac{\theta}{2}\right)$, $r = (F_1^2 + F_2^2)^{\frac{1}{2}}$

$\tan(\theta) = \frac{F_1}{F_2}$, $F_1 = \frac{\rho' \omega^3 \eta'}{(\mu')^2 + (\omega\eta')^2}$, $F_2 = \frac{\alpha^2}{4} - \zeta^2 + \frac{\rho' \omega^2 \mu'}{(\mu')^2 + (\omega\eta')^2}$

3.3.4 Graphical results and discussion

The values of material constants for graphical illustrations are mentioned in Table 3.2.

Fiber-reinforced layer [33]	$\mu_T = 0.35 \times 10^{10}\ N/m^2$	$\mu_L = 0.707 \times 10^{10} N/m^2$	$\rho^F = 1.6 \times 10^3 Kg/m^3$

Viscoelastic layer [33]	$\mu' = 1.987 \times 10^{10}\ N/m^2$	$\frac{\mu'}{\eta'} = 10^{-6}s^{-1}$	$\rho' = 4705\ Kg/m^3$
Couple stress substrate [117]	$\mu^C = 30.5 \times 10^9\ N/m^2$	$-$	$\rho^C = 2717\ Kg/m^3$

Table 3.2 Material parameters

In Figs. (3.13) (a)-(3.21) (b), vertical axis represents dimensionless phase velocity (c/β_1) and horizontal axis represents non-dimensional wave number (ζH_1). In all the figures, phase velocity decreases with increase in wave number, which shows that Love waves are dispersive in nature.

3.3.4.1 The influence of direction of reinforcement parameters $(\boldsymbol{a_1^2, a_2^2})$

For studying the role of reinforced parameters, five combinations of reinforced parameters are considered as $(a_1^2 = 0.75, a_2^2 = 0.25)$, $(a_1^2 = 0.65, a_2^2 = 0.35)$, $(a_1^2 = 0.50, a_2^2 = 0.50)$, $(a_1^2 = 0.35, a_2^2 = 0.65)$ and $(a_1^2 = 0.25, a_2^2 = 0.75)$ and values of other parameters are kept as $l = 0.0001m$, $\alpha H_1 = 0.18$, $H_0 = H_1 = 0.02\ m$ and $\mu^V/\eta^V = 10^{-6}s^{-1}$. It is noticed from Figs. (3.13) (a) & (b), that both phase velocity and damping velocity are affected by reinforced parameters.

3.3.4.2 The influence of microstructural parameter $(\boldsymbol{l})$

To present the impacts of microstructural parameter associated with substrate on propagation behavior of Love waves, graphs are provided by taking four values of microstructural parameter as $l = 0.0001\ m, 0.0004\ m, 0.0006\ m, 0.0008\ m$. Other parameters are kept as $\alpha H_1 = 0.18$, $H_0 = H_1 = 0.02\ m$ and $\mu^V/\eta^V = 10^{-6}s^{-1}$. Figures (3.14) (a) & (b) depict the impacts of microstructural parameter (l) on phase velocity and damping velocity of Love waves in presence of reinforcement parameters $(a_1^2 = 0.50, a_2^2 = 0.50)$. These graphs show that both velocities increase, when the value of microstructural parameter increases. Figures (3.15) (a) & (b) present the impacts of this parameter again on phase and damping velocities, but in absence of reinforcement parameters $(a_1^2 = 0, a_2^2 = 0)$. Trends found here are similar to the trends seen in Figs. (3.14) (a) & (b).

3.3.4.3 The influence of heterogeneity parameter (αH_1)

The impact of heterogeneity parameter (αH_1) of viscoelastic layer on Love waves propagation is shown in (3.16) (a) & (b) and (3.17) (a) & (b). Graphs are taken by taking four values of the heterogeneity parameter as $\alpha H_1 = 0.18, 0.38, 0.58, 0.78$. The values of other parameters are kept as $l = 0.0001\,m$, $H_0 = H_1 = 0.02\,m$, and $\mu^V/\eta^V = 10^{-6}s^{-1}$. Figures (3.16) (a) & (b) are drawn in presence of reinforcement parameters $(a_1^2 = 0.50, a_2^2 = 0.50)$ and Figs. (3.17) (a) & (b) are plotted without reinforcement parameters $(a_1^2 = 0, a_2^2 = 0)$. From all the four figures, both velocities decrease with the increase in heterogeneity.

3.3.4.4 The influence of internal friction

The role of internal friction parameter on Love waves propagation is depicted by taking four values of internal friction parameter as $\mu^V/\eta^V = 6 \times 10^5, 10 \times 10^5, 20 \times 10^5, 30 \times 10^5$. The values of other parameters are kept as $l = 0.0001\,m$, $H_0 = 0.02\,m = H_1$ and $\alpha H_1 = 0.18$. Figures (3.18) (a) & (b) presents the effects of internal friction parameter on phase and damping velocities in presence of fiber-reinforced parameters $(a_1^2 = 0.50, a_2^2 = 0.50)$. Figures (3.19) (a) & (b) are plotted in absence of fiber-reinforced parameters $(a_1^2 = 0, a_2^2 = 0)$. It can be observed from Figs. (3.18) (a) and (3.19) (a) that internal friction parameter has an adverse impact on velocity. It can further be seen from Figs. (3.18) (b) and (3.19) (b) that internal friction parameter favors damping velocity.

3.3.4.5 The influence of width ratio $\left(\frac{H_0}{H_1}\right)$

The effects of width ratio of layers are shown by taking five values of width ratio as $H_0/H_1 = 0.2, 0.5, 1, 1.1, 1.4$ and other parameters are kept as $l = 0.0001\,m$, $\alpha H_1 = 0.18$ and $\mu^V/\eta^V = 10^{-6}s^{-1}$. Figures (3.20) (a) & (b) are generated in the presence of reinforced parameters $(a_1^2 = 0.50, a_2^2 = 0.50)$ and Figs. (3.21) (a) & (b) are generated without reinforced parameters $(a_1^2 = 0, a_2^2 = 0)$. Figures (3.20) (a) and (3.21) (a) are of phase velocity, whereas (3.20) (b) and (3.21) (b) are of damping velocity. From Figs.

(3.20) (a) & (b) and (3.21) (a) & (b), it can be observed that width ratio goes against both the velocities.

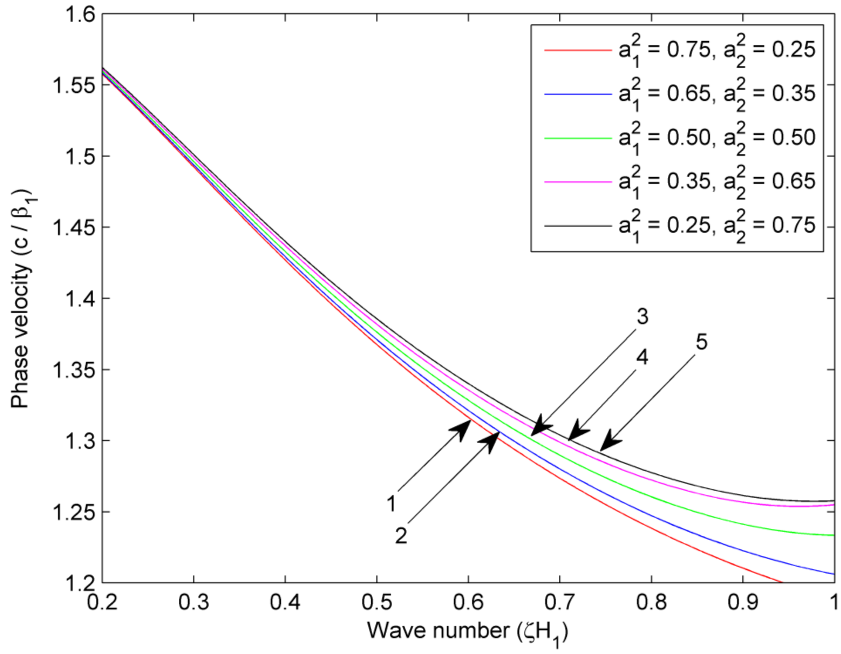

Figure 3.13(a) Plot for showing impacts of reinforced parameters (a_1^2, a_2^2)

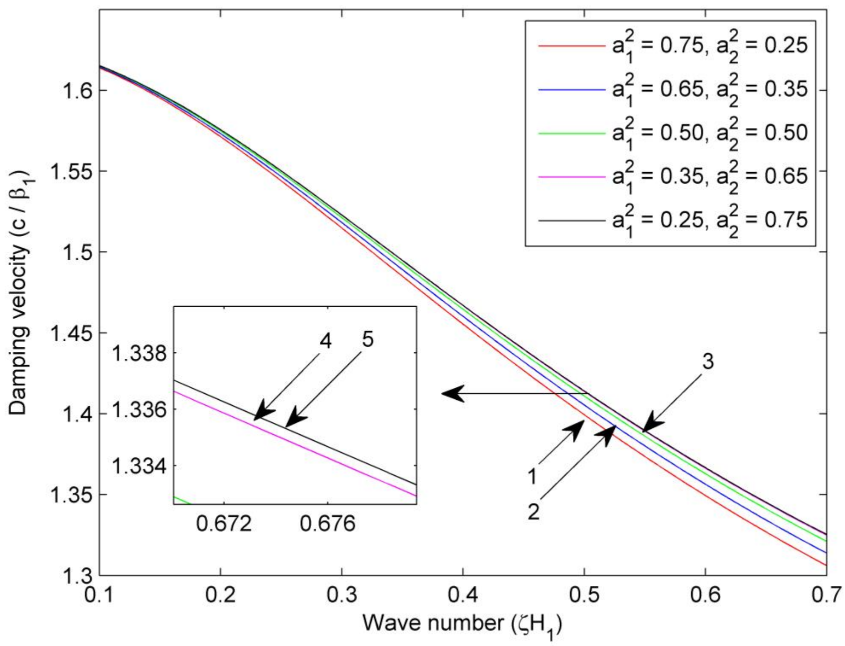

Figure 3.13(b) Plot for showing impacts of reinforced parameters (a_1^2, a_2^2)

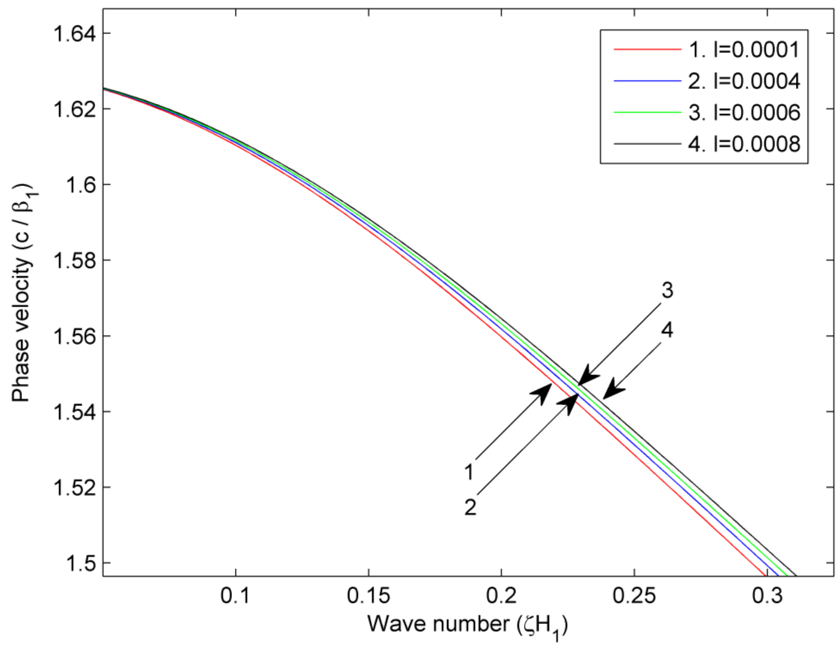

Figure 3.14(a) Plot for showing impacts of characteristic length (l) in the presence of reinforced parameters

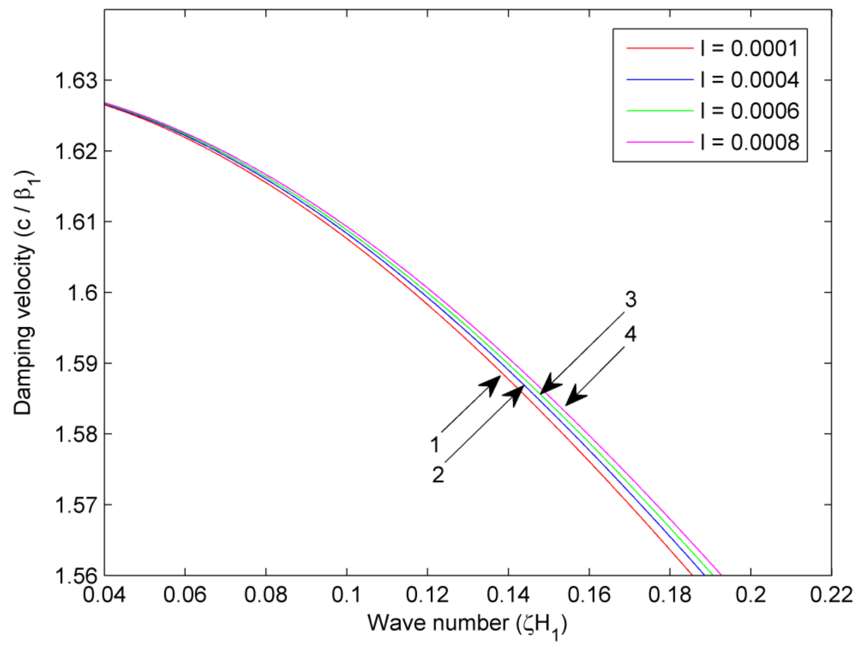

Figure 3.14(b) Plot for showing impacts of characteristic length (l) in the presence of reinforced parameters

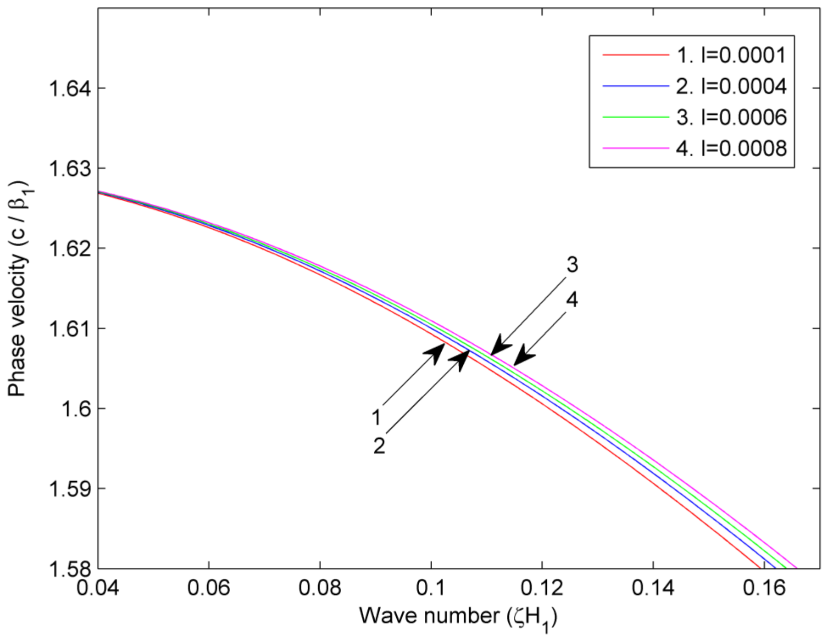

Figure 3.15(a) Plot for showing impacts of characteristic length (l) in the absence of reinforced parameters

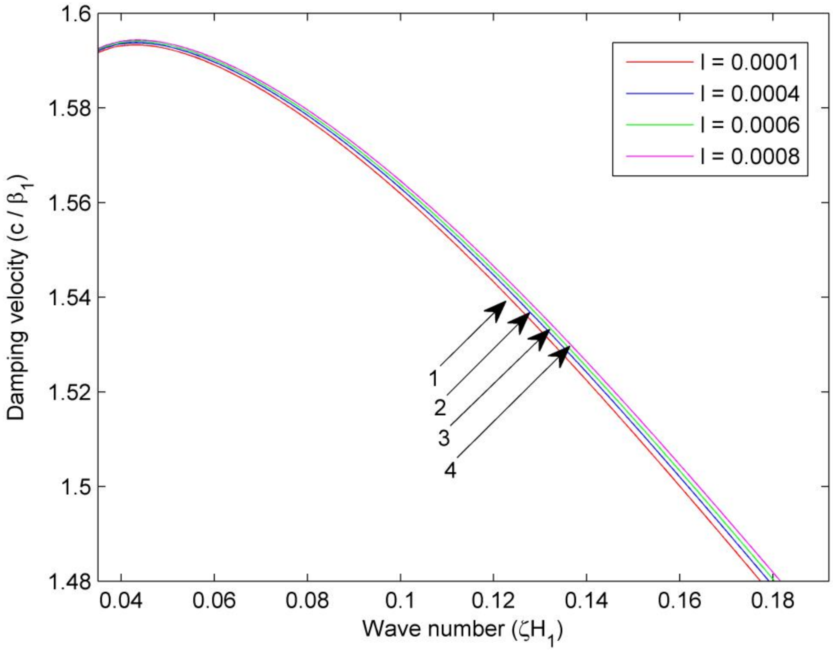

Figure 3.15(b) Plot for showing impacts of characteristic length (l) in the absence of reinforced parameters

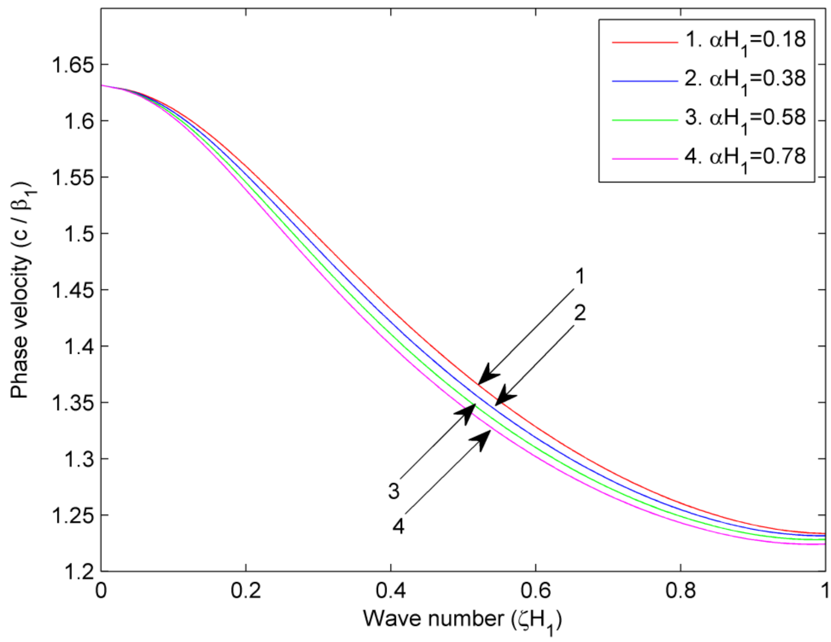

Figure 3.16(a) Plot for showing impacts of heterogeneity (αH_1) parameter in presence of reinforced parameters

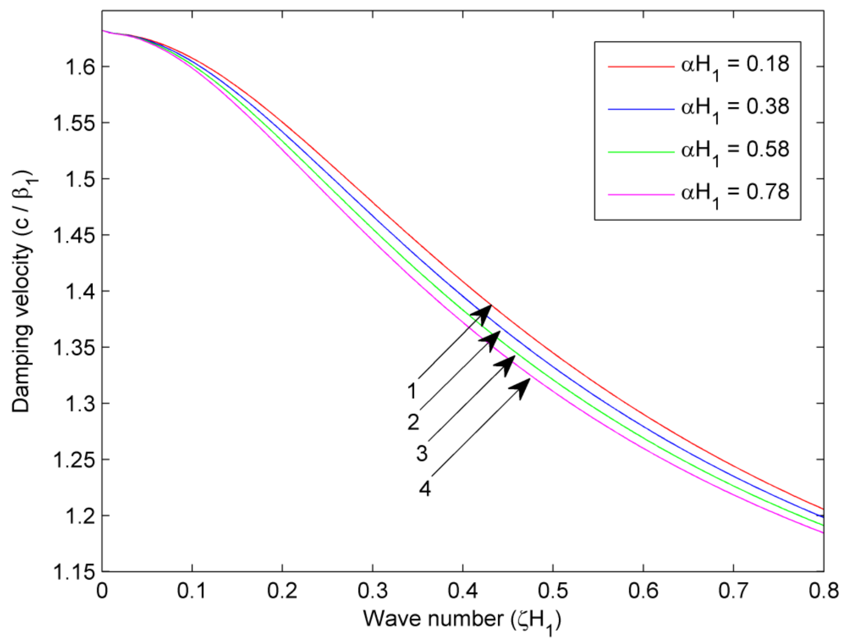

Figure 3.16(b) Plot for showing impacts of heterogeneity (αH_1) parameter in presence of reinforced parameters

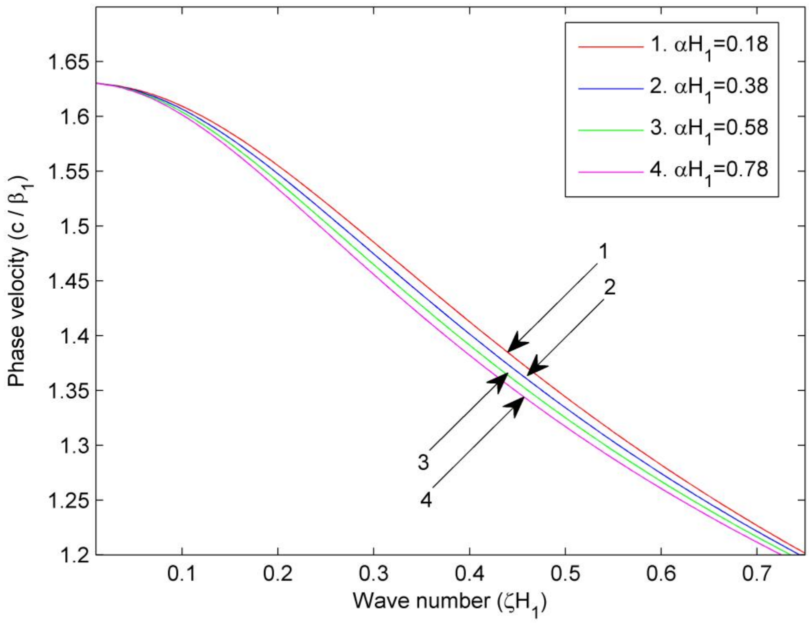

Figure 3.17(a) Plot for showing impacts of heterogeneity parameter (αH_1) in the absence of reinforced parameters

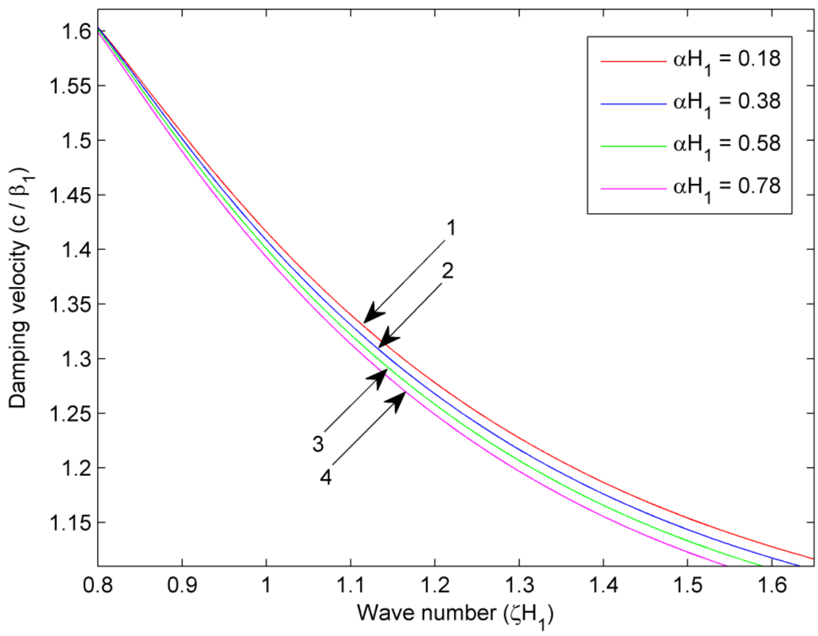

Figure 3.17(b) Plot for showing impacts of heterogeneity parameter (αH_1) in the absence of reinforced parameters

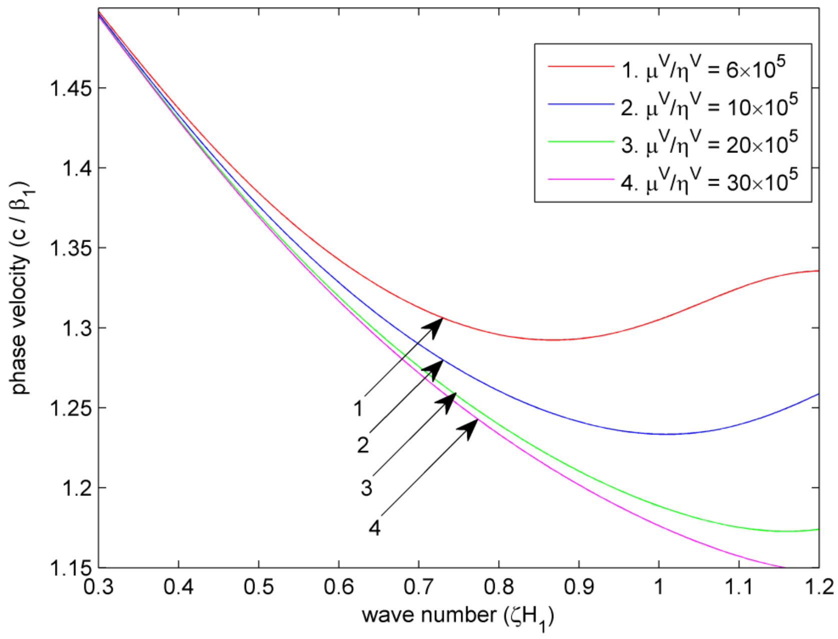

Figure 3.18(a) Plot for showing impacts of internal friction parameter (μ^V/η^V) in the presence of reinforced parameters

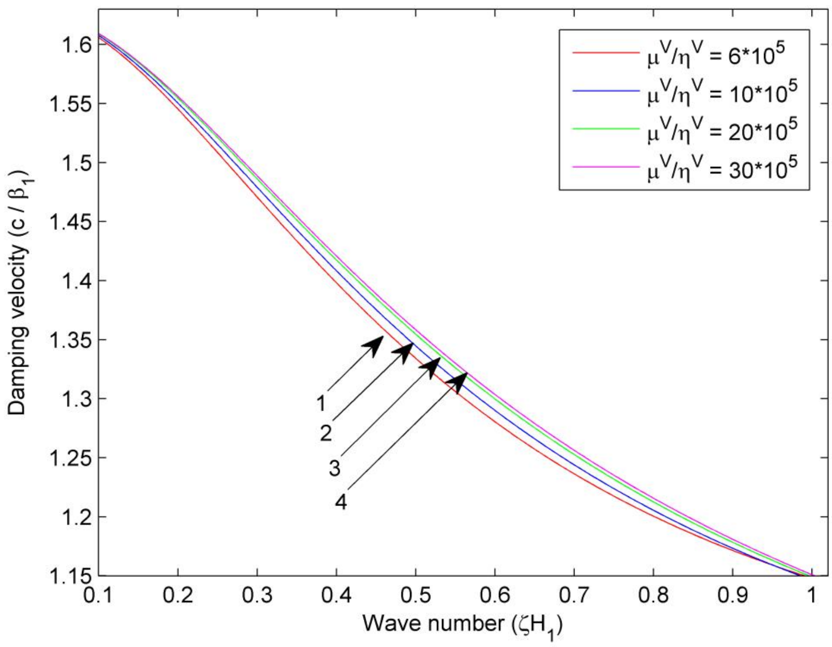

Figure 3.18(b) Plot for showing impacts of internal friction parameter (μ^V/η^V) in the presence of reinforced parameters

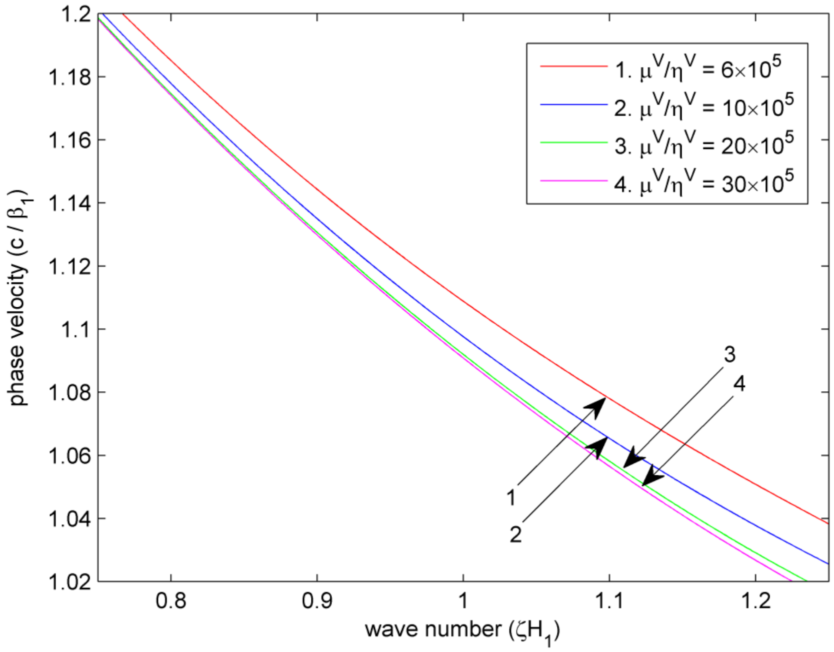

Figure 3.19(a) Plot for showing impacts of internal friction parameter (μ^V/η^V) in the absence of reinforced parameters

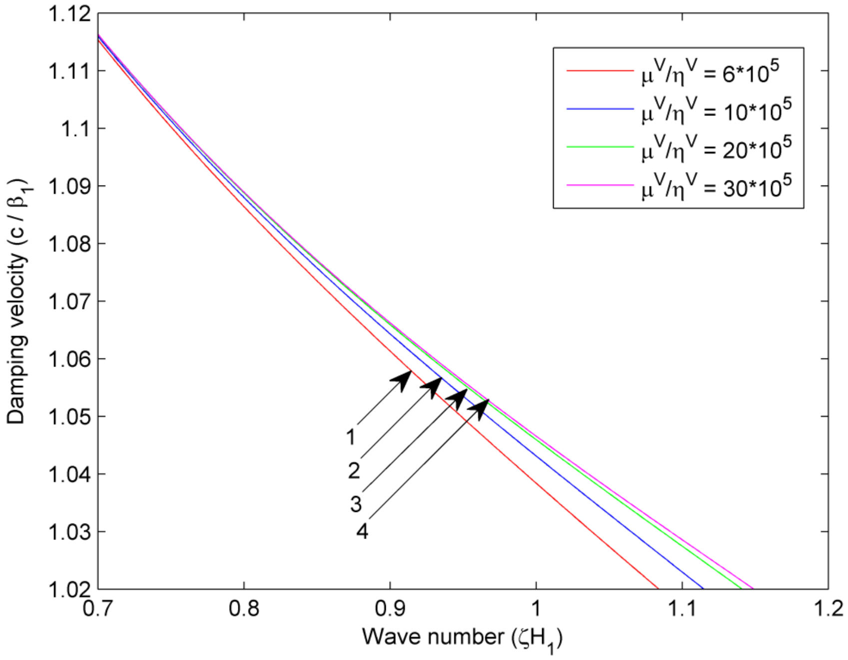

Figure 3.19(b) Plot for showing impacts of internal friction parameter (μ^V/η^V) in the absence of reinforced parameters

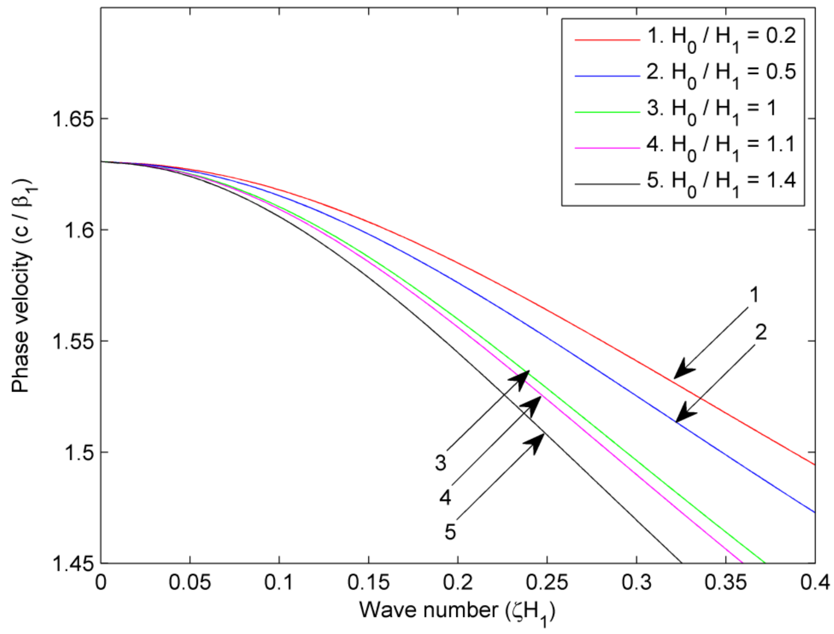

Figure 3.20(a) Plot for showing impacts of width ratio (H_0/H_1) in the presence of reinforced parameters

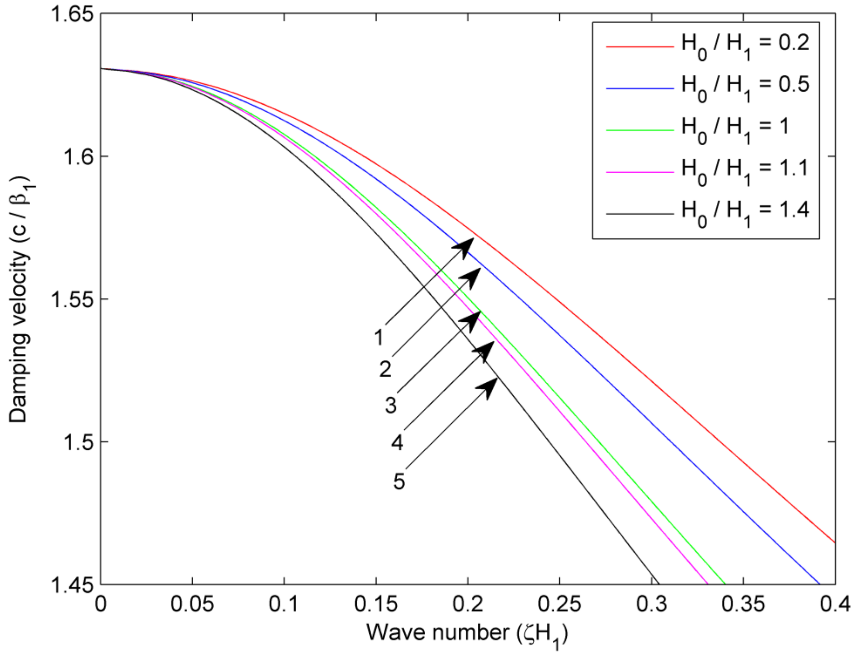

Figure 3.20(b) Plot for showing impacts of width ratio (H_0/H_1) in the presence of reinforced parameters

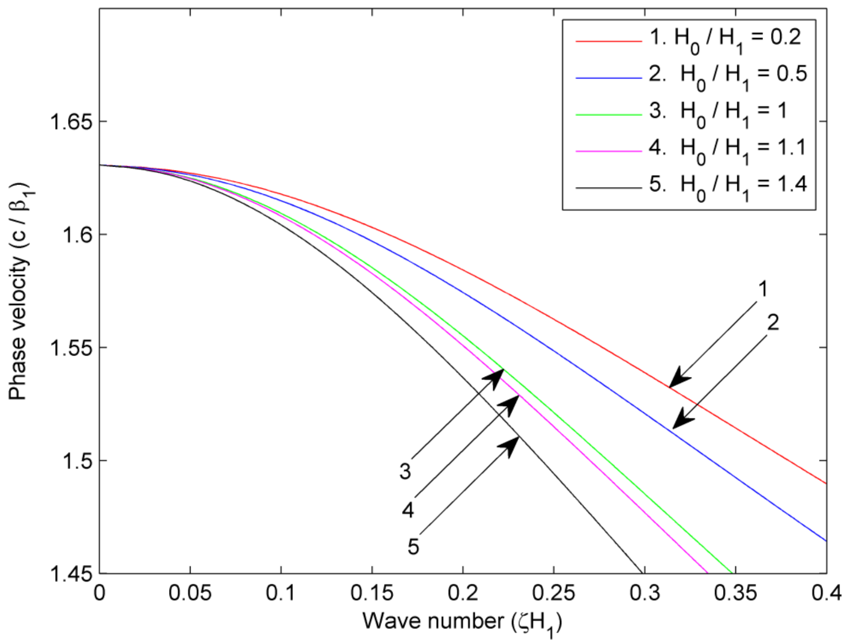

Figure 3.21(a) Plot for showing impacts of width ratio (H_0/H_1) in the absence of reinforced parameters

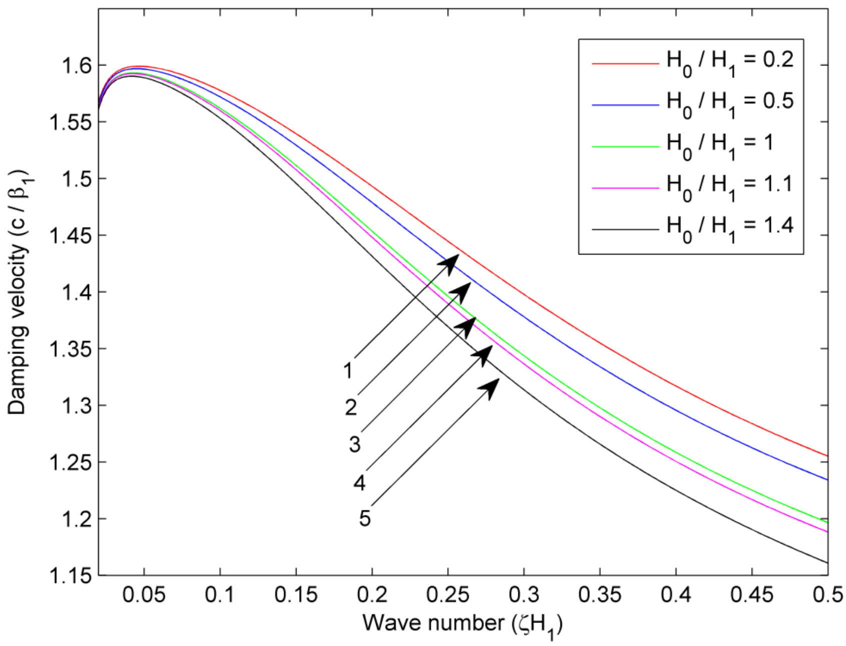

Figure 3.21(b) Plot for showing impacts of width ratio (H_0/H_1) in the absence of reinforced parameters

3.3.5 Conclusion

A systematic investigation is made for the study of Love waves propagation in a viscoelastic layer which is bounded between a fiber-reinforced layer and couple stress substrate which is depicted using consistent couple stress theory. The aim of this problem is to elucidate the effects of reinforced parameter, microstructural parameter known as characteristic length, width ratio of layers, internal friction parameter and heterogeneity parameter on behavior of Love waves. The major outcomes drawn from the study are mentioned below:

- Phase velocity and damping velocity of Love waves are decreasing with increasing value of wave number, which shows dispersive nature of these waves in the considered geometrical model of the problem.
- Fiber-reinforced parameters have shown significant impacts on phase velocity and damping velocity. Phase velocity and damping velocity are changing noticeably with the change in the values of these parameters.
- The microstructural parameter of substrate favors both velocities. As the value of microstructural parameter increases both velocities are increasing. This study is carried out with and without reinforcement parameters and similar results are found for both the cases.
- The impacts of heterogeneity parameter of viscoelastic layer are also depicted on phase and damping velocities and it is found that heterogeneity parameter hinder both velocities. These velocities decrease with the increase in heterogeneity. Results are similar with and without reinforcement parameters.
- Impacts of internal friction parameter of viscoelastic material are quite interesting, as phase velocity decreases, with increase in internal friction parameter, may it be with or without reinforcement parameters. The results of damping velocity are contrary to the results found for phase velocity and damping velocity increases with increase in value of internal friction parameter.

Hence, it shows that internal friction parameter favors damping velocity and works against phase velocity.

- Damping velocity and phase velocity are decreasing with increase in the value of width ratio of fiber-reinforced and viscoelastic layers.

The subject of seismology is developed within the framework of classical mechanics, but interior of the earth is quite heterogeneous, so it is desirable to study problems dealing with earth, using microcontinuum theories. The problem has been solved by keeping internal structure of the earth in mind and further, since the substratum taken in the geometry of the problem is mathematically governed by size-dependent microcontinuum mechanics called consistent couple stress theory, so the study can add something significant to the already known facts of Love waves by predicting their behavior in terms of a microstructural parameter called characteristic length. As Love waves are utilized in SAW devices, biosensors, and sensors, for various non-destructive testing techniques, so the findings can also be vital for these areas.

CHAPTER- 4

RAYLEIGH WAVES IN AN ELASTIC LAYER IMPERFECTLY ATTACHED TO A MICROSTRUCTURAL SUBSTRATE[3]

4.1 INTRODUCTION

The aim of this chapter is to analyse the behavior of Rayleigh waves in an isotropic elastic layer of finite thickness followed by a microcontinuum substrate exhibiting microstructural properties. The substrate is mathematically modeled using size-dependent couple stress theory. The layer is imperfectly attached to the substrate. Dispersion relation for propagation of Rayleigh waves is obtained by using appropriate boundary conditions. Dispersion relation is also obtained, when layer and substrate are in perfect contact with each other. As a special case, dispersion relation is calculated for consistent couple stress substrate under stress-free condition. The role of imperfectness parameters, thickness of the layer and microstructural parameter of the substrate are shown on dispersion behavior of Rayleigh waves. Many researchers have investigated the problems of Rayleigh waves propagation in various geometrical structures [15,51, 13, 100, 45]. The study of Rayleigh waves in layered model has various applications in many fields such as in non-destructive testing techniques for the detection of damages and flaws in materials, SAW devices and in geotechnical and geophysics engineering to explore the interior structure of the earth [27, 111, 72].

4.2 FORMULATION AND SOLUTION OF THE PROBLEM

It is considered that Rayleigh waves are propagating in an elastic layer which is imperfectly attached to a couple stress substrate (Fig. 4.1). The thickness of the layer is

[3]The contents of this chapter are accepted for publication in *Mechanics of Solids*, (Both SCI and Scopus indexed journal, Impact factor- 0.452, SJR- 0.283).

H, origin is considered at joining surface of two media. It is assumed that z-axis is going downward into the substrate and wave is propagating in the direction of x-axis. Displacement components of elastic layer are considered as $u = u(x, z, t)$, $v = 0$, $w = w(x, z, t)$ and displacement components for couple stress substrate are $u^C = u^C(x, z, t)$, $v^C = 0$, $w^C = w^C(x, z, t)$ and field variables are independent of y, so, $\frac{\partial}{\partial y} \equiv 0$.

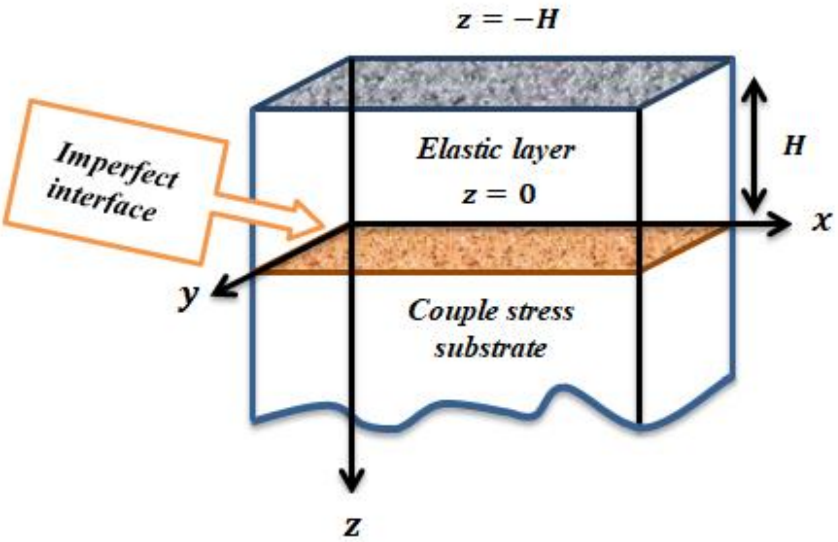

Figure 4.1 Geometrical configuration of the problem

4.2.1 Solution of an elastic layer

For the considered geometry, the equations of motion are [45]

$$\beta_1^2\left(\frac{\partial^2 u}{\partial x^2}+\frac{\partial^2 w}{\partial x \partial z}\right)+\beta_2^2\left(\frac{\partial^2 u}{\partial z^2}-\frac{\partial^2 w}{\partial x \partial z}\right)=\frac{\partial^2 u}{\partial t^2} \tag{4.1}$$

$$\beta_1^2\left(\frac{\partial^2 w}{\partial z^2}+\frac{\partial^2 u}{\partial x \partial z}\right)+\beta_2^2\left(\frac{\partial^2 w}{\partial x^2}-\frac{\partial^2 u}{\partial x \partial z}\right)=\frac{\partial^2 w}{\partial t^2} \tag{4.2}$$

where $\beta_1^2 = \frac{\lambda+2\mu}{\rho}$ and $\beta_2^2 = \frac{\mu}{\rho}$

To solve Eqs. (4.1) and (4.2), consider

$$\left.\begin{aligned} u &= \frac{\partial \phi_1}{\partial x} - \frac{\partial \psi_1}{\partial z} \\ w &= \frac{\partial \phi_1}{\partial z} + \frac{\partial \psi_1}{\partial x} \end{aligned}\right\} \tag{4.3}$$

where $\phi_1$is potential function of longitudinal waves and $\overrightarrow{\psi_1} = (0, \psi_1, 0)$ is potential function of shear waves.

Eqs. (4.1) and (4.2) by using Eq. (4.3) become

$$\nabla^2 \phi_1 = \frac{1}{\beta_1^2} \frac{\partial^2 \phi_1}{\partial t^2} \tag{4.4}$$

$$\nabla^2 \psi_1 = \frac{1}{\beta_2^2} \frac{\partial^2 \psi_1}{\partial t^2} \tag{4.5}$$

Assume the solutions of Eqs. (4.4) and (4.5) as

$$\phi_1 = g_1(z) e^{-i(\omega t - \zeta x)} \tag{4.6}$$

$$\psi_1 = g_2(z) e^{-i(\omega t - \zeta x)} \tag{4.7}$$

Eqs. (4.4) and (4.5) become

$$\frac{d^2 g_1(z)}{dz^2} + \left(\frac{\zeta^2 c^2}{\beta_1^2} - \zeta^2\right) g_1(z) = 0 \tag{4.8}$$

$$\frac{d^2 g_2(z)}{dz^2} + \left(\frac{\zeta^2 c^2}{\beta_2^2} - \zeta^2\right) g_2(z) = 0 \tag{4.9}$$

Eqs. (4.8) and (4.9) become

$$g_1(z) = A_1 \cos(d_1 z) + A_2 \sin(d_1 z) \tag{4.10}$$

$$g_2(z) = A_3 \cos(d_2 z) + A_4 \sin(d_2 z) \tag{4.11}$$

The value of potential functions become

$$\phi_1 = (A_1 \cos(d_1 z) + A_2 \sin(d_1 z)) e^{-i(\omega t - \zeta x)} \tag{4.12}$$

$$\psi_1 = (A_3 \cos(d_2 z) + A_4 \sin(d_2 z)) e^{-i(\omega t - \zeta x)} \tag{4.13}$$

Therefore, the displacement components of an elastic layer are

$$u = \begin{pmatrix} (i\zeta \cos(d_1 z))A_1 + (i\zeta \sin(d_1 z))A_2 + \\ (d_2 \sin(d_2 z))A_3 - (d_2 \cos(d_2 z))A_4 \end{pmatrix} e^{-i(\omega t - \zeta x)} \tag{4.14}$$

$$w = \begin{pmatrix} (-d_1 \sin(d_1 z))A_1 + (d_1 \cos(d_1 z))A_2 + \\ (i\zeta \cos(d_2 z))A_3 + (i\zeta \sin(d_2 z))A_4 \end{pmatrix} e^{-i(\omega t - \zeta x)} \tag{4.15}$$

A_1, A_2, A_3 and A_4 are arbitrary constants and $d_1 = \sqrt{\frac{\zeta^2 c^2}{\beta_1^2} - \zeta^2}$ and $d_2 = \sqrt{\frac{\zeta^2 c^2}{\beta_2^2} - \zeta^2}$

The non-vanishing stress components become

$$\tau_{31} = \mu \begin{Bmatrix} (-2i\zeta d_1 \sin(d_1 z))A_1 + (2i\zeta d_1 \cos(d_1 z))A_2 + \\ \left((d_2^2 - \zeta^2)\cos(d_2 z)\right)A_3 + ((d_2^2 - \zeta^2)\sin(d_2 z))A_4 \end{Bmatrix} e^{-i(\omega t - \zeta x)} \tag{4.16}$$

$$\tau_{33} = \begin{Bmatrix} (T_1 \cos(d_1 z))A_1 + (T_1 \sin(d_1 z))A_2 + \\ (-2i\mu\zeta d_2 \sin(d_2 z))A_3 + (2i\mu\zeta d_2 \cos(d_2 z))A_4 \end{Bmatrix} e^{-i(\omega t - \zeta x)} \tag{4.17}$$

where $T_1 = -(\lambda + 2\mu)d_1^2 - \lambda\zeta^2$

4.2.2 Solution of couple stress substrate

The equation of motion of consistent couple stress substrate mentioned in section (1.3) of chapter-1, becomes

$$\beta_3^2 \left(\frac{\partial^2 u^C}{\partial x^2} + \frac{\partial^2 w^C}{\partial x \partial z}\right) - \beta_4^2 (1 - l^2 \nabla^2) \left(\frac{\partial^2 w^C}{\partial x \partial z} - \frac{\partial^2 u^C}{\partial z^2}\right) = \frac{\partial^2 u^C}{\partial t^2} \tag{4.18}$$

$$\beta_3^2 \left(\frac{\partial^2 u^C}{\partial x \partial z} + \frac{\partial^2 w^C}{\partial z^2}\right) - \beta_4^2 (1 - l^2 \nabla^2) \left(\frac{\partial^2 u^C}{\partial x \partial z} - \frac{\partial^2 w^C}{\partial x^2}\right) = \frac{\partial^2 w^C}{\partial t^2} \tag{4.19}$$

where $\beta_3^2 = \frac{\lambda^C + 2\mu^C}{\rho^C}$ and $\beta_4^2 = \frac{\mu^C}{\rho^C}$

To solve Eqs. (4.18) and (4.19), consider

$$\left.\begin{aligned} u^C &= \frac{\partial \phi_2}{\partial x} - \frac{\partial \psi_2}{\partial z} \\ w^C &= \frac{\partial \phi_2}{\partial z} + \frac{\partial \psi_2}{\partial x} \end{aligned}\right\} \tag{4.20}$$

where ϕ_2 and $\overrightarrow{\psi_2} = (0, \psi_2, 0)$ are the potential functions.

Eqs. (4.18) and (4.19) by using Eq. (4.20) become

$$\nabla^2\phi_2 = \frac{1}{\beta_3^2}\frac{\partial^2\phi_2}{\partial t^2} \tag{4.21}$$

$$\nabla^2\psi_2(1-l^2\nabla^2) = \frac{1}{\beta_4^2}\frac{\partial^2\psi_2}{\partial t^2} \tag{4.22}$$

Assume solutions of Eqs. (4.21) and (4.22) as

$$\phi_2 = h_1(z)e^{-i(\omega t-\zeta x)} \tag{4.23}$$

$$\psi_2 = h_2(z)e^{-i(\omega t-\zeta x)} \tag{4.24}$$

Eqs. (4.21) and (4.22) become

$$\frac{d^2h_1(z)}{dz^2} - \left(\zeta^2 - \frac{\zeta^2c^2}{\beta_3^2}\right)h_1(z) = 0 \tag{4.25}$$

$$\frac{d^4h_2(z)}{dz^4} - \left(\frac{1}{l^2} + 2\zeta^2\right)\frac{d^2h_2(z)}{dz^2} + \left(\zeta^4 + \frac{\zeta^2}{l^2} - \frac{\zeta^2c^2}{l^2\beta_4^2}\right)h_2(z) = 0 \tag{4.26}$$

Eqs. (4.25) and (4.26) become

$$h_1(z) = B_1e^{-p_1z} + B_2e^{p_1z} \tag{4.27}$$

$$h_2(z) = D_1e^{-p_2z} + D_2e^{-p_3z} + D_3e^{p_2z} + D_4e^{p_3z} \tag{4.28}$$

The value of potential functions become

$$\phi_2 = (B_1e^{-p_1z})e^{-i(\omega t-\zeta x)} \tag{4.29}$$

$$\psi_2 = (D_1e^{-p_2z} + D_2e^{-p_3z})e^{-i(\omega t-\zeta x)} \tag{4.30}$$

Therefore, the displacement components of couple stress substrate are

$$u^C = \big((i\zeta e^{-p_1z})B_1 + (p_2e^{-p_2z})D_1 + (p_3e^{-p_3z})D_2\big)e^{-i(\omega t-\zeta x)} \tag{4.31}$$

$$w^C = \big((-p_1e^{-p_1z})B_1 + (i\zeta e^{-p_2z})D_1 + (i\zeta e^{-p_3z})D_2\big)e^{-i(\omega t-\zeta x)} \tag{4.32}$$

$p_1 = \sqrt{\zeta^2 - \frac{\zeta^2c^2}{\beta_3^2}}$, $p_2 = \sqrt{\frac{L_1+\sqrt{L_1^2-4L_2}}{2}}$, $p_3 = \sqrt{\frac{L_1-\sqrt{L_1^2-4L_2}}{2}}$, $L_1 = \frac{1}{l^2} + 2\zeta^2$,

$L_2 = \zeta^4 + \frac{\zeta^2}{l^2} - \frac{\zeta^2c^2}{l^2\beta_4^2}$ and B_1, D_1, D_2 are arbitrary constants.

The non-vanishing stress and couple stress components become

$$\tau_{31}^{C} = \mu^{C}\{(-2i\zeta p_1 e^{-p_1 z})B_1 + (T_2 e^{-p_2 z})D_1 + (T_3 e^{-p_3 z})D_2\}e^{-i(\omega t-\zeta x)} \tag{4.33}$$

$$\tau_{33}^{C} = \{(T_4 e^{-p_1 z})B_1 - (2i\mu^{C}\zeta p_2 e^{-p_2 z})D_1 - (2i\mu^{C}\zeta p_3 e^{-p_3 z})D_2\}e^{-i(\omega t-\zeta x)} \tag{4.34}$$

$$\mu_{32}^{C} = 2\mu^{C} l^2\{(p_2^3 - p_2\zeta^2)e^{-p_2 z}D_1 + (p_3^3 - p_3\zeta^2)e^{-p_3 z}D_2\}e^{-i(\omega t-\zeta x)} \tag{4.35}$$

where $T_2 = l^2(\zeta^2 - p_2^2)^2 - (\zeta^2 + p_2^2)$,

$T_3 = l^2(\zeta^2 - p_3^2)^2 - (\zeta^2 + p_3^2)$,

$T_4 = (\lambda^{C} + 2\mu^{C})p_1^2 - \lambda^{C}\zeta^2$

4.3 BOUNDARY CONDITIONS

(i) Top surface of layer must be stress free, so,

a. $\tau_{31} = 0$ at $z = -H$

b. $\tau_{33} = 0$ at $z = -H$

(ii) Stress components must be continuous at the interface between layer and substrate. Since, layer is assumed to be imperfectly attached to substrate, so, the difference in displacement components must be proportional to stress components.

a. $\tau_{31} = \tau_{31}^{C}$ at $z = 0$

b. $\tau_{33} = \tau_{33}^{C}$ at $z = 0$

c. $\tau_{31}^{C} = K_S(u - u^{C})$ at $z = 0$

d. $\tau_{33}^{C} = K_N(w - w^{C})$ at $z = 0$

K_S and K_N are degrees of imperfectness. If $K_S \to \infty$ and $K_N \to \infty$, displacement components will balance each other at $z = 0$ and it will refer to the case, when layer will be in perfect contact with the substrate. If $K_S = K_N = 0$, it refers to the slippage interface between two media.

(iii) The couple stress coefficient should vanish at interface, that is,

$\mu_{32}^{C} = 0$ at $z = 0$

4.4 DERIVATION OF SECULAR EQUATIONS

By imposing boundary conditions, we get following equations

$$2i\zeta d_1 \sin(d_1H)\, A_1 + 2i\zeta d_1 \cos(d_1H)\, A_2 + (\mathrm{d}_2^2 - \zeta^2)\cos(d_2H)\, A_3 - (\mathrm{d}_2^2 - \zeta^2)\sin(d_2H)\, A_4 = 0 \tag{4.36}$$

$$T_1 \cos(d_1H)\, A_1 - T_1 \sin(d_1H)\, A_2 + 2i\mu\zeta d_2 \sin(d_2H)\, A_3 + 2i\mu\zeta d_2 \cos(d_2H)\, A_4 = 0 \tag{4.37}$$

$$2i\mu\zeta d_1 A_2 + \mu(\mathrm{d}_2^2 - \zeta^2)A_3 + 2i\mu^C\zeta p_1 B_1 - \mu^C T_2 D_1 - \mu^C T_3 D_2 = 0 \tag{4.38}$$

$$T_1 A_1 + 2i\mu\zeta d_2 A_4 - T_4 B_1 + 2i\mu^C\zeta p_2 D_1 + 2i\mu^C\zeta p_3 D_2 = 0 \tag{4.39}$$

$$-i\zeta K_S A_1 + d_2 K_S A_4 + i\zeta(K_S - 2\mu^C p_1)B_1 + (p_2K_S + \mu^C T_2)D_1 + (p_3K_S + \mu^C T_3)D_2 = 0 \tag{4.40}$$

$$-d_1K_N A_2 - i\zeta K_N A_3 + (T_4 - p_1K_N)B_1 + i\zeta(K_N - 2\mu^C p_2)D_1 + i\zeta(K_N - 2\mu^C p_3)D_2 = 0 \tag{4.41}$$

$$(p_2^3 - p_2\zeta^2)D_1 + (p_3^3 - p_3\zeta^2)D_2 = 0 \tag{4.42}$$

To get non-trivial solutions of the Eqs. (4.36)-(4.42), determinant of arbitrary constants must be zero.

$$\begin{vmatrix} 2i\zeta d_1 \sin(d_1H) & 2i\zeta d_1 \cos(d_1H) & \emptyset_1 & -\emptyset_2 & 0 & 0 & 0 \\ T_1\cos(d_1H) & -T_1\sin(d_1H) & \emptyset_3 & \emptyset_4 & 0 & 0 & 0 \\ 0 & 2i\mu\zeta d_1 & \emptyset_5 & 0 & 2i\mu^C\zeta p_1 & -\mu^C T_2 & -\mu^C T_3 \\ T_1 & 0 & 0 & 2i\mu\zeta d_2 & -T_4 & 2i\mu^C\zeta p_2 & 2i\mu^C\zeta p_3 \\ -i\zeta K_S & 0 & 0 & d_2K_S & \emptyset_6 & \emptyset_7 & \emptyset_8 \\ 0 & -d_1K_N & -i\zeta K_N & 0 & T_4 - p_1K_N & \emptyset_9 & \emptyset_{10} \\ 0 & 0 & 0 & 0 & 0 & \varphi_1 & \varphi_2 \end{vmatrix} = 0 \tag{4.43}$$

where $\emptyset_1 = (\mathrm{d}_2^2 - \zeta^2)\cos(d_2H)$, $\emptyset_2 = (\mathrm{d}_2^2 - \zeta^2)\sin(d_2H)$, $\emptyset_3 = 2i\mu\zeta d_2 \sin(d_2H)$, $\emptyset_4 = 2i\mu\zeta d_2 \cos(d_2H)$, $\emptyset_5 = \mu(\mathrm{d}_2^2 - \zeta^2)$, $\emptyset_6 = i\zeta(K_S - 2\mu^C p_1)$, $\emptyset_7 = (p_2K_S + \mu^C T_2)$, $\emptyset_8 = (p_3K_S + \mu^C T_3)$, $\emptyset_9 = i\zeta(K_N - 2\mu^C p_2)$, $\emptyset_{10} = i\zeta(K_N - 2\mu^C p_3)$, $\varphi_1 = p_2^3 - p_2k^2$ and $\varphi_2 = p_3^3 - p_3k^2$.

After solving Eq. (4.43), we get following dispersion relation of Rayleigh waves in an elastic layer which is imperfectly attached to the couple stress substrate

$$t_1 + t_2 \cos(d_1 H)\, cos(d_2 H) + t_3 sin(d_1 H) sin(d_2 H) + t_4 cos(d_1 H) sin(d_2 H) + t_5 sin(d_1 H) cos(d_2 H) = 0 \tag{4.44}$$

where

$t_1 = 8\mu^2\zeta^2 d_1 d_2 T_1 (d_2^2 - \zeta^2)(\varphi_1 Q_1 - \varphi_2 R_1) + 2\mu\mu^C \zeta^2 d_1 d_2 T_1 K_N (3\zeta^2 - d_2^2)(-\varphi_1 Q_2 + \varphi_2 R_2) + 2\mu\zeta^2 d_1 d_2 K_S (d_2^2 - \zeta^2)(T_1 + 2\mu\zeta^2)(-\varphi_1 Q_3 + \varphi_2 R_3) + 2\mu^C \zeta^2 d_1 d_2 K_S K_N (\mu(d_2^2 - \zeta^2) - T_1)(-\varphi_1 Q_4 + \varphi_2 R_4)$,

$t_2 = 8\mu^2\zeta^2 d_1 d_2 T_1 (d_2^2 - \zeta^2)(-\varphi_1 Q_1 + \varphi_2 R_1) + 2\mu\mu^C \zeta^2 d_1 d_2 T_1 K_N (3\zeta^2 - d_2^2)(\varphi_1 Q_2 - \varphi_2 R_2) + 2\mu\zeta^2 d_1 d_2 K_S (d_2^2 - \zeta^2)(T_1 + 2\mu\zeta^2)(\varphi_1 Q_3 - \varphi_2 R_3) + \mu^C d_1 d_2 K_S K_N (4\mu\zeta^4 - T_1(d_2^2 - \zeta^2))(-\varphi_1 Q_4 + \varphi_2 R_4)$,

$t_3 = \big(\mu(T_1^2(d_2^2 - \zeta^2)^2 + 16\mu^2\zeta^4 d_1^2 d_2^2)\big)(-\varphi_1 Q_1 + \varphi_2 R_1) + \Big(\mu^C \zeta^2 K_N \big(8\mu^2\zeta^2 d_1^2 d_2^2 - T_1^2(d_2^2 - \zeta^2)\big)\Big)(-\varphi_1 Q_2 + \varphi_2 R_2) + \big(\mu\zeta^2 K_S (8\mu\zeta^2 d_1^2 d_2^2 + T_1(d_2^2 - \zeta^2)^2)\big)(\varphi_1 Q_3 - \varphi_2 R_3) + \mu^C \zeta^2 K_S K_N (T_1(d_2^2 - \zeta^2) - 4\mu d_1^2 d_2^2)(-\varphi_1 Q_4 + \varphi_2 R_4)$,

$t_4 = 4\mu d_1 d_2^2 \zeta^2 \mu^C K_S (T_1 - 2\mu\zeta^2)(-\varphi_1 Q_5 + \varphi_2 R_5) + \mu d_1 K_N T_1 (d_2^4 - \zeta^4)(\varphi_1 Q_6 - \varphi_2 R_6)$,

$t_5 = \mu^C d_2 K_S T_1 (d_2^2 - \zeta^2)(T_1 - 2\mu\zeta^2)(\varphi_1 Q_5 - \varphi_2 R_5) + 4\mu^2\zeta^2 d_1^2 d_2 K_N (d_2^2 + \zeta^2)(-\varphi_1 Q_6 + \varphi_2 R_6)$,

$Q_1 = \zeta^2 (K_S - 2\mu^C p_1)(K_N - 2\mu^C p_3) + (\mu^C T_3 + p_3 K_S)(T_4 - p_1 K_N)$,

$Q_2 = T_3 K_S + 2p_1 p_3 K_S$, $Q_3 = T_4 K_N - 2\mu^C p_1 p_3 K_N$, $Q_4 = T_3 T_4 + 4\mu^C \zeta^2 p_1 p_3$

$Q_5 = 2p_1\zeta^2 (K_N - 2\mu^C p_3) - T_3 (T_4 - p_1 K_N)$,

$Q_6 = T_4 (\mu^C T_3 + p_3 K_S) - 2\mu^C p_3 \zeta^2 (K_S - 2\mu^C p_1)$,

$R_1 = \zeta^2 (K_S - 2\mu^C p_1)(K_N - 2\mu^C p_2) + (\mu^C T_2 + p_2 K_S)(T_4 - p_1 K_N)$,

$R_2 = T_2 K_S + 2p_1 p_2 K_S$, $R_3 = T_4 K_N - 2\mu^C p_1 p_2 K_N$, $R_4 = T_2 T_4 + 4\mu^C \zeta^2 p_1 p_2$

$R_5 = 2p_1\zeta^2(K_N - 2\mu^C p_2) - T_2(T_4 - p_1K_N),$

$R_6 = T_4(\mu^C T_2 + p_2K_S) - 2\mu^C p_2\zeta^2(K_S - 2\mu^C p_1)$

4.5 PARTICULAR CASES

Case 1: If $H = 0$, then Eq. (4.44) reduces to

$$\left(2\zeta^2 - \left(\frac{\beta_3^2}{\beta_4^2}\right)(\zeta^2 - p_1^2)\right)(-\varphi_2T_2 + \varphi_1T_3) - 4p_1p_2p_3(p_3^2 - p_2^2)k^2 = 0 \tag{4.45}$$

Eq. (4.45) represents the dispersion relation of Rayleigh waves propagation in stress-free couple stress substrate which is same as found in Sharma and Kumar [100].

Case 2: If $K_S \to \infty$, then Eq. (4.44) reduces to

$$t_6 + t_7\cos(d_1H)\,cos(d_2H) + t_8(sin(d_1H)sin(d_2H)) + t_9(cos(d_1H)sin(d_2H)) + t_{10}(sin(d_1H)cos(d_2H)) = 0 \tag{4.46}$$

where

$t_6 = 8\mu\zeta^2d_1d_2T_1(d_2^2 - \zeta^2)(\varphi_1Q_1' - \varphi_2R_1') + 2\mu\mu^C\zeta^2d_1d_2T_1K_N(3\zeta^2 - d_2^2)(-\varphi_1Q_2' + \varphi_2R_2') + 2\mu\zeta^2d_1d_2(d_2^2 - \zeta^2)(T_1 + 2\mu\zeta^2)(-\varphi_1Q_3 + \varphi_2R_3) + 2\mu^C\zeta^2d_1d_2K_N(\mu(d_2^2 - \zeta^2) - T_1)(-\varphi_1Q_4 + \varphi_2R_4)$

$t_7 = 8\mu^2\zeta^2d_1d_2T_1(d_2^2 - \zeta^2)(-\varphi_1Q_1' + \varphi_2R_1') + 2\mu\mu^C\zeta^2d_1d_2T_1K_N(3\zeta^2 - d_2^2)(\varphi_1Q_2' - \varphi_2R_2') + 2\mu\zeta^2d_1d_2(d_2^2 - \zeta^2)(T_1 + 2\mu\zeta^2)(\varphi_1Q_3 - \varphi_2R_3) + \mu^Cd_1d_2K_N\left(4\mu k^4 - T_1(d_2^2 - \zeta^2)\right)(-\varphi_1Q_4 + \varphi_2R_4)$

$t_8 = \left(\mu(T_1^2(d_2^2 - \zeta^2)^2 + 16\mu^2\zeta^4d_1^2d_2^2)\right)(-\varphi_1Q_1' + \varphi_2R_1') + \left(\mu^C\zeta^2K_N\left(8\mu^2\zeta^2d_1^2d_2^2 - T_1^2(d_2^2 - \zeta^2)\right)\right)(-\varphi_1Q_2' + \varphi_2R_2') + \left(\mu\zeta^2(8\mu\zeta^2d_1^2d_2^2 + T_1(d_2^2 - \zeta^2)^2)\right)(\varphi_1Q_3 - \varphi_2R_3) + \mu^C\zeta^2K_N(T_1(d_2^2 - \zeta^2) - 4\mu d_1^2d_2^2)(-\varphi_1Q_4 + \varphi_2R_4)$

$t_9 = 4\mu d_1d_2^2\zeta^2\mu^C(T_1 - 2\mu\zeta^2)(-\varphi_1Q_5 + \varphi_2R_5) + \mu d_1K_NT_1(d_2^4 - \zeta^4)(\varphi_1Q_6' - \varphi_2R_6')$

$t_{10} = \mu^C d_2 T_1 (d_2^2 - \zeta^2)(T_1 - 2\mu\zeta^2)(\varphi_1 Q_5 - \varphi_2 R_5) + 4\mu^2\zeta^2 d_1^2 d_2 K_N (d_2^2 + \zeta^2)(-\varphi_1 Q_6' + \varphi_2 R_6')$

$Q_1' = \zeta^2(K_N - 2\mu^C p_3) + (p_3 T_4 - p_1 p_3 K_N)$, $Q_2' = T_3 + 2p_1 p_3$, $Q_6' = T_4 p_3 - 2\mu^C p_3 \zeta^2$

$R_1' = \zeta^2(K_N - 2\mu^C p_2) + (p_2 T_4 - p_1 p_2 K_N)$, $R_2' = T_2 + 2p_1 p_2$, $R_6' = T_4 p_2 - 2\mu^C p_2 \zeta^2$

Case 3: If $K_N \to \infty$, then Eq. (4.44) reduces to

$$t_{11} + t_{12}\cos(d_1 H)\,cos(d_2 H) + t_{13} sin(d_1 H) sin(d_2 H) + t_{14} cos(d_1 H) sin(d_2 H) + t_{15} sin(d_1 H) cos(d_2 H) = 0 \quad (4.47)$$

where

$t_{11} = 8\mu^2\zeta^2 d_1 d_2 T_1 (d_2^2 - \zeta^2)(\varphi_1 Q_1'' - \varphi_2 R_1'') + 2\mu\mu^C\zeta^2 d_1 d_2 T_1 (3\zeta^2 - d_2^2)(-\varphi_1 Q_2 + \varphi_2 R_2) + 2\mu\zeta^2 d_1 d_2 K_S (d_2^2 - \zeta^2)(T_1 + 2\mu\zeta^2)(-\varphi_1 Q_3'' + \varphi_2 R_3'') + 2\mu^C\zeta^2 d_1 d_2 K_S (\mu(d_2^2 - \zeta^2) - T_1)(-\varphi_1 Q_4 + \varphi_2 R_4)$

$t_{12} = 8\mu^2\zeta^2 d_1 d_2 T_1 (d_2^2 - \zeta^2)(-\varphi_1 Q_1'' + \varphi_2 R_1'') + 2\mu\mu^C\zeta^2 d_1 d_2 T_1 (3\zeta^2 - d_2^2)(\varphi_1 Q_2 - \varphi_2 R_2) + 2\mu\zeta^2 d_1 d_2 K_S (d_2^2 - k^2)(T_1 + 2\mu\zeta^2)(\varphi_1 Q_3'' - \varphi_2 R_3'') + \mu^C d_1 d_2 K_S (4\mu\zeta^4 - T_1(d_2^2 - \zeta^2))(-\varphi_1 Q_4 + \varphi_2 R_4)$

$t_{13} = \left(\mu(T_1^2(d_2^2 - \zeta^2)^2 + 16\mu^2\zeta^4 d_1^2 d_2^2)\right)(-\varphi_1 Q_1'' + \varphi_2 R_1'') + \left(\mu^C\zeta^2\left(8\mu^2\zeta^2 d_1^2 d_2^2 - T_1^2(d_2^2 - \zeta^2)\right)\right)(-\varphi_1 Q_2 + \varphi_2 R_2) + \left(\mu\zeta^2 K_S (8\mu\zeta^2 d_1^2 d_2^2 + T_1(d_2^2 - \zeta^2)^2)\right)(\varphi_1 Q_3'' - \varphi_2 R_3'') + \mu^C\zeta^2 K_S (T_1(d_2^2 - \zeta^2) - 4\mu d_1^2 d_2^2)(-\varphi_1 Q_4 + \varphi_2 R_4)$

$t_{14} = 4\mu d_1 d_2^2 \zeta^2 \mu^C p_1 K_S (T_1 - 2\mu\zeta^2)(-\varphi_1 Q_5'' + \varphi_2 R_5'') + \mu d_1 T_1 (d_2^4 - \zeta^4)(\varphi_1 Q_6 - \varphi_2 R_6)$

$t_{15} = \mu^C d_2 T_1 p_1 K_S (d_2^2 - \zeta^2)(T_1 - 2\mu\zeta^2)(\varphi_1 Q_5'' - \varphi_2 R_5'') + 4\mu^2\zeta^2 d_1^2 d_2 K_N (d_2^2 + \zeta^2)(-\varphi_1 Q_6 + \varphi_2 R_6)$

$Q_1'' = \zeta^2(K_S - 2\mu^C p_1) - (p_1\mu^C T_3 + p_1 p_3 K_S)$, $Q_3'' = T_4 - 2\mu^C p_1 p_3$, $Q_5'' = 2\zeta^2 + T_3$

$R_1'' = \zeta^2(K_S - 2\mu^C p_1) - (p_1\mu^C T_2 + p_1 p_2 K_S)$, $R_3'' = T_4 - 2\mu^C p_1 p_2$, $R_5'' = 2\zeta^2 + T_2$

Case 4: If $K_S \to \infty$, $K_N \to \infty$, then Eq. (4.44) reduces to

$t_{16} + t_{17}\cos(d_1H)\,cos(d_2H) + t_{18}sin(d_1H)sin(d_2H) + t_{19}cos(d_1H)sin(d_2H) + t_{20}sin(d_1H)cos(d_2H) = 0$ (4.48)

Eq. (4.48) represents frequency equation of Rayleigh waves in an elastic layer which is perfectly attached to the couple stress substrate.

where

$t_{16} = 8\mu^2\zeta^2 d_1 d_2 T_1(d_2^2 - \zeta^2)(\varphi_1 Q_1''' - \varphi_2 R_1''') + 2\mu\mu^C\zeta^2 d_1 d_2 T_1(3\zeta^2 - d_2^2)(-\varphi_1 Q_2' + \varphi_2 R_2') + 2\mu\zeta^2 d_1 d_2(d_2^2 - \zeta^2)(T_1 + 2\mu\zeta^2)(-\varphi_1 Q_3'' + \varphi_2 R_3'') + 2\mu^C\zeta^2 d_1 d_2(\mu(d_2^2 - \zeta^2) - T_1)(-\varphi_1 Q_4 + \varphi_2 R_4)$

$t_{17} = 8\mu^2\zeta^2 d_1 d_2 T_1(d_2^2 - \zeta^2)(-\varphi_1 Q_1''' + \varphi_2 R_1''') + 2\mu\mu^C\zeta^2 d_1 d_2 T_1(3\zeta^2 - d_2^2)(\varphi_1 Q_2' - \varphi_2 R_2') + 2\mu\zeta^2 d_1 d_2(d_2^2 - k^2)(T_1 + 2\mu\zeta^2)(\varphi_1 Q_3'' - \varphi_2 R_3'') + \mu^C d_1 d_2(4\mu\zeta^4 - T_1(d_2^2 - \zeta^2))(-\varphi_1 Q_4 + \varphi_2 R_4)$

$t_{18} = \left(\mu(T_1^2(d_2^2 - \zeta^2)^2 + 16\mu^2\zeta^4 d_1^2 d_2^2)\right)(-\varphi_1 Q_1''' + \varphi_2 R_1''') + \left(\mu^C\zeta^2\left(8\mu^2\zeta^2 d_1^2 d_2^2 - T_1^2(d_2^2 - \zeta^2)\right)\right)(-\varphi_1 Q_2' + \varphi_2 R_2') + \left(\mu\zeta^2(8\mu\zeta^2 d_1^2 d_2^2 + T_1(d_2^2 - \zeta^2)^2)\right)(\varphi_1 Q_3'' - \varphi_2 R_3'') + \mu^C\zeta^2(T_1(d_2^2 - \zeta^2) - 4\mu d_1^2 d_2^2)(-\varphi_1 Q_4 + \varphi_2 R_4)$

$t_{19} = 4\mu d_1 d_2^2\zeta^2\mu^C p_1(T_1 - 2\mu\zeta^2)(-\varphi_1 Q_5'' + \varphi_2 R_5'') + \mu d_1 T_1(d_2^4 - \zeta^4)(\varphi_1 Q_6''' - \varphi_2 R_6''')$

$t_{20} = \mu^C d_2 T_1 p_1(d_2^2 - \zeta^2)(T_1 - 2\mu\zeta^2)(\varphi_1 Q_5'' - \varphi_2 R_5'') + 4\mu^2\zeta^2 d_1^2 d_2(d_2^2 + \zeta^2)(-\varphi_1 Q_6''' + \varphi_2 R_6''')$

$Q_1''' = \zeta^2 - p_1 p_3$, $Q_6''' = T_4 p_3 - 2\mu^C p_3\zeta^2$, $R_1''' = \zeta^2 - p_1 p_2$, $R_6''' = T_4 p_2 - 2\mu^C p_2\zeta^2$

4.6 GRAPHICAL RESULTS AND DISCUSSION

The values of material constants for graphical illustrations are mentioned in Table 4.1.

Material Constants	Young's modulus	Poisson ratio	Density of material

Elastic layer [45]	$E = 78\ GPa$	$\nu = 0.44$	$\rho = 19{,}400\ kg/m^3$
Couple stress substrate [100]	$E^C = 14\ GPa$	$\nu^C = 0.37$	$\rho^C = 1500\ kg/m^3$

Table 4.1 Material parameters

Graphical illustrations showing the impacts of various parameters such as thickness of the layer, characteristic length associated with substrate, and imperfectness parameters on the dispersion curves, are presented in Figs. (4.2)-(4.8). In Figs. (4.2), (4.3), (4.4), (4.7) and (4.8), vertical axis represents dimensionless phase velocity (c/β_4) and horizontal axis represents non-dimensional wave number (ζH). In Figs. (4.5) and (4.6), vertical axis represents dimensionless phase velocity (c/β_4) and horizontal axis represents non-dimensional wave number (ζl).

Figure (4.2) represents general trend of dispersion curves for Rayleigh waves. The values of other parameters taken to plot Fig. (4.2) are kept as $l = 0.0004m$, $H = 0.001m$. For the case, when layer is imperfectly attached to substrate, the values of imperfectness parameters are kept as $K_S = K_N = 4 \times 10^{15}$. It is observed that Rayleigh waves are dispersive in the considered model, as Rayleigh waves speed is decreasing sharply with the increasing wave number. It is further found that Rayleigh waves speed is higher when layer and substrate are imperfectly attached to each other.

Parameters	l	H	K_S	K_N
Fig.4.3	$-$	0.001	∞	∞
Fig. 4.4	$-$	0.001	4×10^{15}	4×10^{15}
Fig. 4.5	0.0004	$-$	∞	∞
Fig. 4.6	0.0004	$-$	4×10^{15}	4×10^{15}
Fig. 4.7	0.0004	0.001	$-$	4×10^{15}
Fig. 4.8	0.0004	0.001	4×10^{15}	$-$

Table 4.2 Values of various parameters

4.6.1 The influence of microstructural parameter $(\boldsymbol{l})$

The impacts of internal microstructure length scale parameter (l) have been presented in Figs. (4.3) and (4.4). Figure (4.3) is plotted, when an elastic layer is perfectly attached to the substrate. Figure (4.4) is shown by taking layer to be imperfectly attached with the couple stress substrate. In both the figures, graphs are plotted by taking four values of microstructural parameter as $l = 0.0002m, 0.0004m, 0.0006m$ & $0.0008m$ andother parameters are given in Table 4.2. From both the figures, it can observe that phase velocity increases, when value of microstructural parameter increases.

4.6.2 The influence of thickness (H) of layer

Impacts of thickness (H) parameter are depicted in Figs. (4.5) and (4.6). Figure (4.5) elucidates the impacts, when an elastic layer is perfectly attached to the substrate, whereas in Fig. (4.6) layer is imperfectly attached to the microstructural substrate. Figs. (4.5) and (4.6) are plotted by taking four values of thickness parameter as $H = 0.001m, 0.002m, 0.003m$ & $0.004m$ and other parameters are mentioned in Table 4.2. From both the figures, it is found that velocity decreases, when value of thickness parameter increases.

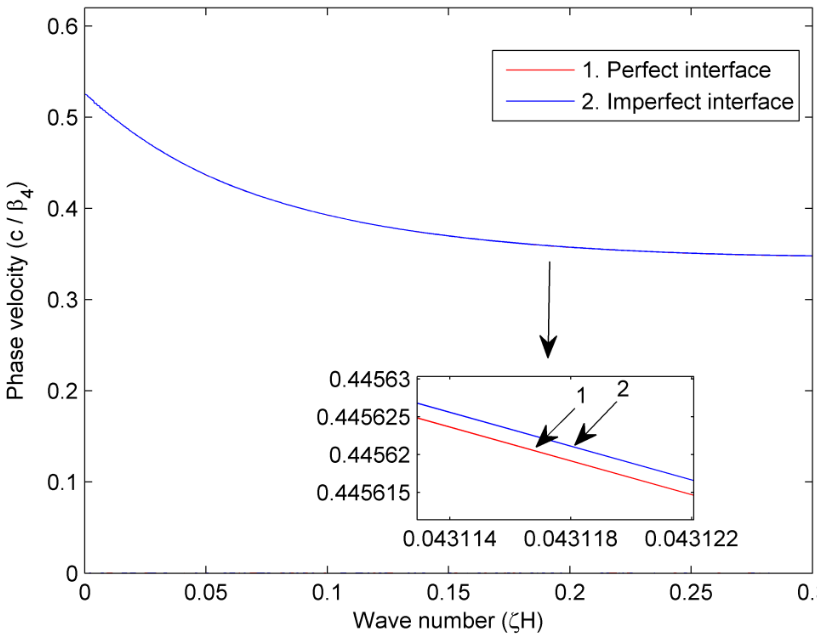

Figure 4.2 Dispersion curves for perfect and imperfect interfaces

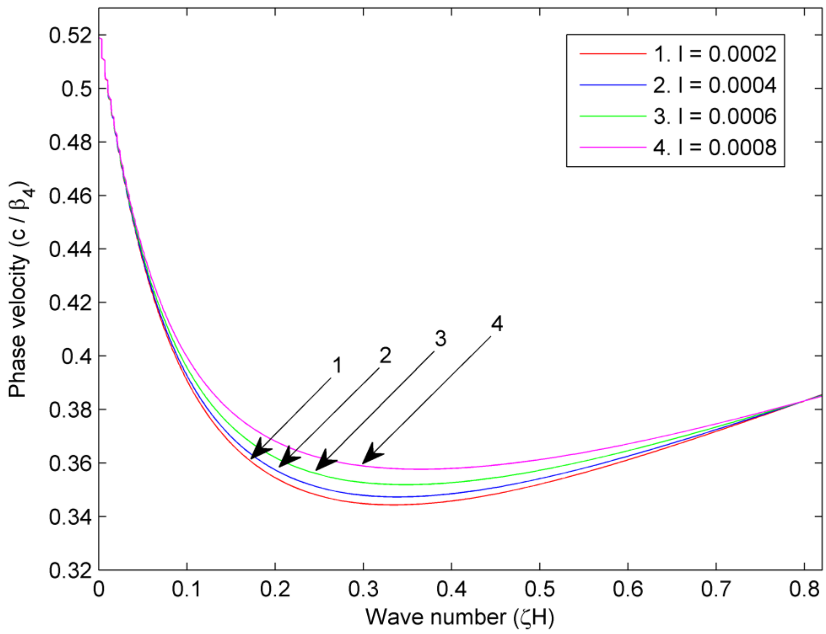

Figure 4.3 Plot for showing impacts of characteristic length (l) with perfect interface

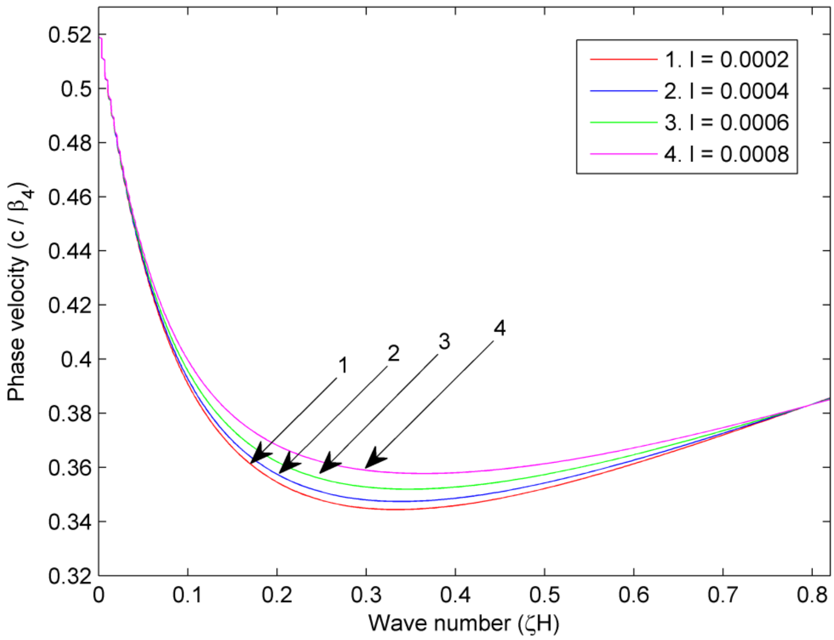

Figure 4.4 Plot for showing impacts of characteristic length (l) with imperfect interface

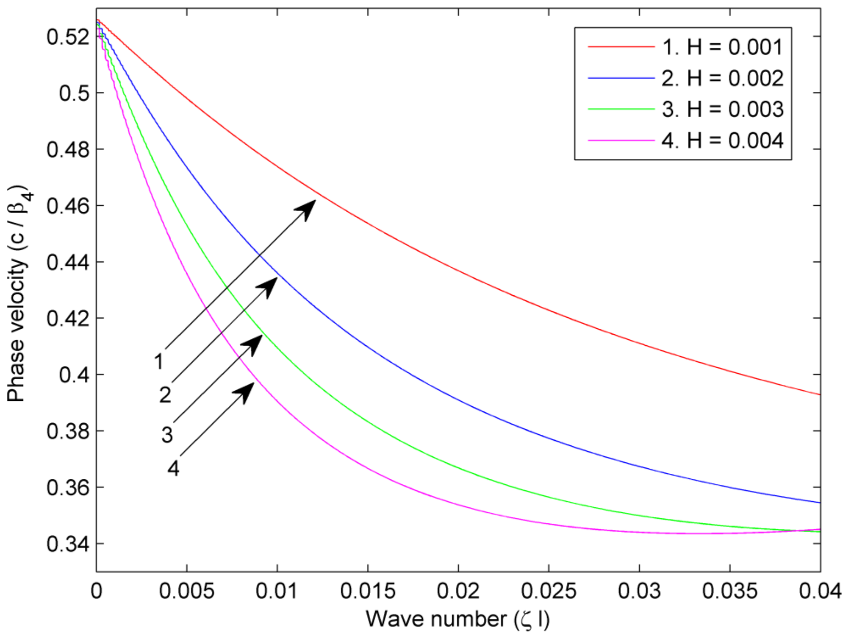

Figure 4.5 Plot for showing impacts of thickness parameter (H) with perfect interface

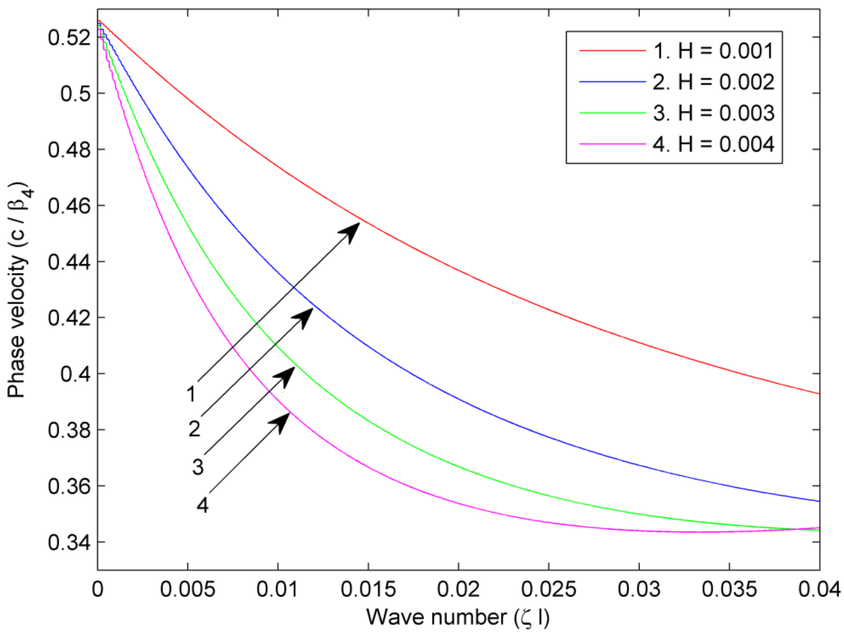

Figure 4.6 Plot for showing impacts of thickness parameter (H) with imperfect interface

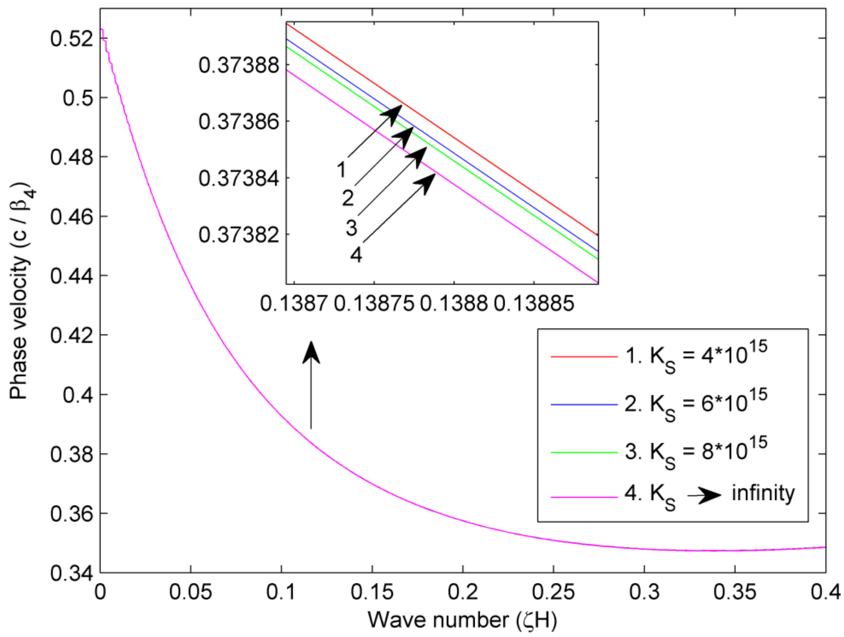

Figure 4.7 Plot for showing impacts of imperfectness parameter (K_S)

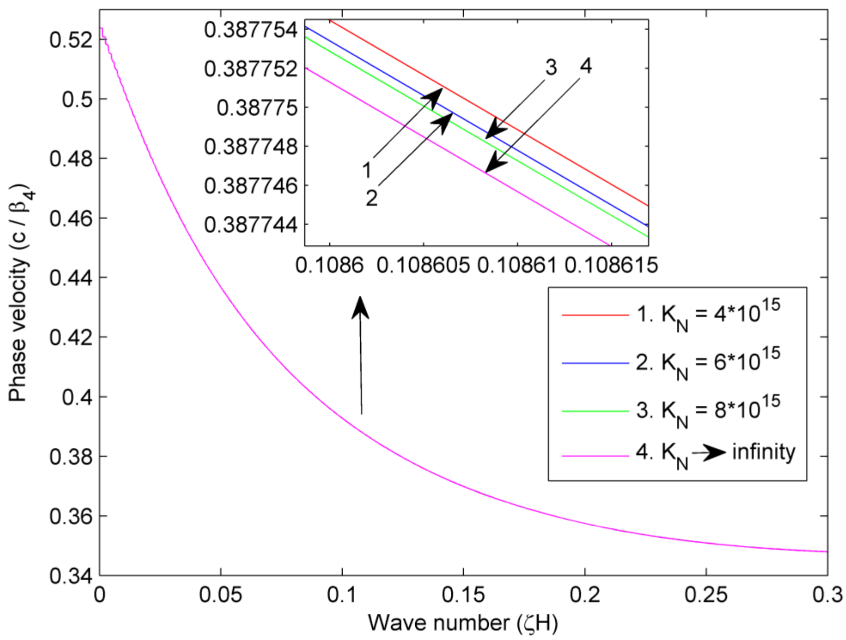

Figure 4.8 Plot for showing impacts of imperfectness parameter (K_N)

4.6.3 The influence of imperfectness parameters $(\boldsymbol{K_S}$ & $\boldsymbol{K_N})$

The impacts of degree of imperfectness of joining surface between two media are presented in Figs. (4.7) and (4.8) using parameters K_S and K_N. Figure (4.7) has been plotted by taking four values of imperfectness parameter K_S as $4 \times 10^{15}, 6 \times 10^{15}, 8 \times 10^{15}$ and $K_S \to \infty$ and other parameters are mentioned in Table 4.2. It is noticed in Fig. (4.7), when the value of parameter K_S increases, phase velocity decreases. In Fig. (4.8), the values of parameter K_N is considered as $4 \times 10^{15}, 6 \times 10^{15}, 8 \times 10^{15}$ and $K_N \to \infty$ and other parameters are mentioned in Table 4.2. The results obtained in Fig. (4.8) are similar as the results observed in Fig. (4.7).

4.7 CONCLUSION

This chapter analyse propagation behavior of Rayleigh waves in an elastic layer followed by a microstructural substrate. The contact between layer and substrate is assumed to be imperfect in nature. The frequency equation is obtained by using the appropriate boundary conditions. Outcomes found in the problem are given below.

- It is observed that Rayleigh waves are dispersive in nature as phase velocity decreases with increase in the value of wave number.
- Characteristic length parameter associated with substrate favors velocity of Rayleigh waves. The pattern is same whether layer and substrate are perfectly or imperfectly attached to each other.
- Impacts of thickness (H) of layer are presented on phase velocity. The velocity decreases with increase in the value of thickness parameter. Similar kind of results are obtained irrespective of the nature of bonding between two media.
- The imperfectness parameters K_S & K_N which measure the degree of imperfectness at joining surface between layer and half-space affects velocity. Phase velocity decreases with increase in the value of imperfectness parameters K_S and K_N .

As the problem is dealt using microcontinuum theory known as consistent couple stress theory, so it brings the role of size dependency in the problem, hence, the results found in the problem can amend some facts about Rayleigh waves which were established using classical elasticity. The outcomes of the study can also find applications in other fields such as seismology, NDT techniques, and geophysics etc.

CHAPTER- 5

SH-WAVES IN AN INHOMOGENEOUS FIBER-REINFORCED LAYER SANWICHED BETWEEN TWO MICROSTRUCTURAL SUBSTRATES[4]

5.1 INTRODUCTION

The problem is about the study of propagation of shear horizontal waves in a layer of finite thickness which is lying between two microstructural substrates. The substrates are modeled using consistent couple stress theory and the layer is assumed to be made of fiber-reinforced material. It is assumed that layer is imperfectly attached to both the substrates. Dispersion equations are obtained, when the layer is imperfectly/perfectly attached to both the substrates by using suitable boundary conditions. The impacts of characteristic lengths $(l_1$ & $l_3)$ associated with substrates, inhomogeneity parameter, reinforcement parameter, and imperfectness parameter are shown on phase velocity of SH-waves. Many researchers have studied propagation of shear horizontal waves in layered structures [84, 110, 118, 54, 94, 98, 43]. SH-waves have numerous applications in different areas such as healthcare [87, 61] and non-destructive testing techniques [30, 42].

5.2 FORMULATION AND SOLUTION OF THE PROBLEM

It is assumed that an inhomogeneous fiber-reinforced layer (M_2) of finite thickness H is sandwiched between two microstructural substrates (M_1 and M_3) as shown in Fig. (5.1). Both the substrates are mathematically modeled using consistent couple stress theory. It is assumed that three media are imperfectly attached to each other at the interfacial surfaces I_1 and I_2, origin (O) is considered at joining surface of M_1 and M_2. It is considered that y-axis is going vertically downward into the substrate (M_1) and

[4] Communicated to SCI indexed journal.

wave is propagating in the direction of x-axis. As per geometry, propagation of SH-waves is causing displacement in the direction of z-axis, so displacement components for $M_1(u^{C_1}, v^{C_1}, w^{C_1})$, $M_2(u^F, v^F, w^F)$ and $M_3(u^{C_3}, v^{C_3}, w^{C_3})$ are taken as $u^{C_1} = v^{C_1} = 0,\ w^{C_1} = w^{C_1}(x, y, t), u^F = v^F = 0, w^F = w^F(x, y, t)$ and $u^{C_3} = v^{C_3} = 0, w^{C_3} = w^{C_3}(x, y, t)$. All the field variables are assumed to be independent of z-coordinate, so, $\frac{\partial}{\partial z} \equiv 0$.

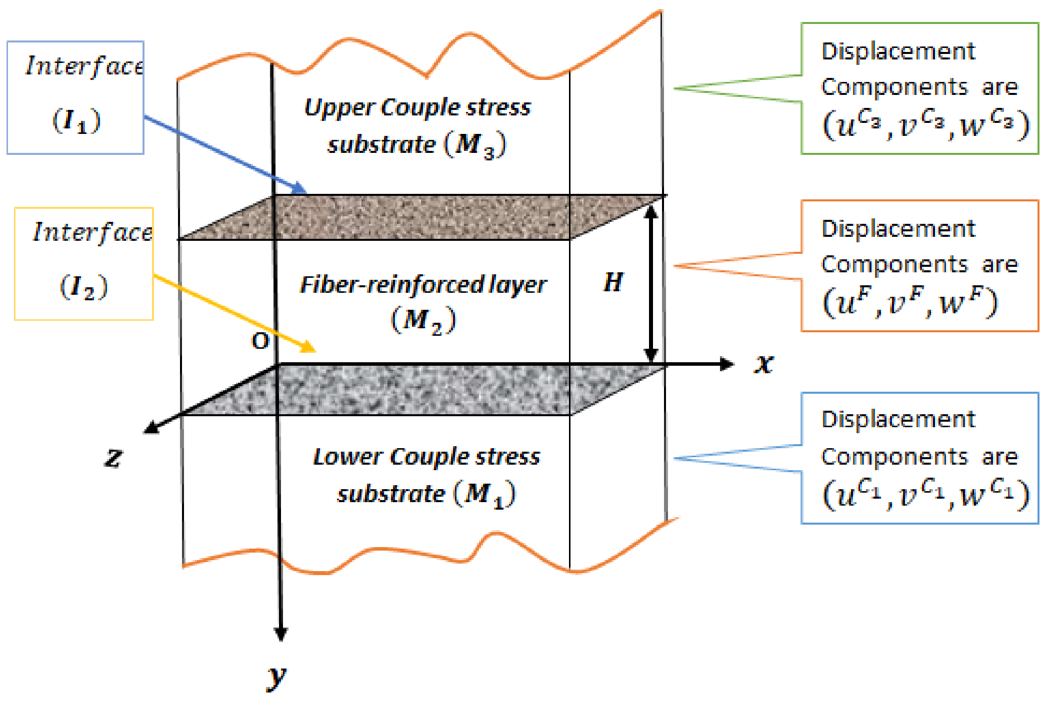

Figure 5.1 Geometrical configuration of the problem

5.2.1 Solution for the upper couple stress substrate

Equation of motion is given as [37]

$$(\lambda^{C_3} + \mu^{C_3} + \eta^{C_3}\nabla^2)\nabla(\nabla.\overrightarrow{w^{C_3}}) + (\mu^{C_3} - \eta^{C_3}\nabla^2)\nabla^2\overrightarrow{w^{C_3}} = \rho^{C_3}\frac{\partial^2\overrightarrow{w^{C_3}}}{\partial t^2} \tag{5.1}$$

The parameters λ^{C_3}, μ^{C_3}, ρ^{C_3}, η_3^C are discussed in section (1.3) of chapter 1 and $\overrightarrow{w^{C_3}} = (u^{C_3}, v^{C_3}, w^{C_3})$ is displacement vector.

Equation of motion in Eq. (5.1) reduces to

$$\left(\frac{\partial^2 w^{C_3}}{\partial x^2}+\frac{\partial^2 w^{C_3}}{\partial y^2}\right)-l_3^2\left(\frac{\partial^4 w^{C_3}}{\partial x^4}+\frac{\partial^4 w^{C_3}}{\partial y^4}+2\frac{\partial^4 w^{C_3}}{\partial x^2\partial y^2}\right)=\frac{1}{\beta_3^2}\frac{\partial^2 w^{C_3}}{\partial t^2} \tag{5.2}$$

where $\beta_3^2=\frac{\mu^{C_3}}{\rho^{C_3}}$

Assume the solution of Eq. (5.2) as

$$w^{C_3}(x,y,t)=F_3(y)e^{-i(\omega t-\zeta x)} \tag{5.3}$$

Eq. (5.2) becomes

$$\frac{d^4F_3}{dy^4}-L_1\frac{d^2F_3}{dy^2}+L_2F_3=0 \tag{5.4}$$

where $L_1=2\zeta^2+\frac{1}{l_3^2}$ and $L_2=\zeta^4+\frac{\zeta^2}{l_3^2}-\frac{\zeta^2c^2}{\beta_3^2 l_3^2}$

SH-waves are confined to the surface only, so, it is expected that amplitude of wave must vanish as they travel away from the surface. So, for upper substrate magnitude of wave must vanish as $y\to-\infty$. Hence, solution of Eq. (5.4) is

$$F_3(y)=A_3e^{p_3y}+B_3e^{q_3y} \tag{5.5}$$

where $p_3=\sqrt{\frac{L_1+\sqrt{L_1^2-4L_2}}{2}}$ and $q_3=\sqrt{\frac{L_1-\sqrt{L_1^2-4L_2}}{2}}$

Therefore, the displacement component of couple stress substrate (M_3) is

$$w^{C_3}(x,y,t)=(A_3e^{p_3y}+B_3e^{q_3y})e^{-i(\omega t-\zeta x)} \tag{5.6}$$

A_3 and B_3 are arbitrary constants.

The constitutive relations are [37]

$$\tau_{ji}^{C_3}=\lambda^{C_3}w_{k,k}^{C_3}\delta_{ij}+\mu^{C_3}\left(w_{i,j}^{C_3}+w_{j,i}^{C_3}\right)-\eta^{C_3}\nabla^2(w_{i,j}^{C_3}-w_{j,i}^{C_3}) \tag{5.7}$$

$$\mu_{ji}^{C_3}=4\eta^{C_3}(\omega_{i,j}-\omega_{j,i}) \tag{5.8}$$

where $\omega_i=\frac{1}{2}\epsilon_{ijk}w_{k,j}^{C_3}$ is a rotation vector. The parameters $\tau_{ji}^{C_3}$, $\mu_{ji}^{C_3}$ are discussed in section (1.3) of chapter 1.

The non-vanishing force stress and couple stress components become

$$\tau_{23}^{C_3} = \mu^{C_3}\begin{bmatrix} p_3(1 + l_3^2\zeta^2 - p_3^2 l_3^2)e^{p_3 y}A_3 + \\ q_3(1 + l_3^2\zeta^2 - q_3^2 l_3^2)e^{q_3 y}B_3 \end{bmatrix} e^{-i(\omega t - \zeta x)} \tag{5.9}$$

$$\mu_{21}^{C_3} = 2\mu^{C_3} l_3^2[(p_3^2 - \zeta^2)e^{p_3 y}A_3 + (q_3^2 - \zeta^2)e^{q_3 y}B_3]e^{-i(\omega t - \zeta x)} \tag{5.10}$$

5.2.2 Solution for intermediate inhomogeneous fiber-reinforced layer

Equation of motion is written as [48]

$$\frac{\partial \tau_{31}^F}{\partial x} + \frac{\partial \tau_{32}^F}{\partial y} + \frac{\partial \tau_{33}^F}{\partial z} = \rho^F \frac{\partial^2 w^F}{\partial t^2} \tag{5.11}$$

ρ^F is the density

The constitutive relation is given in section (1.4) of chapter 1. According to the geometry of the problem, direction of reinforcement may be considered as $(a_1, a_2, 0)$.

The non-vanishing stress components from constitutive equation are

$$\left.\begin{aligned} \tau_{31}^F &= \mu_T \frac{\partial w^F}{\partial x} + (\mu_L - \mu_T)\left(a_1^2 \frac{\partial w^F}{\partial x} + a_1 a_2 \frac{\partial w^F}{\partial y}\right) \\ \tau_{32}^F &= \mu_T \frac{\partial w^F}{\partial y} + (\mu_L - \mu_T)\left(a_1 a_2 \frac{\partial w^F}{\partial x} + a_2^2 \frac{\partial w^F}{\partial y}\right) \end{aligned}\right\} \tag{5.12}$$

The heterogeneity in fiber-reinforced layer is taken as

$$\mu_L = \mu_L' e^{\alpha y}, \mu_T = \mu_{\mathrm{T}}' e^{\alpha y}, \rho^F = \rho' e^{\alpha y} \tag{5.13}$$

where α is heterogeneity parameter having dimension of inverse of length, ρ' is fixed value of ρ^F, μ_L' is fixed value of μ_L and μ_T' is fixed value of μ_T.

By using Eqs. (5.12) and (5.13), Eq. (5.11) becomes

$$P\frac{\partial^2 w^F}{\partial x^2} + R\frac{\partial^2 w^F}{\partial y^2} + Q\frac{\partial^2 w^F}{\partial x \partial y} + S\frac{\partial w^F}{\partial x} + T\frac{\partial w^F}{\partial y} = \rho' \frac{\partial^2 w^F}{\partial t^2} \tag{5.14}$$

where $P = \mu_{\mathrm{T}}' + (\mu_L' - \mu_{\mathrm{T}}')a_1^2$, $R = \mu_{\mathrm{T}}' + (\mu_L' - \mu_{\mathrm{T}}')a_2^2$, $Q = 2(\mu_L' - \mu_{\mathrm{T}}')a_1 a_2$, $S = \alpha(\mu_L' - \mu_{\mathrm{T}}')a_1 a_2$ and $T = \alpha(\mu_{\mathrm{T}}' + (\mu_L' - \mu_{\mathrm{T}}')a_2^2)$

Assume solution of Eq. (5.14) as

$$w^F(x,y,t) = F_2(y)e^{-i(\omega t - \zeta x)} \tag{5.15}$$

Eq. (5.14) becomes

$$R\frac{d^2F_2}{dy^2} + (i\zeta Q + T)\frac{dF_2}{dy} + (i\zeta S + \rho'\zeta^2c^2 - \zeta^2P)F_2(y) = 0 \tag{5.16}$$

The solution of Eq. (5.16) is

$$F_2(y) = A_2e^{m_1y} + B_2e^{m_2y} \tag{5.17}$$

$m_1 = \frac{-T+i(r^{\frac{1}{2}}-\zeta Q)}{2R}$, $m_2 = \frac{-T+i(-r^{\frac{1}{2}}-\zeta Q)}{2R}$ and $r = \zeta^2Q^2 + 4\rho'\zeta^2c^2R - T^2 - 4\zeta^2PR$

Therefore, displacement component of fiber-reinforced layer (M_2) is

$$w^F(x,y,t) = (A_2e^{m_1y} + B_2e^{m_2y})e^{-i(\omega t - \zeta x)} \tag{5.18}$$

A_2 and B_2 are arbitrary constants.

The stress component becomes

$$\tau_{23}^F = \left[\left(-\frac{T}{2} + \frac{ir^{1/2}}{2}\right)e^{(\alpha+m_1)y}A_2 + \left(-\frac{T}{2} - \frac{ir^{1/2}}{2}\right)e^{(\alpha+m_2)y}B_2\right]e^{-i(\omega t - \zeta x)} \tag{5.19}$$

5.2.3 Solution for the lower couple stress substrate

Equation of motion is given as [37]

$$(\lambda^{C_1} + \mu^{C_1} + \eta^{C_1}\nabla^2)\nabla(\nabla.\overrightarrow{w^{C_1}}) + (\mu^{C_1} - \eta^{C_1}\nabla^2)\nabla^2\overrightarrow{w^{C_1}} = \rho^{C_1}\frac{\partial^2\overrightarrow{w^{C_1}}}{\partial t^2} \tag{5.20}$$

The parameters λ^{C_1}, μ^{C_1}, ρ^{C_1} and η^{C_1} are discussed in section (1.3) of chapter 1 and $\overrightarrow{w^{C_1}} = (u^{C_1}, v^{C_1}, w^{C_1})$ is displacement vector.

By imposing the conditions for SH-waves, the equation of motion in Eq. (5.20) reduces to

$$\left(\frac{\partial^2w^{C_1}}{\partial x^2} + \frac{\partial^2w^{C_1}}{\partial y^2}\right) - l_1^2\left(\frac{\partial^4w^{C_1}}{\partial x^4} + \frac{\partial^4w^{C_1}}{\partial y^4} + 2\frac{\partial^4w^{C_1}}{\partial x^2\partial y^2}\right) = \frac{1}{\beta_1^2}\frac{\partial^2w^{C_1}}{\partial t^2} \tag{5.21}$$

where $\beta_1^2 = \frac{\mu^{C_1}}{\rho^{C_1}}$

Assume the solution of Eq. (5.21) as

$$w^{C_1}(x,y,t) = F_1(y)e^{-i(\omega t - \zeta x)} \tag{5.22}$$

The solution of Eq. (5.21) by using Eq. (5.22) is

$$\frac{d^4F_1}{dy^4} - L_3\frac{d^2F_1}{dy^2} + L_4F_1 = 0 \tag{5.23}$$

where $L_3 = 2\zeta^2 + \frac{1}{l_1^2}$ and $L_4 = \zeta^4 + \frac{\zeta^2}{l_1^2} - \frac{\zeta^2 c^2}{\beta_1^2 l_1^2}$

Eq. (5.23) becomes

$$F_1(y) = A_1e^{-p_1y} + B_1e^{-q_1y} \tag{5.24}$$

where $p_1 = \sqrt{\frac{L_3+\sqrt{L_3^2-4L_4}}{2}}$ and $q_1 = \sqrt{\frac{L_3-\sqrt{L_3^2-4L_4}}{2}}$

Therefore, displacement component of couple stress substrate (M_1) is

$$w^{C_1}(x,y,t) = (A_1e^{-p_1y} + B_1e^{-q_1y})e^{-i(\omega t - \zeta x)} \tag{5.25}$$

A_1 and B_1 are arbitrary constants.

The constitutive equations are

$$\tau_{ji}^{C_1} = \lambda^{C_1}w_{k,k}^{C_1}\delta_{ij} + \mu^{C_1}\left(w_{i,j}^{C_1} + w_{j,i}^{C_1}\right) - \eta^{C_1}\nabla^2(w_{i,j}^{C_1} - w_{j,i}^{C_1}) \tag{5.26}$$

$$\mu_{ji}^{C_1} = 4\eta^{C_1}(\omega_{i,j} - \omega_{j,i}) \tag{5.27}$$

where $\omega_i = \frac{1}{2}\epsilon_{ijk}w_{k,j}^{C_1}$ is a rotation vector. The parameters $\tau_{ji}^{C_1}$ and $\mu_{ji}^{C_1}$ are discussed in section (1.3) of chapter 1.

The non-vanishing force stress and couple stress components become

$$\tau_{23}^{C_1} = \mu^{C_1}\begin{bmatrix} p_1(p_1^2l_1^2 - 1 - l_1^2\zeta^2)e^{-p_1y}A_1 + \\ q_1(q_1^2l_1^2 - 1 - l_1^2\zeta^2)e^{-q_1y}B_1 \end{bmatrix} e^{-i(\omega t - \zeta x)} \tag{5.28}$$

$$\mu_{21}^{C_1} = 2\mu^{C_1}l_1^2[(p_1^2 - \zeta^2)e^{-p_1y}A_1 + (q_1^2 - \zeta^2)e^{-q_1y}B_1]e^{-i(\omega t - \zeta x)} \tag{5.29}$$

5.3 BOUNDARY CONDITIONS

5.3.1 Boundary conditions for a perfect interface

Boundary conditions at the interface $(\boldsymbol{I_1}: \boldsymbol{y = -H})$:

(i) Upper substrate (M_3) and layer (M_2) are perfectly bonded to each other, so the stress and displacement components must be continuous, that is,

a. $\tau_{23}^{C_3} = \tau_{23}^{F}$ at $y = -H$

b. $w^{C_3}(x, y, t) = w^{F}(x, y, t)$ at $y = -H$

(ii) The couple stress coefficient of upper substrate (M_3) should vanish, that is, $\mu_{21}^{C_3} = 0$ at $y = -H$.

Boundary conditions at the interface $(\boldsymbol{I_2}: \boldsymbol{y = 0})$:

(i) Substrate (M_1) and layer (M_2) are perfectly bonded to each other, so the stress and displacement components must be continuous, that is,

a. $\tau_{23}^{F} = \tau_{23}^{C_1}$ at $y = 0$

b. $w^{F}(x, y, t) = w^{C_1}(x, y, t)$ at $y = 0$

(ii) The couple stress coefficient of lower substrate (M_1) should vanish, that is, $\mu_{21}^{C_1} = 0$ at $y = 0$.

5.3.2 Boundary conditions for an imperfect interface

Boundary conditions at the interface $(\boldsymbol{I_1}: \boldsymbol{y = -H})$:

(i) At interface $y = -H$, substrate (M_3) and layer (M_2) are imperfectly attached to each other, so stress components will be continuous and difference between displacement components of two media will be linearly proportional to the stress component, that is,

a. $\tau_{23}^{C_3} = \tau_{23}^{F}$ at $y = -H$

b. $\tau_{23}^{F} = G_1(w^{C_3} - w^{F})$ at $y = -H$, where G_1 measures degree of imperfectness at interface I_1.

(ii) The couple stress coefficient of substrate (M_3) should vanish, that is,

$\mu_{21}^{C_3} = 0$ at $y = -H$.

Boundary conditions at the interface $(\boldsymbol{I_2}: \boldsymbol{y = 0})$:

(i) The layer (M_2) and substrate (M_1) are imperfectly attached to each other, so stress components will be continuous at the interface $y = 0$ and difference between displacement components of two media will be linearly proportional to the stress component, that is,

a. $\tau_{23}^{F} = \tau_{23}^{C_1}$ at $y = 0$

b. $\tau_{23}^{F} = G_2(w^{C_1} - w^{F})$ at $y = 0$, where G_2 measures degree of imperfectness at interface I_2.

(ii) The couple stress coefficient of substrate (M_1) should vanish, that is,

$\mu_{21}^{C_1} = 0$ at $y = 0$.

5.4 DERIVATION OF SECULAR EQUATIONS

5.4.1 Derivation of secular equation with perfect interface

By using boundary conditions, we obtain following six equations as

$$t_1 e^{-p_3 H} A_3 + t_2 e^{-q_3 H} B_3 - \Omega_1 e^{-(\alpha+m_1)H} A_2 - \Omega_2 e^{-(\alpha+m_2)H} B_2 = 0 \tag{5.30}$$

$$e^{-p_3 H} A_3 + e^{-q_3 H} B_3 - e^{-m_1 H} A_2 - e^{-m_2 H} B_2 = 0 \tag{5.31}$$

$$(p_3^2 - \zeta^2) e^{-p_3 H} A_3 + (q_3^2 - \zeta^2) e^{-q_3 H} B_3 = 0 \tag{5.32}$$

$$\Omega_1 A_2 + \Omega_2 B_2 - t_3 A_1 - t_4 B_1 = 0 \tag{5.33}$$

$$A_2 + B_2 - A_1 - B_1 = 0 \tag{5.34}$$

$$(p_1^2 - \zeta^2) A_1 + (q_1^2 - \zeta^2) B_1 = 0 \tag{5.35}$$

For the non-trivial solution of Eqs. (5.30)-(5.35), determinant of the arbitrary coefficients should vanish.

$$\begin{vmatrix} t_1 e^{-p_3 H} & t_2 e^{-q_3 H} & -\varphi^* & -\varphi^{**} & 0 & 0 \\ e^{-p_3 H} & e^{-q_3 H} & -e^{-m_1 H} & -e^{-m_2 H} & 0 & 0 \\ \varphi_1 e^{-p_3 H} & \varphi_2 e^{-q_3 H} & 0 & 0 & 0 & 0 \\ 0 & 0 & \Omega_1 & \Omega_2 & -t_3 & -t_4 \\ 0 & 0 & 1 & 1 & -1 & -1 \\ 0 & 0 & 0 & 0 & \varphi_3 & \varphi_4 \end{vmatrix} = 0 \qquad (5.36)$$

where $\varphi_1 = (p_3^2 - \zeta^2)$, $\varphi_2 = (q_3^2 - \zeta^2)$, $\varphi_3 = (p_1^2 - \zeta^2)$, $\varphi_4 = (q_1^2 - \zeta^2)$,

$t_1 = \mu_3 p_3 + \mu_3 l_3^2 \zeta^2 p_3 - \mu_3 p_3^3 l_3^2$, $t_2 = \mu_3 q_3 + \mu_3 l_3^2 \zeta^2 q_3 - \mu_3 q_3^3 l_3^2$,

$t_3 = \mu_1 p_1^3 l_1^2 - \mu_1 l_1^2 \zeta^2 p_1 - \mu_1 p_1$, $t_4 = \mu_1 q_1^3 l_1^2 - \mu_1 l_1^2 \zeta^2 q_1 - \mu_1 q_1$,

$\varphi^* = \Omega_1 e^{-(\alpha+m_1)H}$, $\varphi^{**} = \Omega_2 e^{-(\alpha+m_2)H}$, $\Omega_1 = -\frac{T}{2} + \frac{ir^{1/2}}{2}$ and $\Omega_2 = -\frac{T}{2} - \frac{ir^{1/2}}{2}$

By expanding the determinant in Eq. (5.36), we get following equation of shear horizontal waves, when layer is perfectly attached to both the microstructural substrates.

$$\left[s_1 \sin\left(\frac{r^{1/2}H}{2R}\right) \sin\left(\frac{\zeta QH}{2R}\right) - s_2 \cos\left(\frac{r^{1/2}H}{2R}\right) \sin\left(\frac{\zeta QH}{2R}\right)\right] + i\left[s_1 \sin\left(\frac{r^{1/2}H}{2R}\right) \cos\left(\frac{\zeta QH}{2R}\right) - s_2 \cos\left(\frac{r^{1/2}H}{2R}\right) \cos\left(\frac{\zeta QH}{2R}\right)\right] = 0 \qquad (5.37)$$

From real part of Eq. (5.37), we get dispersion relation as

$$\sin\left(\frac{\zeta QH}{2R}\right)\left(s_1 \sin\left(\frac{r^{1/2}H}{2R}\right) - s_2 \cos\left(\frac{r^{1/2}H}{2R}\right)\right) = 0 \qquad (5.38)$$

and from imaginary part of Eq. (5.37), we get damping relation as

$$\cos\left(\frac{\zeta QH}{2R}\right)\left(s_1 \sin\left(\frac{r^{1/2}H}{2R}\right) - s_2 \cos\left(\frac{r^{1/2}H}{2R}\right)\right) = 0 \qquad (5.39)$$

where

$$s_1 = -N_1 N_2 - \frac{(T^2+r)e^{-\alpha H}(p_1^2-q_1^2)(p_3^2-q_3^2)}{4} + \frac{N_1 T e^{-\alpha H}(p_3^2-q_3^2)}{2} + \frac{N_2 T(p_1^2-q_1^2)}{2}$$

$$s_2 = \frac{r^{1/2}\left(N_2(p_1^2-q_1^2) - N_1 e^{-\alpha H}(p_3^2-q_3^2)\right)}{2},$$

$N_1 = t_3(q_1^2 - \zeta^2) - t_4(p_1^2 - \zeta^2)$,

$$N_2 = t_1(q_3^2 - \zeta^2) - t_2(p_3^2 - \zeta^2)$$

5.4.2 Derivation of secular equation with an imperfect interface

By imposing boundary conditions, we obtain following system of homogeneous linear equations

$$t_1 e^{-p_3 H} A_3 + t_2 e^{-q_3 H} B_3 - \Omega_1 e^{-(\alpha+m_1)H} A_2 - \Omega_2 e^{-(\alpha+m_2)H} B_2 = 0 \tag{5.40}$$

$$-G_1 e^{-p_3 H} A_3 - G_1 e^{-q_3 H} B_3 + \left(\Omega_1 e^{-(\alpha+m_1)H} + G_1 e^{-m_1 H}\right) A_2 + \left(\Omega_2 e^{-(\alpha+m_2)H} + G_1 e^{-m_2 H}\right) B_2 = 0 \tag{5.41}$$

$$(p_3^2 - \zeta^2) e^{-p_3 H} A_3 + (q_3^2 - \zeta^2) e^{-q_3 H} B_3 = 0 \tag{5.42}$$

$$\Omega_1 A_2 + \Omega_2 B_2 - t_3 A_1 - t_4 B_1 = 0 \tag{5.43}$$

$$(\Omega_1 + G_2) A_2 + (\Omega_2 + G_2) B_2 - G_2 A_1 - G_2 B_1 = 0 \tag{5.44}$$

$$(p_1^2 - \zeta^2) A_1 + (q_1^2 - \zeta^2) B_1 = 0 \tag{5.45}$$

For the non-trivial solution of Eqs. (5.40)-(5.45), determinant of arbitrary constants should vanish.

$$\begin{vmatrix} t_1 e^{-p_3 H} & t_2 e^{-q_3 H} & -\varphi^* & -\varphi^{**} & 0 & 0 \\ -G_1 e^{-p_3 H} & -G_1 e^{-q_3 H} & \varphi^* + G_1 e^{-m_1 H} & \varphi^{**} + G_1 e^{-m_2 H} & 0 & 0 \\ \varphi_1 e^{-p_3 H} & \varphi_2 e^{-q_3 H} & 0 & 0 & 0 & 0 \\ 0 & 0 & \Omega_1 & \Omega_2 & -t_3 & -t_4 \\ 0 & 0 & \Omega_1 + G_2 & \Omega_2 + G_2 & -G_2 & -G_2 \\ 0 & 0 & 0 & 0 & \varphi_3 & \varphi_4 \end{vmatrix} = 0 \tag{5.46}$$

By solving Eq. (5.46), we get following equation of shear horizontal waves in a fiber-reinforced layer which is not in perfect contact with both the microstructural substrates.

$$\left[n_1 \sin\left(\frac{r^{1/2} H}{2R}\right) \sin\left(\frac{\zeta Q H}{2R}\right) - n_2 \cos\left(\frac{r^{1/2} H}{2R}\right) \sin\left(\frac{\zeta Q H}{2R}\right)\right] + i\left[n_1 \sin\left(\frac{r^{1/2} H}{2R}\right) \cos\left(\frac{\zeta Q H}{2R}\right) - n_2 \cos\left(\frac{r^{1/2} H}{2R}\right) \cos\left(\frac{\zeta Q H}{2R}\right)\right] = 0 \tag{5.47}$$

From real part of Eq. (5.47), we get dispersion relation as

$$\sin\left(\frac{\zeta Q H}{2R}\right)\left(n_1 \sin\left(\frac{r^{1/2} H}{2R}\right) - n_2 \cos\left(\frac{r^{1/2} H}{2R}\right)\right) = 0 \tag{5.48}$$

and from imaginary part of Eq. (5.47), we get damping relation as

$$\cos\left(\frac{\zeta QH}{2R}\right)\left(n_1 \sin\left(\frac{r^{1/2}H}{2R}\right) - n_2 \cos\left(\frac{r^{1/2}H}{2R}\right)\right) = 0 \tag{5.49}$$

where

$$n_1 = \frac{(T^2+r)e^{-\alpha H}(T_{11}-T_{22})}{4} + G_1G_2N_1N_2 - \frac{G_1G_2N_2T(p_1^2-q_1^2)}{2} - \frac{G_1G_2N_1Te^{-\alpha H}(p_3^2-q_3^2)}{2} - \frac{G_1N_1N_2T}{2} - \frac{G_2N_1N_2e^{-\alpha H}T}{2},$$

$$n_2 = r^{1/2}\left[-\frac{G_1G_2N_2(p_1^2-q_1^2)}{2} + \frac{G_1G_2N_1e^{-\alpha H}(p_3^2-q_3^2)}{2} - \frac{G_1N_1N_2}{2} + \frac{G_2N_1N_2e^{-\alpha H}}{2}\right],$$

$$T_{11} = G_2N_2(p_1^2 - q_1^2) + G_1N_1(p_3^2 - q_3^2),$$

$$T_{22} = -G_1G_2(p_1^2 - q_1^2)(p_3^2 - q_3^2) - N_1N_2$$

5.5 PARTICULAR CASES

5.5.1 Particular cases for perfect interface

Case 1: When reinforcement parameters of the fiber-reinforced layers are neglected, that is, $a_1 = a_2 = 0$, then we get following dispersion equation

$$\tan\left(\frac{\zeta r_1^{1/2}H}{2\mu'}\right) = \frac{\zeta r_1^{1/2}s_4}{s_3} \tag{5.50}$$

Eq. (5.50) represents dispersion relation of shear horizontal waves in a heterogeneous layer sandwiched between two microstructural substrates. Eq. (5.50) can also get from Eq. (5.38), if we take second term, that is, $s_1 \sin\left(\frac{r^{1/2}H}{2R}\right) - s_2 \cos\left(\frac{r^{1/2}H}{2R}\right) = 0$.

where

$$\mu' = \mu_T',\ r_1 = \mu'\left(4\rho' c^2 - \frac{\alpha^2\mu'}{\zeta^2} - 4\mu'\right),$$

$$s_3 = -N_1N_2 - \frac{((\alpha\mu')^2+\zeta^2 r_1)e^{-\alpha H}(p_1^2-q_1^2)(p_3^2-q_3^2)}{4} + \frac{\alpha\mu' N_1e^{-\alpha H}(p_3^2-q_3^2)}{2} + \frac{\alpha\mu' N_2(p_1^2-q_1^2)}{2},$$

$$s_4 = \frac{N_2(p_1^2-q_1^2)-N_1e^{-\alpha H}(p_3^2-q_3^2)}{2}$$

Case 2: If the heterogeneity parameter, $\alpha = 0$, then dispersion relation in Eq. (5.38) reduces to

$$\sin\left(\frac{\zeta QH}{2R}\right)\left(s_5 \sin\left(\frac{\zeta r_2^{1/2} H}{2R}\right) - s_6 \cos\left(\frac{\zeta r_2^{1/2} H}{2R}\right)\right) = 0 \tag{5.51}$$

Eq. (5.51) represents dispersion relation of shear horizontal waves in a fiber-reinforced layer without heterogeneity

and damping relation in Eq. (5.39) reduces to

$$\cos\left(\frac{\zeta QH}{2R}\right)\left(s_5 \sin\left(\frac{\zeta r_2^{1/2} H}{2R}\right) - s_6 \cos\left(\frac{\zeta r_2^{1/2} H}{2R}\right)\right) = 0 \tag{5.52}$$

Eq. (5.52) represents damping relation of shear horizontal waves in a fiber-reinforced layer without heterogeneity

where

$$r_2 = Q^2 + 4\rho' c^2 R - 4PR$$

$$s_5 = -N_1 N_2 - \frac{\zeta^2 r_2 (p_1^2 - q_1^2)(p_3^2 - q_3^2)}{4}$$

$$s_6 = \zeta r_2^{1/2} \left(\frac{N_2 (p_1^2 - q_1^2) - N_1 (p_3^2 - q_3^2)}{2}\right)$$

Case 3: When the heterogeneity and reinforcement parameters of the intermediate layer are both neglected, that is, $\alpha = 0$, $\mu_L' = \mu_{\mathrm{T}}' = \mu'$ and $a_1 = a_2 = 0$, then dispersion relation in Eq. (5.38) reduces to

$$tan\left(\zeta H \sqrt{\frac{c^2}{\beta_2^2} - 1}\right) = \frac{s_8 \mu' \zeta}{s_7} \sqrt{\frac{c^2}{\beta_2^2} - 1} \tag{5.53}$$

Eq. (5.53) represents dispersion equation of shear horizontal waves in a homogeneous isotropic layer sandwiched between two substrates.

where

$$\beta_2 = \sqrt{\frac{\mu'}{\rho'}},\ s_7 = -N_1 N_2 - \frac{\zeta^2 r_3 (p_1^2 - q_1^2)(p_3^2 - q_3^2)}{4},$$

$r_3 = 4\rho'\mu'c^2 - 4(\mu')^2$,

$s_8 = N_2(p_1^2 - q_1^2) - N_1(p_3^2 - q_3^2)$

5.5.2 Particular cases for an imperfect interface

Case 1: When reinforcement parameters of the fiber-reinforced layers are neglected, that is, $a_1 = a_2 = 0$, then we get following dispersion equation

$$\tan\left(\frac{\zeta r_1^{1/2} H}{2\mu'}\right) = \frac{\zeta r_1^{1/2} n_4}{n_3} \tag{5.54}$$

Eq. (5.54) represents dispersion equation of shear horizontal waves in a heterogeneous layer sandwiched between two microstructural substrates. Eq. (5.54) can also get from Eq. (5.48), if we take second term, that is, $n_1 \sin\left(\frac{r^{1/2}H}{2R}\right) - n_2 \cos\left(\frac{r^{\frac{1}{2}}H}{2R}\right) = 0.$

where

$\mu' = \mu'_T$

$n_3 = \frac{((\alpha\mu')^2 + \zeta^2 r_1)e^{-\alpha H}(T_{11} - T_{22})}{4} + G_1G_2N_1N_2 - \frac{\alpha\mu' G_1G_2N_2(p_1^2 - q_1^2)}{2} - \frac{G_1G_2N_1\alpha\mu' e^{-\alpha H}(p_3^2 - q_3^2)}{2} - \frac{\alpha\mu' G_1N_1N_2}{2} - \frac{\alpha\mu' G_2N_1N_2e^{-\alpha H}}{2}$,

$n_4 = -\frac{G_1G_2N_2(p_1^2 - q_1^2)}{2} + \frac{G_1G_2N_1e^{-\alpha H}(p_3^2 - q_3^2)}{2} - \frac{G_1N_1N_2}{2} + \frac{G_2N_1N_2e^{-\alpha H}}{2}$

Case 2: If the heterogeneity parameter, $\alpha = 0$, then dispersion relation in Eq. (5.48) reduces to

$$\sin\left(\frac{\zeta QH}{2R}\right)\left(n_5 \sin\left(\frac{\zeta r_2^{1/2} H}{2R}\right) - n_6 \cos\left(\frac{\zeta r_2^{1/2} H}{2R}\right)\right) = 0 \tag{5.55}$$

Eq. (5.55) represents dispersion relation of shear horizontal waves in a fiber-reinforced layer without heterogeneity

and damping relation in Eq. (5.49) reduces to

$$\cos\left(\frac{\zeta QH}{2R}\right)\left(n_5 \sin\left(\frac{\zeta r_2^{1/2} H}{2R}\right) - n_6 \cos\left(\frac{\zeta r_2^{1/2} H}{2R}\right)\right) = 0 \tag{5.56}$$

Eq. (5.56) represents damping relation of shear horizontal waves in a fiber-reinforced layer without heterogeneity which is imperfectly attached to both the substrates.

where

$$n_5 = \frac{\zeta^2 r_2 (T_{11} - T_{22})}{4} + G_1 G_2 N_1 N_2 ,$$

$$n_6 = \zeta r_2^{1/2}\left[-\frac{G_1 G_2 N_2 (p_1^2 - q_1^2)}{2} + \frac{G_1 G_2 N_1 (p_3^2 - q_3^2)}{2} - \frac{G_1 N_1 N_2}{2} + \frac{G_2 N_1 N_2}{2}\right]$$

Case 3: When the heterogeneity and reinforcement parameters of fiber-reinforced layer are neglected, that is, $\alpha = 0$, $\mu'_L = \mu'_T = \mu'$ and $a_1 = a_2 = 0$, then dispersion equation in Eq. (5.48) reduces to

$$tan\left(\zeta H \sqrt{\frac{c^2}{\beta_2^2} - 1}\right) = \frac{n_8 \mu' \zeta}{n_7} \sqrt{\frac{c^2}{\beta_2^2} - 1} \tag{5.57}$$

Eq. (5.57) represents dispersion relation of shear horizontal waves in a homogeneous isotropic layer which is imperfectly attached with the substrates.

where

$$n_7 = \frac{\zeta^2 r_3 (T_{11} - T_{22})}{4} + G_1 G_2 N_1 N_2 ,$$

$$n_8 = -\frac{G_1 G_2 N_2 (p_1^2 - q_1^2)}{2} + \frac{G_1 G_2 N_1 (p_3^2 - q_3^2)}{2} - \frac{G_1 N_1 N_2}{2} + \frac{G_2 N_1 N_2}{2}$$

Case 4: If $G_1 \to \infty$, then upper substrate (M_3) and the layer (M_2) will be perfectly attached to each other and dispersion equation in Eq. (5.48) reduces to

$$\sin\left(\frac{\zeta QH}{2R}\right)\left(n_9 \sin\left(\frac{r^{1/2} H}{2R}\right) - n_{10} \cos\left(\frac{r^{1/2} H}{2R}\right)\right) = 0 \tag{5.58}$$

and damping equation in Eq. (5.49) reduces to

$$\cos\left(\frac{\zeta QH}{2R}\right)\left(n_9 \sin\left(\frac{r^{1/2} H}{2R}\right) - n_{10} \cos\left(\frac{r^{1/2} H}{2R}\right)\right) = 0 \tag{5.59}$$

where

$$n_9 = \frac{(T^2+r)e^{-\alpha H}}{4}\left((p_3^2 - q_3^2)N_1 + G_2(p_1^2 - q_1^2)(p_3^2 - q_3^2)\right) + G_2N_1N_2 - \frac{G_2N_2T(p_1^2-q_1^2)}{2} - \frac{G_2N_1Te^{-\alpha H}(p_3^2-q_3^2)}{2} - \frac{N_1N_2T}{2},$$

$$n_{10} = r^{1/2}\left[-\frac{G_2N_2(p_1^2-q_1^2)}{2} + \frac{G_2N_1e^{-\alpha H}(p_3^2-q_3^2)}{2} - \frac{N_1N_2}{2}\right]$$

Case 5: When $G_1 \to \infty$ and $\alpha = 0$, dispersion relation in Eq. (5.48) reduces to

$$\sin\left(\frac{\zeta QH}{2R}\right)\left(n_{11}\sin\left(\frac{\zeta r_2^{1/2}H}{2R}\right) - n_{12}\cos\left(\frac{\zeta r_2^{1/2}H}{2R}\right)\right) = 0 \tag{5.60}$$

and damping equation in Eq. (5.49) reduces to

$$\cos\left(\frac{\zeta QH}{2R}\right)\left(n_{11}\sin\left(\frac{\zeta r_2^{1/2}H}{2R}\right) - n_{12}\cos\left(\frac{\zeta r_2^{1/2}H}{2R}\right)\right) = 0 \tag{5.61}$$

where

$$n_{11} = \frac{\zeta^2 r_2}{4}\left((p_3^2 - q_3^2)N_1 + G_2(p_1^2 - q_1^2)(p_3^2 - q_3^2)\right) + G_2N_1N_2,$$

$$n_{12} = \zeta r_2^{1/2}\left[-\frac{G_2N_2(p_1^2-q_1^2)}{2} + \frac{G_2N_1(p_3^2-q_3^2)}{2} - \frac{N_1N_2}{2}\right]$$

Case 6: When $G_1 \to \infty$, $\alpha = 0$, $\mu'_L = \mu'_{\mathrm{T}} = \mu'$ and $a_1 = a_2 = 0$, dispersion equation in Eq. (5.48) reduces to

$$tan\left(\zeta H\sqrt{\frac{c^2}{\beta_2^2} - 1}\right) = \frac{n_{14}\mu'\zeta}{n_{13}}\sqrt{\frac{c^2}{\beta_2^2} - 1} \tag{5.62}$$

where

$$n_{13} = \frac{\zeta^2 r_3}{4}\left((p_3^2 - q_3^2)N_1 + G_2(p_1^2 - q_1^2)(p_3^2 - q_3^2)\right) + G_2N_1N_2,$$

$$n_{14} = -\frac{G_2N_2(p_1^2-q_1^2)}{2} + \frac{G_2N_1(p_3^2-q_3^2)}{2} - \frac{N_1N_2}{2}$$

Case 7: If $G_2 \to \infty$, then lower substrate (M_1) and the layer (M_2) will be perfectly attached and dispersion equation in Eq. (5.48) reduces to

$$\sin\left(\frac{\zeta QH}{2R}\right)\left(n_{15}\sin\left(\frac{r^{1/2}H}{2R}\right) - n_{16}\cos\left(\frac{r^{1/2}H}{2R}\right)\right) = 0 \tag{5.63}$$

and damping equation in Eq. (5.49) reduces to

$$\cos\left(\frac{\zeta QH}{2R}\right)\left(n_{15}\sin\left(\frac{r^{1/2}H}{2R}\right)-n_{16}\cos\left(\frac{r^{1/2}H}{2R}\right)\right)=0 \tag{5.64}$$

where

$$n_{15}=\frac{(T^2+r)e^{-\alpha H}}{4}\left((p_1^2-q_1^2)N_2+G_1(p_1^2-q_1^2)(p_3^2-q_3^2)\right)+G_1N_1N_2-$$
$$\frac{G_1N_2T(p_1^2-q_1^2)}{2}-\frac{G_1N_1Te^{-\alpha H}(p_3^2-q_3^2)}{2}-\frac{N_1N_2e^{-\alpha H}T}{2},$$

$$n_{16}=r^{1/2}\left[-\frac{G_1N_2(p_1^2-q_1^2)}{2}+\frac{G_1N_1e^{-\alpha H}(p_3^2-q_3^2)}{2}+\frac{N_1N_2e^{-\alpha H}}{2}\right]$$

Case 8: If $G_2\to\infty$ and $\alpha=0$, dispersion relation in Eq. (5.48) reduces to

$$\sin\left(\frac{\zeta QH}{2R}\right)\left(n_{17}\sin\left(\frac{\zeta r_2^{1/2}H}{2R}\right)-n_{18}\cos\left(\frac{\zeta r_2^{1/2}H}{2R}\right)\right)=0 \tag{5.65}$$

and damping equation in Eq. (5.49) reduces to

$$\cos\left(\frac{\zeta QH}{2R}\right)\left(n_{17}\sin\left(\frac{\zeta r_2^{1/2}H}{2R}\right)-n_{18}\cos\left(\frac{\zeta r_2^{1/2}H}{2R}\right)\right)=0 \tag{5.66}$$

where

$$n_{17}=\frac{\zeta^2r_2}{4}\left((p_1^2-q_1^2)N_2+G_1(p_1^2-q_1^2)(p_3^2-q_3^2)\right)+G_1N_1N_2\,,$$

$$n_{18}=\zeta r_2^{1/2}\left[-\frac{G_1N_2(p_1^2-q_1^2)}{2}+\frac{G_1N_1(p_3^2-q_3^2)}{2}+\frac{N_1N_2}{2}\right]$$

Case 9: If $G_2\to\infty$, $\alpha=0$, $\mu_L'=\mu_T'=\mu'$ and $a_1=a_2=0$, dispersion relation in Eq. (5.48) reduces to

$$tan\left(\zeta H\sqrt{\frac{c^2}{\beta_2^2}-1}\right)=\frac{n_{20}\mu'\zeta}{n_{19}}\sqrt{\frac{c^2}{\beta_2^2}-1} \tag{5.67}$$

where

$$n_{19}=\frac{\zeta^2r_3}{4}\left((p_1^2-q_1^2)N_2+G_1(p_1^2-q_1^2)(p_3^2-q_3^2)\right)+G_1N_1N_2\,,$$

$$n_{20}=-\frac{G_1N_2(p_1^2-q_1^2)}{2}+\frac{G_1N_1(p_3^2-q_3^2)}{2}+\frac{N_1N_2}{2}$$

Case 10: If $G_1 \to \infty$ and $G_2 \to \infty$, then heterogeneous fiber-reinforced layer is perfectly attached to both the substrates and dispersion relation in Eq. (5.48) reduces to

$$\sin\left(\frac{\zeta QH}{2R}\right)\left(n_{21}\sin\left(\frac{r^{1/2}H}{2R}\right) - n_{22}\cos\left(\frac{r^{1/2}H}{2R}\right)\right) = \sin\left(\frac{\zeta QH}{2R}\right)\left(s_1\sin\left(\frac{r^{1/2}H}{2R}\right) - s_2\cos\left(\frac{r^{1/2}H}{2R}\right)\right) = 0 \tag{5.68}$$

and damping relation in Eq. (5.49) reduces to

$$\cos\left(\frac{\zeta QH}{2R}\right)\left(n_{21}\sin\left(\frac{r^{1/2}H}{2R}\right) - n_{22}\cos\left(\frac{r^{1/2}H}{2R}\right)\right) = \cos\left(\frac{\zeta QH}{2R}\right)\left(s_1\sin\left(\frac{r^{1/2}H}{2R}\right) - s_2\cos\left(\frac{r^{1/2}H}{2R}\right)\right) = 0 \tag{5.69}$$

Eqs. (5.68) & (5.69) are same as the Eqs. (5.38) & (5.39) respectively.

5.6 GRAPHICAL RESULTS AND DISCUSSION

The values of material constants for graphical illustrations are mentioned in Table 5.1.

Couple stress substrates (M_1&M_3) [117]	$\mu^C = 30.5 \times 10^9\ N/m^2$	$-$	$\rho^{C_1} = \rho^{C_3} = 2717\ Kg/m^3$
Fiber-reinforced layer [102]	$\mu'_T = 3.50 \times 10^9\ N/m^2$	$\mu'_L = 7.07 \times 10^9\ N/m^2$	$\rho' = 1600\ Kg/m^3$

Table 5.1 Material parameters

Parameters	l_3	l_1	αH	(a_1^2, a_2^2)	H	G_1	G_2
Fig. 5.2	0.0004	0.0004	0.1	$-$	0.3	∞	∞
Fig. 5.3	0.0004	0.0004	0.1	$-$	0.3	∞	∞
Fig. 5.4	0.0004	0.0004	0.1	$-$	0.3	30.5×10^9	30.5×10^9
Fig. 5.5	0.0004	0.0004	0.1	$-$	0.3	30.5×10^9	30.5×10^9
Fig. 5.6	$-$	0.0004	0.1	$(0.5, 0.5)$	0.3	∞	∞
Fig. 5.7	$-$	0.0004	0.1	$(0.5, 0.5)$	0.3	∞	∞

Fig. 5.8	$-$	0.0004	0.1	$(0.5, 0.5)$	0.3	30.5×10^9	30.5×10^9
Fig. 5.9	$-$	0.0004	0.1	$(0.5, 0.5)$	0.3	30.5×10^9	30.5×10^9
Fig. 5.10	0.0004	$-$	0.1	$(0.5, 0.5)$	0.3	∞	∞
Fig. 5.11	0.0004	$-$	0.1	$(0.5, 0.5)$	0.3	∞	∞
Fig. 5.12	0.0004	$-$	0.1	$(0.5, 0.5)$	0.3	30.5×10^9	30.5×10^9
Fig. 5.13	0.0004	$-$	0.1	$(0.5, 0.5)$	0.3	30.5×10^9	30.5×10^9
Fig. 5.14	0.0004	0.0004	$-$	$(0.5, 0.5)$	0.3	∞	∞
Fig. 5.15	0.0004	0.0004	$-$	$(0.5, 0.5)$	0.3	∞	∞
Fig. 5.16	0.0004	0.0004	$-$	$(0.5, 0.5)$	0.3	30.5×10^9	30.5×10^9
Fig. 5.17	0.0004	0.0004	$-$	$(0.5, 0.5)$	0.3	30.5×10^9	30.5×10^9
Fig. 5.18	0.0004	0.0004	0.1	$(0.5, 0.5)$	0.3	$-$	30.5×10^9
Fig. 5.19	0.0004	0.0004	0.1	$(0.5, 0.5)$	0.3	$-$	30.5×10^9
Fig. 5.20	0.0004	0.0004	0.1	$(0.5, 0.5)$	0.3	30.5×10^9	$-$
Fig. 5.21	0.0004	0.0004	0.1	$(0.5, 0.5)$	0.3	30.5×10^9	$-$

Table 5.2 Values of various parameters

In Figs. (5.2), (5.4), (5.6), (5.8), (5.10), (5.12), (5.14), (5.16), (5.18), (5.20), vertical axis represents non-dimensional phase velocity (c/β_2) and horizontal axis represents non-dimensional wave number (ζH). In Figs. (5.3), (5.5), (5.7), (5.9), (5.11), (5.13), (5.15), (5.17), (5.19), (5.21), vertical axis represents dimensionless damped velocity (c/β_2) and horizontal axis represents non-dimensional wave number (ζH). Figures (5.2), (5.3), (5.6), (5.7), (5.10), (5.11), (5.14), (5.15) are plotted when layer is perfectly attached to both the substrates and Figs. (5.4), (5.5), (5.8), (5.9), (5.12), (5.13), (5.16), (5.17) are plotted when layer is imperfectly attached to both the substrates.

5.6.1 The influence of reinforced parameters (a_1^2, a_2^2)

Figures (5.2), (5.3), (5.4) and (5.5) represented the impacts of reinforced parameters (a_1^2, a_2^2) on propagation behavior of SH-waves. In Figs. (5.2) and (5.3), intermediate layer is perfectly attached to the substrates and in Figs. (5.4) and (5.5), layer is taken to be imperfectly attached to both the substrates. All four figures are plotted by taking five values of the reinforced parameters (a_1^2, a_2^2) as $(0.25, 0.75)$, $(0.35, 0.65)$,

$(0.50, 0.50)$, $(0.65, 0.35)$ and $(0.75, 0.25)$ and other parameters are mentioned in Table 5.2. In Figs. (5.2) and (5.3), it is found that phase velocity and damping velocity increase with increase in value of reinforcement parameters. In Figs. (5.4) and (5.5), it can be observed that the trend of the curves changes at a particular value of wave number.

5.6.2 The influence of characteristic length parameters $(\boldsymbol{l_1}$ & $\boldsymbol{l_3})$

Figures (5.6), (5.7), (5.8) and (5.9) illustrate the impacts of the microstructural characteristic length parameter (l_3) on the propagation behavior of shear waves. Figures (5.6) and (5.7) are plotted by considering that intermediate layer is perfectly attached to both the substrates, whereas Figs. (5.8) and (5.9) are shown by considering layer to be imperfectly attached to the substrates. All four figures are plotted by taking three values of microstructural parameter as $l_3 = 0.0001, 0.0004$ and 0.0006 and other parameters are mentioned in Table 5.2. It can be observed that effects of this parameter are very meager on both velocities of SH-waves. To depict these results, graphs have been zoomed, and it is seen that both velocities increase, when value of microstructural parameter increases.

Figures (5.10), (5.11), (5.12) and (5.13) depict the impacts of microstructural parameter (l_1) on behavior of SH-waves. In Figs. (5.10) and (5.11) intermediate layer is perfectly attached to the substrates and in Fig. (5.12) and (5.13) layer is taken to be imperfectly attached to both the substrates. For all four figures, three values of microstructural parameter are taken as $l_1 = 0.0001, 0.0004$ and 0.0006 and other parameters are mentioned in Table 5.2. It is noticed from all four figures that characteristic length parameter (l_1) favors phase velocity and damped velocity of SH-waves.

In Figs. (5.6), (5.8), (5.10), and (5.12), results are shown in the presence as well as absence of reinforcement parameters. In Figs. (5.7), (5.9), (5.11), and (5.13), results are shown in the presence of reinforcement parameters.

5.6.3 The influence of heterogeneity parameter (αH)

Figures (5.14), (5.15), (5.16) and (5.17) depict the impacts of heterogeneity parameter (αH) on propagation behavior of SH-waves. Figures (5.14) and (5.15) are plotted by considering that intermediate layer is perfectly attached to both the substrates, whereas Figs. (5.16) and (5.17) are shown by considering layer to be imperfectly attached to the substrates. To plot all these four figures, we have considered three values of heterogeneity parameter as $\alpha H = 0.1, 0.2, 0.3$ and other parameters are mentioned in Table 5.2. In Figs. (5.14) and (5.15), it is found that both velocities increase, when value of heterogeneity parameter increases. In Figs. (5.16) and (5.17), initially the velocity increases with increase in the value of heterogeneity parameter and then trend reverses after a particular wave number.

In Figs. (5.14) and (5.16), trends are shown in the presence as well as absence of reinforcement parameters. In Figs. (5.15) and (5.17), trends are shown in the presence of reinforcement parameters.

5.6.4 The influence of imperfectness parameter (G_1)

Figures (5.18) and (5.19) elucidate the effects of imperfectness parameter (G_1) of interface (I_1). The figures have been plotted by taking the values of the imperfectness parameter G_1 as 30.5×10^9, $4 \times 30.5 \times 10^9$ and $G_1 \to \infty$ and other parameters are mentioned in Table 5.2. In both figures, it is found that both velocities decrease as value of imperfectness parameter G_1 increases. As value of parameter G_1 increases, the bonding between layer and upper substrate tend to become better and when $G_1 \to \infty$, the layer is perfectly attached to the substrate. In Fig. (5.18), trends are shown in the presence as well as absence of reinforcement parameters. In Fig. (5.19), trends are shown in the presence of reinforcement parameters.

5.6.5 The influence of imperfectness parameter (G_2)

The impacts of imperfectness parameter (G_2) of the interface (I_2) are elucidated in Figs. (5.20) and (5.21). The graphs have been plotted by taking values of the imperfectness parameter G_2 as 30.5×10^9, $4 \times 30.5 \times 10^9$, $G_2 \to \infty$ and other parameters are mentioned in Table 5.2. From Figs. (5.20) and (5.21), it is noticed that imperfectness parameter (G_2) favours the velocities and both velocities increase with increase in value of imperfectness parameter G_2. When $G_2 \to \infty$, it refers to the case when two media are perfectly attached, and it can be observed that phase velocity is highest for this case. In Fig. (5.20), trends are shown in the presence as well as absence of reinforcement parameters. In Fig. (5.21), trends are shown in the presence of reinforcement parameters.

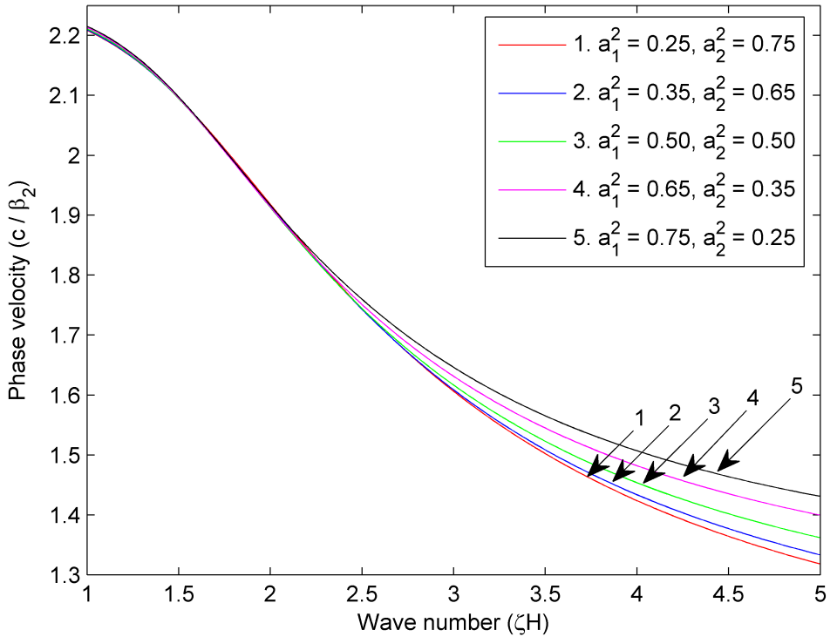

Figure 5.2 Plots for showing impacts of reinforced parameters (a_1^2, a_2^2) with perfect interface

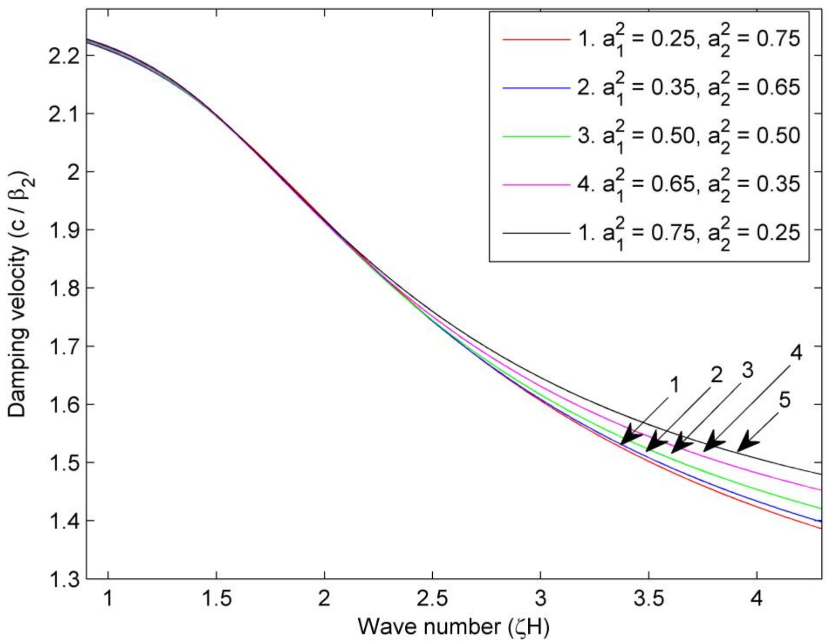

Figure 5.3 Plots for showing impacts of reinforced parameters (a_1^2, a_2^2) with perfect interface

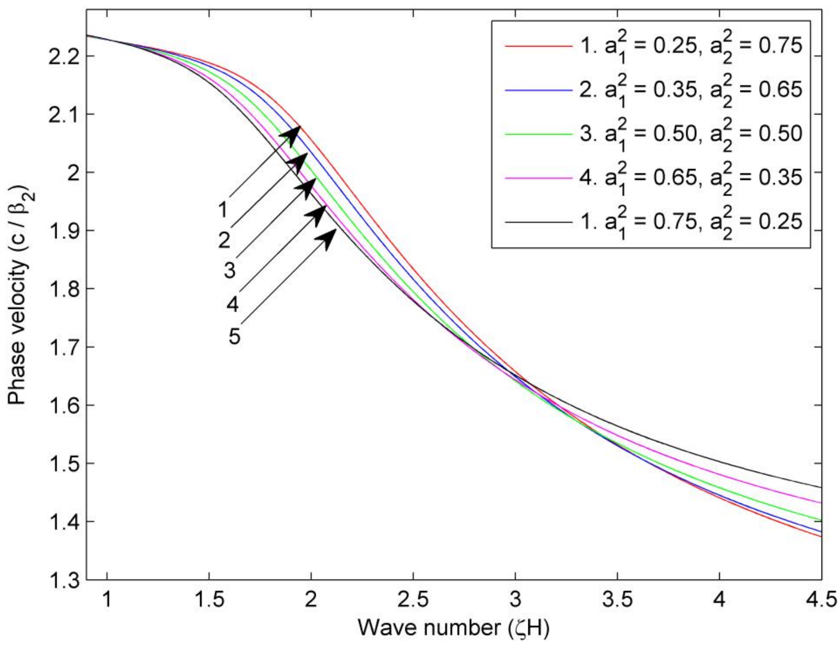

Figure 5.4 Plots for showing impacts of reinforced parameters (a_1^2, a_2^2) with imperfect interface

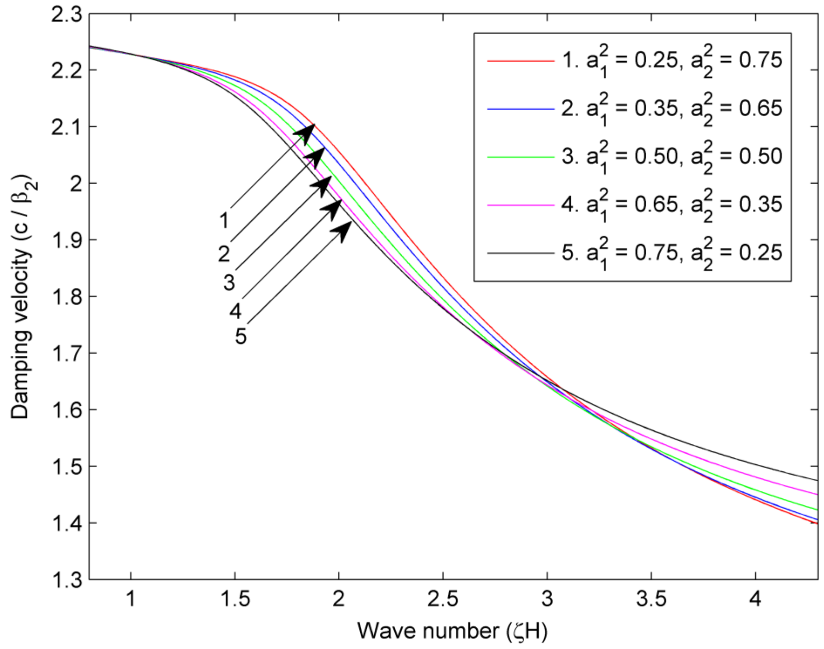

Figure 5.5 Plots for showing impacts of reinforced parameters (a_1^2, a_2^2) with imperfect interface

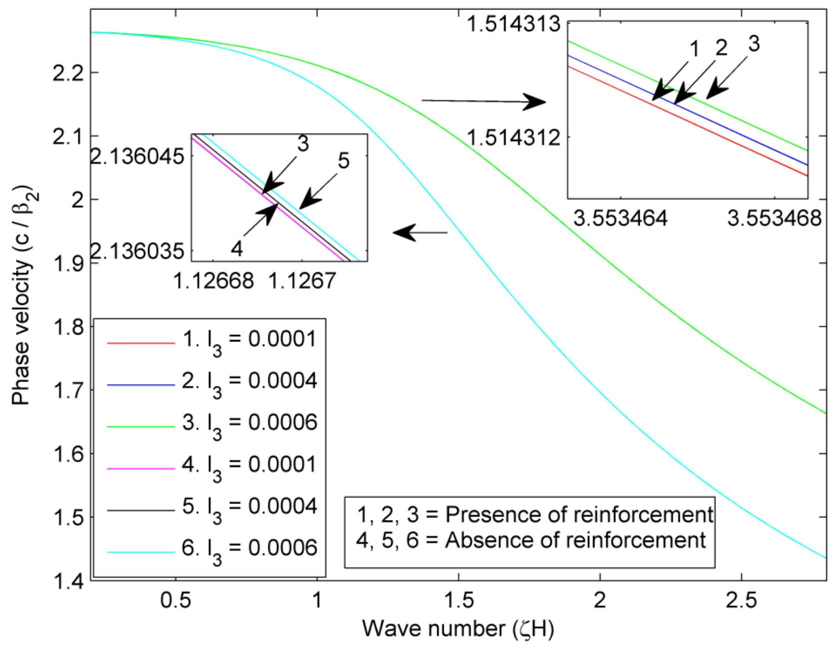

Figure 5.6 Plots for showing impacts of characteristic length (l_3) with perfect interface

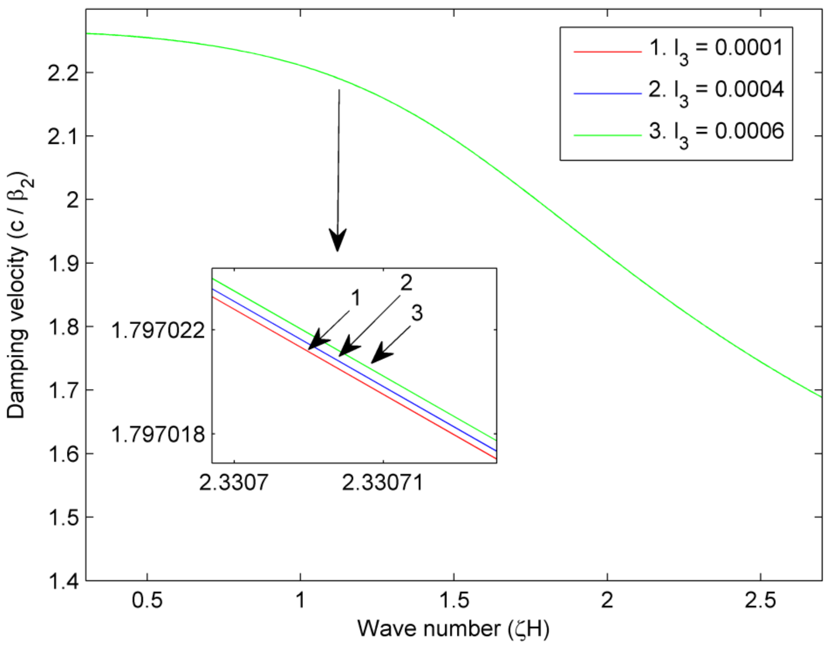

Figure 5.7 Plots for showing impacts of characteristic length (l_3) with perfect interface

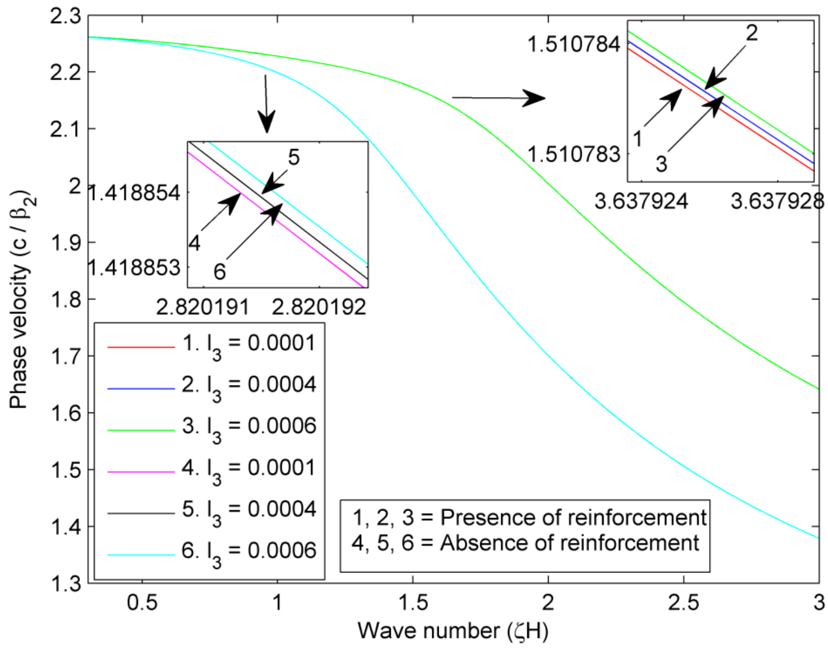

Figure 5.8 Plots for showing impacts of characteristic length (l_3) with imperfect interface

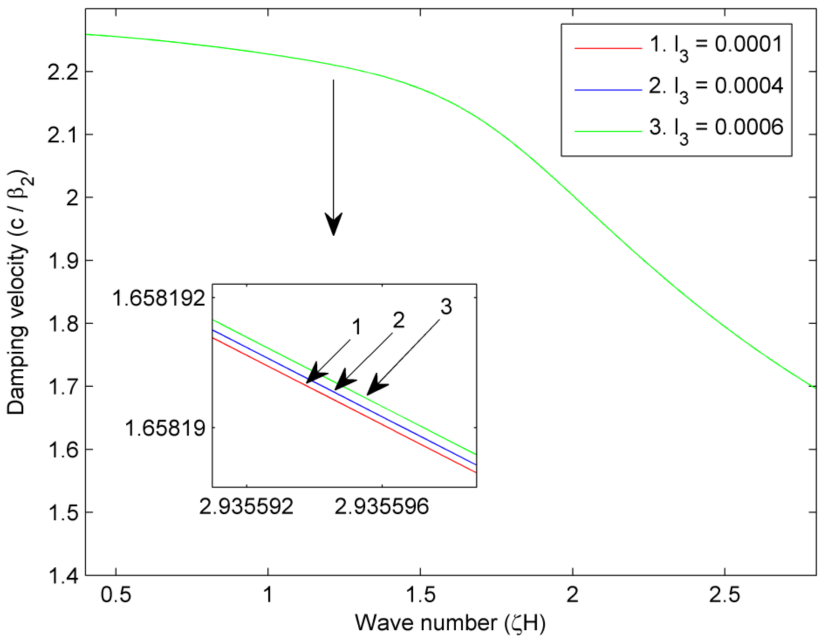

Figure 5.9 Plots for showing impacts of characteristic length (l_3) with imperfect interface

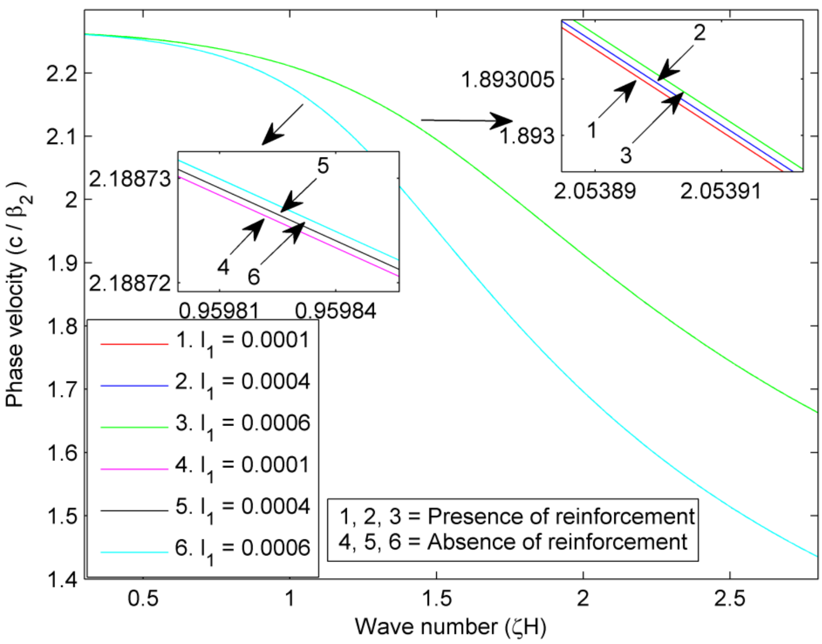

Figure 5.10 Plots for showing impacts of characteristic length (l_1) with perfect interface

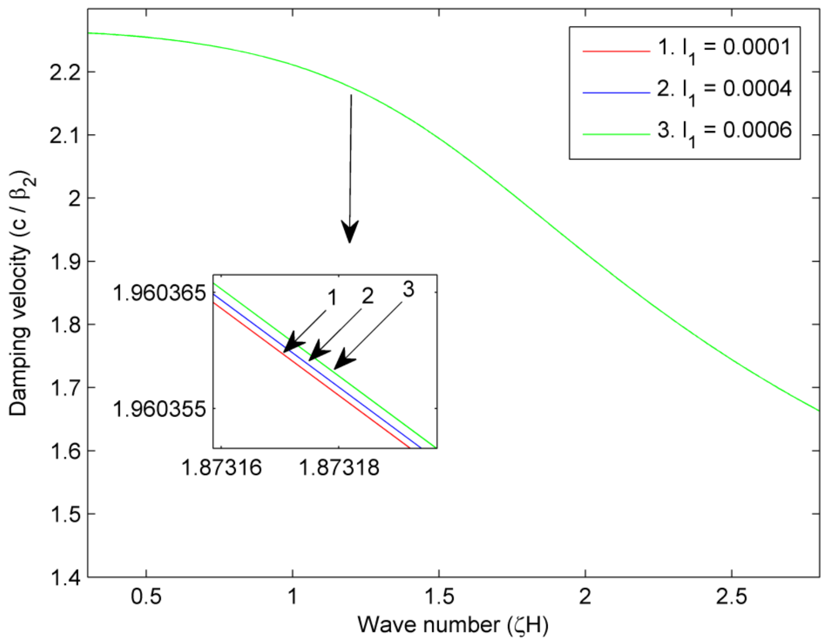

Figure 5.11 Plots for showing impacts of characteristic length (l_1) with perfect interface

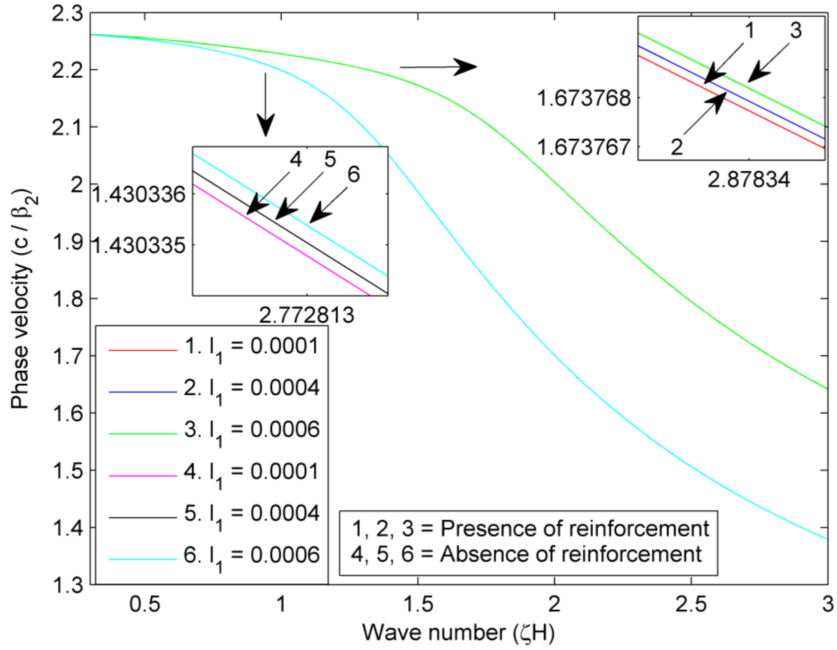

Figure 5.12 Plots for showing impacts of characteristic length (l_1) with imperfect interface

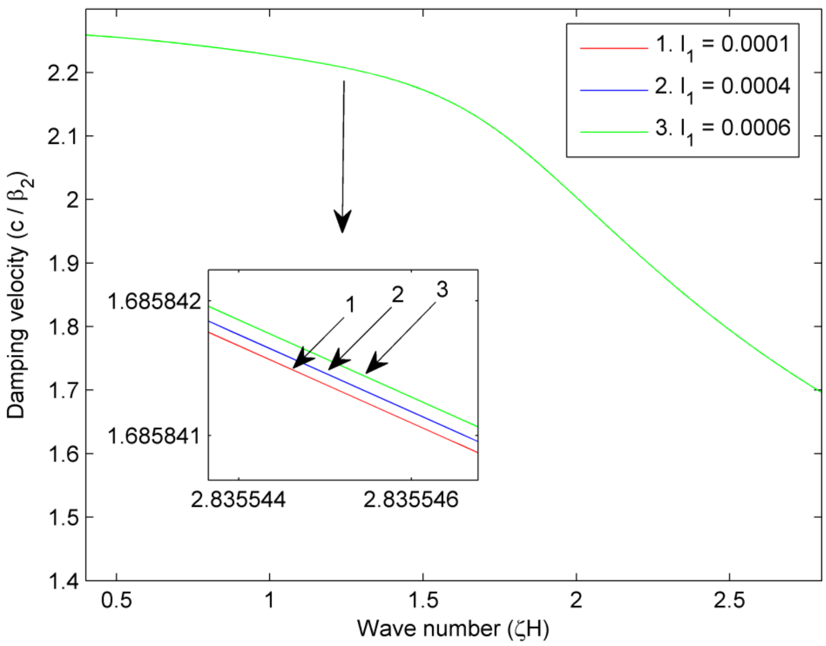

Figure 5.13 Plots for showing impacts of characteristic length (l_1) with imperfect interface

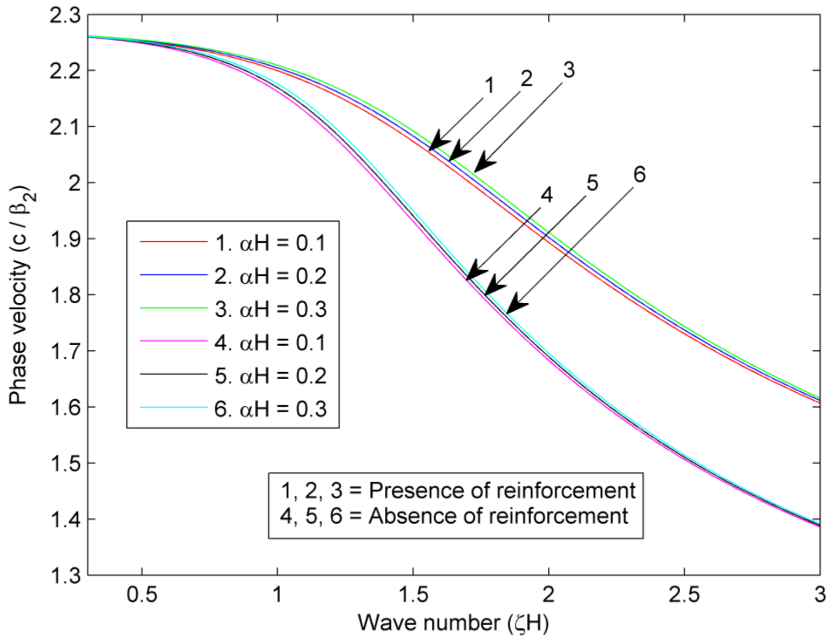

Figure 5.14 Plots for showing impacts of inhomogeneity parameter (αH) with perfect interface

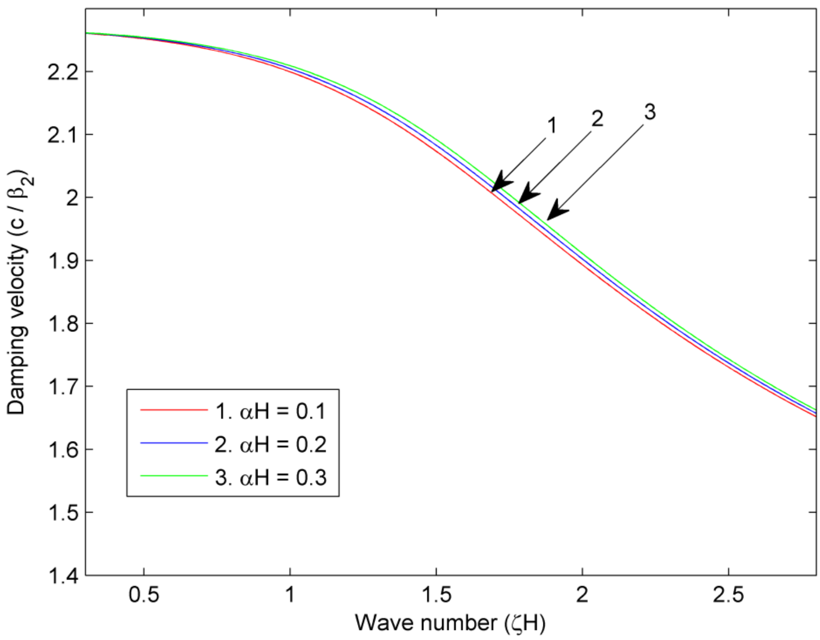

Figure 5.15 Plots for showing impacts of inhomogeneity parameter (αH) with perfect interface

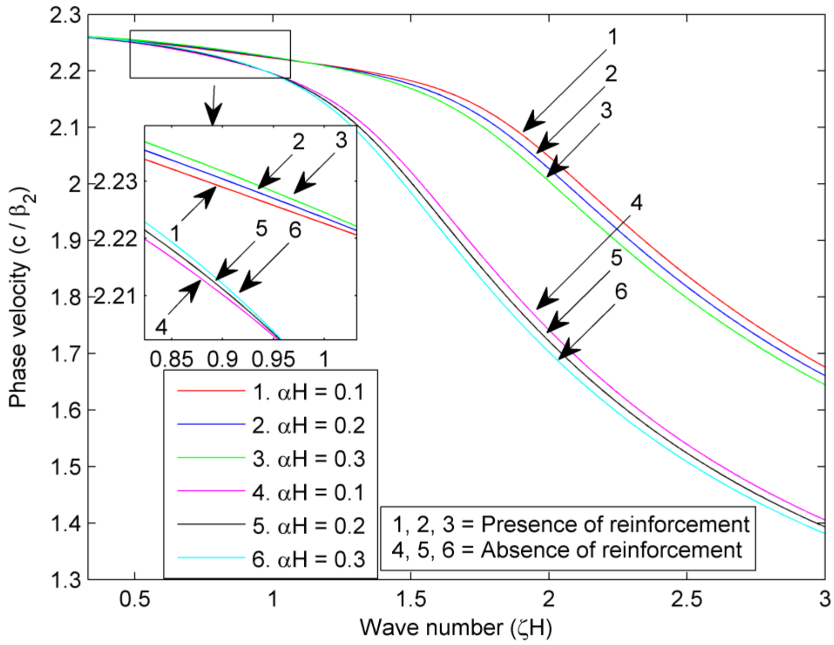

Figure 5.16 Plots for showing impacts of inhomogeneity parameter (αH) with imperfect interface

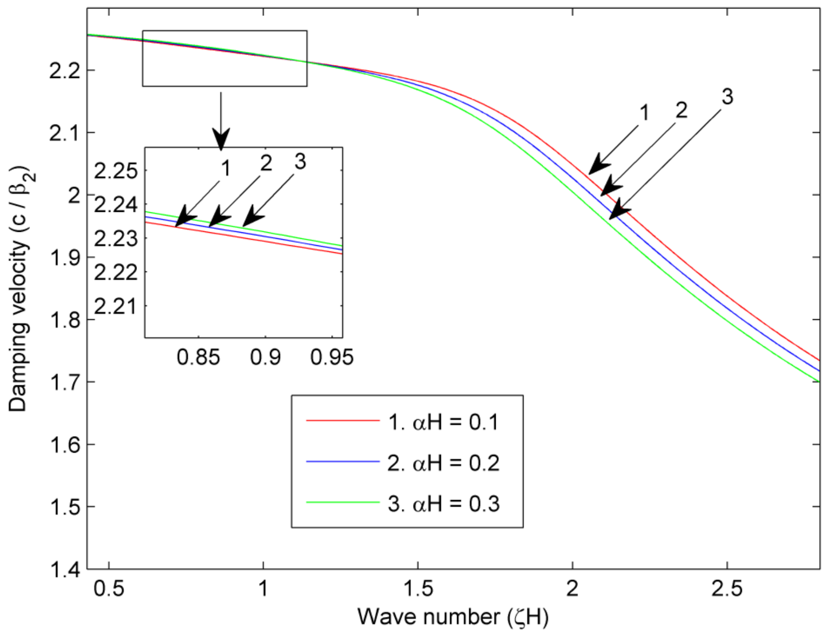

Figure 5.17 Plots for showing impacts of inhomogeneity parameter (αH) with imperfect interface

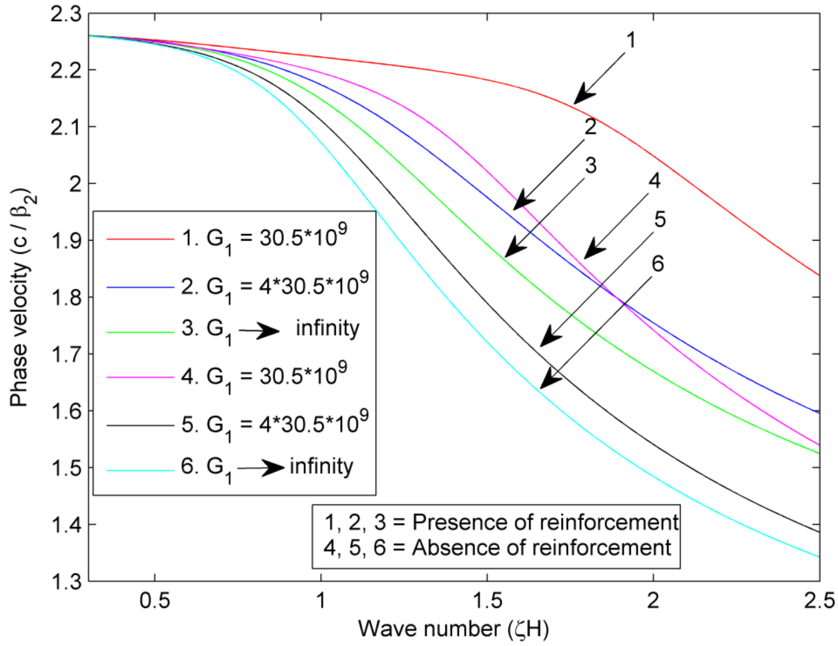

Figure 5.18 Plots for showing impacts of imperfectness parameter (G_1)

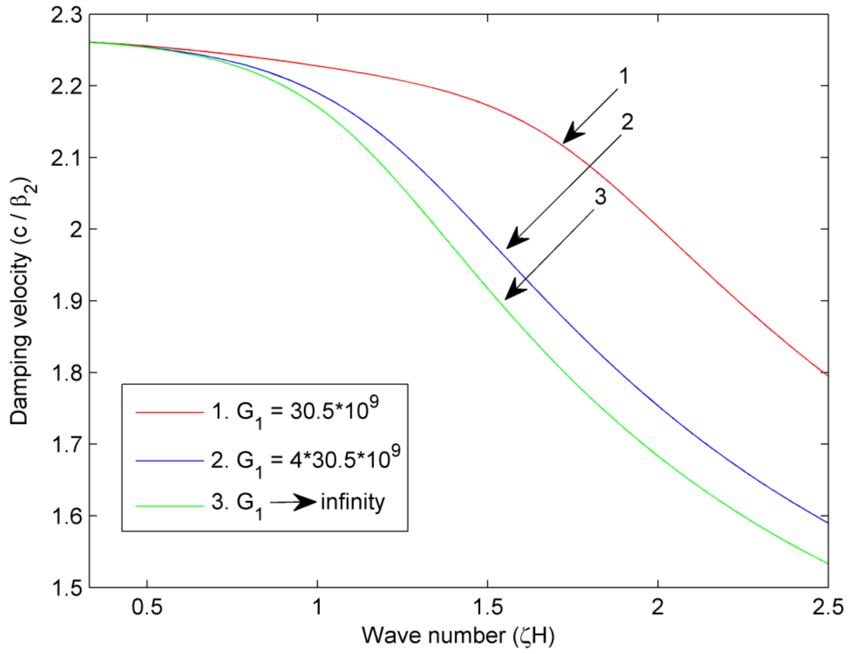

Figure 5.19 Plots for showing impacts of imperfectness parameter (G_1)

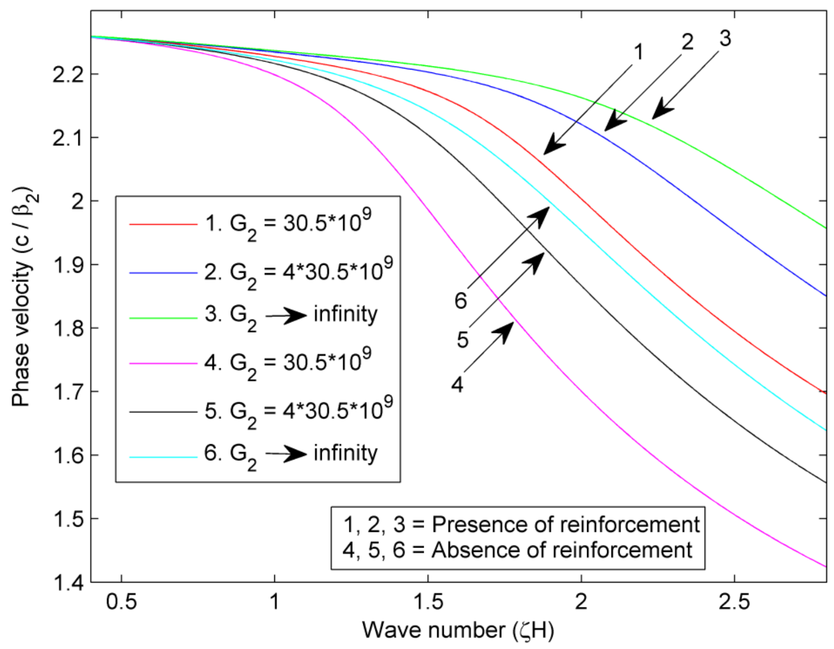

Figure 5.20 Plots for showing impacts of imperfectness parameter (G_2)

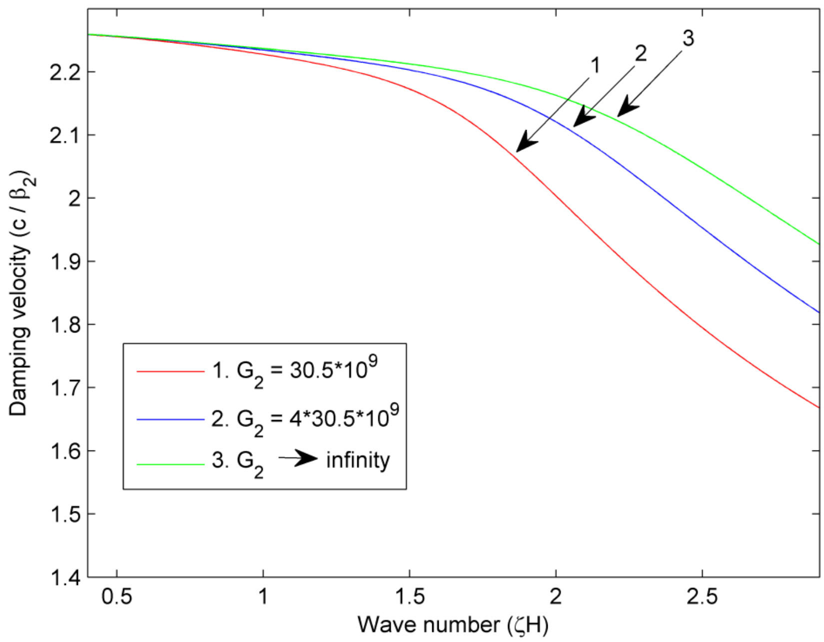

Figure 5.21 Plots for showing impacts of imperfectness parameter (G_2)

5.7 CONCLUSION

The problem investigates propagation behavior of shear horizontal waves in an inhomogeneous fiber-reinforced layer lying between two couple stress substrates. The analysis has been done in two scenarios, firstly when the layer is perfectly attached to both the substrates and secondly, when layer is imperfectly attached to both the substrates. The secular equations are calculated to observe the impacts of various parameters. The main outcomes are drawn from the obtained results

- Initially the velocities decrease with increase in the values of reinforced parameters (a_1^2, a_2^2) and then trend changes after a particular wave number. This kind of pattern is seen in the case, when layer is imperfectly attached to the substrates. When layer is perfectly attached to both the substrates, phase and damping velocities increase with increase in value of reinforcement parameters.
- Both velocities increase with increase in the values of two characteristic lengths $(l_1$ & $l_3)$ associated with the substrates. These results are independent of the situation whether layer is perfectly or imperfectly attached to the substrates.

- When the intermediate layer is perfectly attached to the substrates, it is noticed that both velocities increase with increase in values of heterogeneity (αH). When layer is imperfectly attached with substrates, both velocities firstly increase with increase in values of heterogeneity parameter (αH) and then pattern changes after a particular value of wave number.
- The results of imperfectness parameters $(G_1$ & $G_2)$ are contrary to each other. Phase velocity and damping velocity decrease with increase in values of the imperfectness parameter G_1 of interface I_1 and both velocities of shear waves increase with increase in the values of the imperfectness parameter G_2 of interface I_2.

As SH-waves are used in NDT techniques for material evaluation, so, present analysis may also find some applications in this area. The problem has been dealt using size-dependent couple stress theory, which can enhance the results, established in non-destructive testing techniques using classical theory. As the geometrical configuration of the problem is inspired from earth, so the results found in the problem can help to find solutions to mitigate the devasting effects of earthquakes. Fiber-reinforced materials are widely used in constructions works and architectural designs, so the present study may also find some applications in civil engineering, geophysics, and geomechanics.

SUGGESTION FOR FUTURE WORK

Following suggestions have been made for the extension and further use of the present research work:

- In this thesis, we have studied about the propagation of Rayleigh waves in an elastic layer attached to a microstructural couple stress half-space, so as an extension of this work, propagation behavior of Rayleigh waves can be studied in double layered structure. Another suggestion for the extension of the work done in thesis is to study Rayleigh waves in one or more layers attached to microstructural couple stress half-space in the presence of gravity.
- We have studied about the propagation of SH-waves in a layer which is imperfectly attached to two couple stress substrates. Problems of Love waves are also studied in single and double layered structures. A suggestion for the extension of this work is to study about the propagation behavior of SH-waves or Love waves in a layer attached to half-space with irregular surfaces.
- Plate waves (Lamb waves or SH-waves) can also be studied in a layered structure.

BIBLIOGRAPHY

[1] Abbas, I. A., & Othman, M. I. (2011). Generalized magneto-thermoelasticity in a fiber-reinforced anisotropic half-space. *International Journal of Thermophysics*, *32*(5), 1071-1085.

[2] Abd-Alla, A. M., Hammad, H. A. H., & Abo-Dahab, S. M. (2004). Rayleigh waves in a magnetoelastic half-space of orthotropic material under influence of initial stress and gravity field. *Applied Mathematics and Computation*, *154*(2), 583-597.

[3] Abd-Alla, A. M., Nofal, T. A., Abo-Dahab, S. M., & Al-Mullise, A. (2013). Surface waves propagation in fibre-reinforced anisotropic elastic media subjected to gravity field. *International Journal of Physical Sciences*, *8*(14), 574-584.

[4] Ahmed, S. M., & Abo-Dahab, S. M. (2010). Propagation of Love waves in an orthotropic granular layer under initial stress overlying a semi-infinite granular medium. *Journal of Vibration and Control*, *16*(12), 1845-1858.

[5] Ajri, M., Fakhrabadi, M. M. S., & Rastgoo, A. (2018). Analytical solution for nonlinear dynamic behavior of viscoelastic nano-plates modeled by consistent couple stress theory. *Latin American Journal of Solids and Structures*, *15*.

[6] Akbarov, S. D., & Negin, M. (2017). Near-surface waves in a system consisting of a covering layer and a half-space with imperfect interface under two-axial initial stresses. *Journal of Vibration and Control*, *23*(1), 55-68.

[7] Akgöz, B., & Civalek, Ö. (2013). Modeling and analysis of micro-sized plates resting on elastic medium using the modified couple stress theory. *Meccanica*, *48*(4), 863-873.

[8] Alam, P., Kundu, S., & Gupta, S. (2017). Dispersion and attenuation of torsional wave in a viscoelastic layer bonded between a layer and a half-space of dry sandy media. *Applied Mathematics and Mechanics*, *38*(9), 1313-1328.

[9] Alam, P., Kundu, S., Gupta, S., & Saha, A. (2018). Study of torsional wave in a poroelastic medium sandwiched between a layer and a half-space of heterogeneous dry sandy media. *Waves in Random and Complex Media*, *28*(1), 182-201.

[10] Ardanuy, M., Claramunt, J., & Toledo Filho, R. D. (2015). Cellulosic fiber reinforced cement-based composites: A review of recent research. *Construction and building materials*, *79*, 115-128.

[11] Bayones, F. S. (2020). Effect of initial stress and gravity field on shear wave propagation in an inhomogeneous anisotropic incompressible sandy medium. *Mechanics of Advanced Materials and Structures*, *27*(5), 403-408.

[12] Belfield, A. J., Rogers, T. G., & Spencer, A. J. M. (1983). Stress in elastic plates reinforced by fibres lying in concentric circles. *Journal of the Mechanics and Physics of Solids*, *31*(1), 25-54.

[13] Bhattacharya, S. N. (2017). Limits of transversely isotropic elastic parameters for the existence of classical Rayleigh waves. *Journal of Seismology*, *21*(1), 237-241.

[14] Carcione, J. M. (1990). Wave propagation in anisotropic linear viscoelastic media: theory and simulated wavefields. *Geophysical Journal International*, *101*(3), 739-750.

[15] Chadwick, P. (1976). Surface and interfacial waves of arbitrary form in isotropic elastic media. *Journal of Elasticity*, *6*(1), 73-80.

[16] Chattopadhyay, A., & Choudhury, S. (1990). Propagation, reflection and transmission of magnetoelastic shear waves in a self-reinforced medium. *International Journal of Engineering Science*, *28*(6), 485-495.

[17] Chattopadhyay, A., Gupta, S., Samal, S. K., & Sharma, V. K. (2009). Torsional waves in self-reinforced medium. *International Journal of Geomechanics*, *9*(1), 9-13.

[18] Chattopadhyay, A., Singh, A. K., & Dhua, S. (2014). Effect of heterogeneity and reinforcement on propagation of a crack due to shear waves. *International Journal of Geomechanics*, *14*(4), 04014013.

[19] Chaudhary, S., Kaushik, V. P., & Tomar, S. K. (2005). Transmission of shear waves through a self-reinforced layer sandwiched between two inhomogeneous viscoelastic half-spaces. *International journal of mechanical sciences*, *47*(9), 1455-1472.

[20] Chen, S., & Wang, T. (2001). Strain gradient theory with couple stress for crystalline solids. *European Journal of Mechanics-A/Solids*, *20*(5), 739-756.

[21] Cheng, T. H., Ren, M., Li, Z. Z., & Shen, Y. D. (2015). Vibration and damping analysis of composite fiber reinforced wind blade with viscoelastic damping control. *Advances in Materials Science and Engineering*, *2015*.

[22] Chimenti, D. E., Nayfeh, A. H., & Butler, D. L. (1982). Leaky Rayleigh waves on a layered halfspace. *Journal of Applied Physics*, *53*(1), 170-176.

[23] Chiriţă, S. (2013). On the Rayleigh surface waves on an anisotropic homogeneous thermoelastic half space. *Acta Mechanica*, *224*(3), 657-674.

[24] Cosserat, E., & Cosserat, F. (1909). *Théorie des corps déformables (Theory of deformable bodies)*. A. Hermann et Fils, Paris.

[25] Deresiewicz, H. (1961). A note on thermoelastic Rayleigh waves. *Journal of the Mechanics and Physics of Solids*, *9*(3), 191-195.

[26] Dey, S., Gupta, A. K., Gupta, S., & Prasad, A. M. (2000). Torsional surface waves in nonhomogeneous anisotropic medium under initial stress. *Journal of engineering mechanics*, *126*(11), 1120-1123.

[27] Drafts, B. (2001). Acoustic wave technology sensors. *IEEE Transactions on microwave theory and techniques*, *49*(4), 795-802.

[28] Ejaz, K., & Shams, M. (2019). Love waves in compressible elastic materials with a homogeneous initial stress. *Mathematics and Mechanics of Solids*, *24*(8), 2576-2590.

[29] Eskandari, M., & Shodja, H. M. (2008). Love waves propagation in functionally graded piezoelectric materials with quadratic variation. *Journal of Sound and Vibration*, *313*(1-2), 195-204.

[30] Fortunko, C. M., & Moulder, J. C. (1982). Ultrasonic inspection of stainless steel butt welds using horizontally polarized shear waves. *Ultrasonics*, *20*(3), 113-117.

[31] Goyal, R., & Kumar, S. (2019). Dispersion of Love waves in size-dependent substrate containing finite piezoelectric and viscoelastic layers. *International Journal of Mechanics and Materials in Design*, *15*(4), 767-790.

[32] Goyal, R., & Kumar, S. (2019). Quantifying viscoelastic, piezoelectric and couple stress effects on Love-type wave propagation. *Smart Materials and Structures*, *28*(10), 105021.

[33] Gubbins, D. (1990). *Seismology and plate tectonics*. Cambridge University Press.

[34] Gupta, S., Dwivedi, R., & Dutta, R. (2021). Rayleigh wave propagation at the boundary surface of dry sandy ($ SiO_2 $) thermoelastic solids. *Engineering Computations*. DOI:10.1108/EC-04-2020-0231.

[35] Gupta, S., Pramanik, A., & Ahmed, M. (2018). Impact of pre-stress, inhomogeneity and porosity on the propagation of Love wave. *Acta Geophysica*, *66*(5), 855-866.

[36] Güven, U. (2011). The investigation of the nonlocal longitudinal stress waves with modified couple stress theory. *Acta Mechanica*, *221*(3), 321-325.

[37] Hadjesfandiari, A. R., & Dargush, G. F. (2011). Couple stress theory for solids. *International Journal of Solids and Structures*, *48*(18), 2496-2510.

[38] Hawwa, M. A. (2017). Shear waves in an initially stressed elastic plate with periodic corrugations. *Arabian Journal for Science and Engineering*, *42*(5), 1831-1840.

[39] Hua, L. I. U., YANG, J. L., & LIU, K. X. (2007). Love waves in layered graded composite structures with imperfectly bonded interface. *Chinese Journal of Aeronautics*, *20*(3), 210-214.

[40] Hudson, J. A. (1962). Love waves in a heterogeneous medium. *Geophysical Journal International*, *6*(2), 131-147.

[41] Hussien, N. S., & Bayones, F. S. (2019). Effect of rotation on Rayleigh waves in a fiber-reinforced solid anisotropic magneto-thermo-viscoelastic media. *Mechanics of Advanced Materials and Structures*, *26*(20), 1711-1718.

[42] Ilyashenko, A. V., & Kuznetsov, S. V. (2017). Theoretical aspects of applying love and SH-waves to nondestructive testing of stratified media. *Russian Journal of Nondestructive Testing*, *53*(9), 597-603.

[43] Ilyashenko, A. V., & Kuznetsov, S. V. (2018). Horizontally polarized shear waves in stratified anisotropic (monoclinic) media. *Archives of Mechanics*, *70*(4), 305-315.

[44] Isobe, A., Hikita, M., & Asai, K. (2005). Love-wave-type/Rayleigh-wave-type SAW resonators with thick Al-grating structure. *Electronics and Communications in Japan (Part II: Electronics)*, *88*(4), 1-8.

[45] Jia, N., Peng, Z., Li, J., Yao, Y., & Chen, S. (2021). Dispersive behavior of high frequency Rayleigh waves propagating on an elastic half space. *Acta Mechanica Sinica*, *37*(4), 562-569.

[46] Kaplunov, J., Prikazchikov, D., & Sultanova, L. (2019). Rayleigh-type waves on a coated elastic half-space with a clamped surface. *Philosophical Transactions of the Royal Society A*, *377*(2156), 20190111.

[47] Kaur, B., & Singh, B. (2021). Rayleigh-type surface wave in nonlocal isotropic diffusive materials. *Acta Mechanica*, *232*(9), 3407-3416.

[48] Kaur, T., Kumar, S., & Singh, A. K. (2018). Love wave propagation in vertical heterogeneous fiber-reinforced stratum imperfectly bonded to a micropolar elastic substrate. *International Journal of Geomechanics*, *18*(2), 04017146.

[49] Kaur, T., Sharma, S. K., & Singh, A. K. (2016). Effect of reinforcement, gravity and liquid loading on Rayleigh-type wave propagation. *Meccanica*, *51*(10), 2449-2458.

[50] Ke, L. L., Wang, Y. S., Yang, J., & Kitipornchai, S. (2012). Free vibration of size-dependent Mindlin microplates based on the modified couple stress theory. *Journal of Sound and Vibration*, *331*(1), 94-106.

[51] Kiselev, A. P. (2004). Rayleigh wave with a transverse structure. *Proceedings of the Royal Society of London. Series A: Mathematical, Physical and Engineering Sciences*, *460*(2050), 3059-3064.

[52] Koiter, W. T. (1964). Couple stresses in the theory of elasticity, I and II. *KoninKlije Nederlandse Akademie van Wetenshappen, SeriesB*, *67*, 17–44.

[53] Kończak, Z. (1989). The propagation of Love waves in a fluid-saturated porous anisotropic layer. *Acta Mechanica*, *79*(3), 155-168.

[54] Kong, Y., Liu, J., & Nie, G. (2015). Propagation characteristics of SH wave in an mm2 piezoelectric layer on an elastic substrate. *AIP Advances*, *5*(9), 097135.

[55] Kumari, N., Chattopadhyay, A., Kumar, S., & Singh, A. K. (2017). Propagation of SH-waves in two anisotropic layers bonded to an isotropic half-space under gravity. *Waves in Random and Complex Media*, *27*(2), 195-212.

[56] Kundu, S., & Maity, M. (2017). Edge wave propagation in an initially stressed dry sandy plate. *Procedia engineering*, *173,* 1029-1033.

[57] Kundu, S., Manna, S., & Gupta, S. (2014). Love wave dispersion in pre-stressed homogeneous medium over a porous half-space with irregular boundary surfaces. *International Journal of Solids and Structures*, *51*(21-22), 3689-3697.

[58] Kuznetsov, S. V. (2010). Love waves in nondestructive diagnostics of layered composites. Survey. *Acoustical Physics*, *56*(6), 877-892.

[59] Kuznetsov, S. V. (2021). Weiskopf model for sandy materials: Rayleigh–Lamb wave dispersion. *Mechanics of Advanced Materials and Structures,* 1-6.

[60] Landau, L. D., & Lifšic, E. M. (1975). *Theory of elasticity: Transl. from the Russian by JB Sykes and WH Reid*. Pergamon Press.

[61] Lee, S., Kim, K. B., & Kim, Y. I. (2011). Love wave SAW biosensors for detection of antigen-antibody binding and comparison with SPR biosensor. *Food Science and Biotechnology*, *20*(5), 1413-1418.

[62] Liu, H., Wang, Z. K., & Wang, T. J. (2001). Effect of initial stress on the propagation behavior of Love waves in a layered piezoelectric structure. *International Journal of Solids and Structures*, *38*(1), 37-51.

[63] Liu, J. (2014). A theoretical study on Love wave sensors in a structure with multiple viscoelastic layers on a piezoelectric substrate. *Smart materials and structures*, *23*(7), 075015.

[64] Lord, R. (1887), "On waves propagating along the plane surface of an elastic solid", *Proceedings of the London Mathematical Society*, *17,* 4-11.

[65] Love, A. E. H. (1911). *A treatise on the mathematical theory of elasticity*. Cambridge University Press, Cambridge. Dover Publications, New York, First American Printing 1944.

[66] Ma, Q., Jiao, J., Hu, P., Zhong, X., Wu, B., & He, C. (2014). Excitation and detection of shear horizontal waves with electromagnetic acoustic transducers for nondestructive testing of plates. *Chinese Journal of Mechanical Engineering, 27*(2), 428-436.

[67] Meral, F. C., Royston, T. J., & Magin, R. L. (2011). Rayleigh–Lamb wave propagation on a fractional order viscoelastic plate. *The Journal of the Acoustical Society of America*, *129*(2), 1036-1045.

[68] Mindlin, R. D., & Eshel, N. N. (1968). On first strain-gradient theories in linear elasticity. *International Journal of Solids and Structures*, *4*, 109-124.

[69] Mindlin, R. D., & Tiersten, H.F. (1962). Effects of couple-stresses in linear elasticity. *Archive for Rational Mechanics and Analysis*, *11*, 415–448.

[70] Moradi, S., & Innanen, K. A. (2015). Scattering of homogeneous and inhomogeneous seismic waves in low-loss viscoelastic media. *Geophysical Journal International*, *202*(3), 1722-1732.

[71] Müller, G. (2007). *Theory of elastic waves*. Potsdam: Geoforschungszentrum.

[72] Na, J. K., Blackshire, J. L., & Kuhr, S. (2008). Design, fabrication, and characterization of single-element interdigital transducers for NDT applications. *Sensors and Actuators A: Physical*, *148*(2), 359-365.

[73] Novotny, O. (1999). Seismic surface waves. *Bahia, Salvador: Instituto de Geociencias*, *61*.

[74] Nowacki, W. (1974). *Micropolar Elasticity*. International Center for Mechanical Sciences, Courses and Lectures No. 151, Udine, Springer-Verlag, Wien-New York.

[75] Ono, K. (2019). Rayleigh wave calibration of acoustic emission sensors and ultrasonic transducers. *Sensors*, *19*(14), 3129.

[76] Ottosen, N. S., Ristinmaa, M., & Ljung, C. (2000). Rayleigh waves obtained by the indeterminate couple-stress theory. *European Journal of Mechanics-A/Solids*, *19*(6), 929-947.

[77] Ozisik, M. (2021). Dispersion of generalized Rayleigh waves in the half-plane covered with pre-stretched two layers under complete contact. *Thermal Science*, *25*(Spec. issue 2), 247-253.

[78] Pal, P. C., & Mandal, D. (2014). Generation of SH-type waves due to shearing stress discontinuity in a sandy layer overlying an isotropic and inhomogeneous elastic half-space. *Acta Geophysica*, *62*(1), 44-58.

[79] Pal, P. C., Kumar, S., & Bose, S. (2015). Propagation of Rayleigh waves in anisotropic layer overlying a semi-infinite sandy medium. *Ain Shams Engineering Journal*, *6*(2), 621-627.

[80] Pal, P. C., Kumar, S., & Mandal, D. (2016). Surface wave propagation in sandy layer overlying a liquid saturated porous half-space and lying under a uniform liquid layer. *Mechanics of Advanced Materials and Structures*, *23*(1), 59-65.

[81] Pang, Y., Liu, J. X., Wang, Y. S., & Zhao, X. F. (2008). Propagation of Rayleigh-type surface waves in a transversely isotropic piezoelectric layer on a piezomagnetic half-space. *Journal of Applied Physics*, *103*(7), 074901.

[82] Papadakis, G., Tsortos, A., & Gizeli, E. (2009). Triple-helix DNA structural studies using a Love wave acoustic biosensor. *Biosensors and Bioelectronics*, *25*(4), 702-707.

[83] Pasternak, M. (2008). New approach to Rayleigh wave propagation in the elastic halfspace-viscoelastic layer interface. *Acta Physica Polonica A*, *114*(6A), A-169.

[84] Qian, Z., Jin, F., Wang, Z., & Kishimoto, K. (2004). Dispersion relations for SH-wave propagation in periodic piezoelectric composite layered structures. *International Journal of Engineering Science*, *42*(7), 673-689.

[85] Rajak, D. K., Pagar, D. D., Menezes, P. L., & Linul, E. (2019). Fiber-reinforced polymer composites: Manufacturing, properties, and applications. *Polymers*, *11*(10), 1667.

[86] Ravindra, R. (1968). Usual assumptions in the treatment of wave propagation in heterogeneous elastic media. *pure and applied geophysics*, *70*(1), 12-17.

[87] Rostocki, A. J., Siegoczyński, R. M., Kiełczyński, P., & Szalewski, M. (2010). An application of Love SH waves for the viscosity measurement of triglycerides at high pressures. *High Pressure Research*, *30*(1), 88-92.

[88] Rushchitsky, J. (2011). *Theory of waves in materials*. Bookboon.

[89] Saha, A. N. U. P., Kundu, S., Gupta, S., & Vaishnav, P. K. (2015). Love waves in a heterogeneous orthotropic layer under initial stress overlying a gravitating porous half-space. In *Proc Indian Natl Sci Acad*, *81*(5), 1193-1205.

[90] Sahu, S. A., Saroj, P. K., & Dewangan, N. (2014). SH-waves in viscoelastic heterogeneous layer over half-space with self-weight. *Archive of Applied Mechanics*, *84*(2), 235-245

[91] Scholte, J. G. (1947). On Rayleigh waves in visco-elastic media. *Physica*, *13*(4-5), 245-250.

[92] Sengupta, P. R., & Nath, S. (2001). Surface waves in fibre-reinforced anisotropic elastic media. *Sadhana*, *26*(4), 363-370.

[93] Sethi, M., Gupta, K. C., & Rani, M. (2012). Propagation of torsional surface waves in a non-homogeneous crustal layer over a viscoelastic mantle. *Mathematica Aeterna*, *2*(10), 879-900.

[94] Sethi, M., Sharma, A., & Sharma, A. (2016). Propagation of SH waves in a double non-homogeneous crustal layers of finite depth lying over an homogeneous half-space. *Latin American Journal of Solids and Structures*, *13*(14), 2628-2642.

[95] Sharma, J. N., & Kumar, S. (2009). Lamb waves in micropolar thermoelastic solid plates immersed in liquid with varying temperature. *Meccanica*, *44*(3), 305-319.

[96] Sharma, J. N., Kumar, S., & Sharma, Y. D. (2009). Effect of micropolarity, microstretch and relaxation times on Rayleigh surface waves in thermoelastic solids. *Inernational Journal of Applied Mathematics and Mechanics*, *5*(2), 17-38.

[97] Sharma, V., & Kumar, S. (2014). Velocity dispersion in an elastic plate with microstructure: effects of characteristic length in a couple stress model. *Meccanica*, *49*(5), 1083-1090.

[98] Sharma, V., & Kumar, S. (2016). Influence of microstructure, heterogeneity and internal friction on SH waves propagation in a viscoelastic layer overlying a couple stress substrate. *Structural engineering and mechanics: An international journal*, *57*(4), 703-716.

[99] Sharma, V., & Kumar, S. (2017). Dispersion of SH waves in a viscoelastic layer imperfectly bonded with a couple stress substrate. *Journal of Theoretical and Applied Mechanics*, *55*(2), 535-546.

[100] Sharma, V., & Kumar, S. (2018). Effects of microstructure and liquid loading on velocity dispersion of leaky Rayleigh waves at liquid–solid interface. *Canadian Journal of Physics*, *96*(1), 11-17.

[101] Sharma, V., & Kumar, S. (2020). Caliberating length scale parameter and micropolarity on transference of Love-type waves in composite of $CoFe_2O_4$ and Aluminium-Epoxy laden with Newtonian liquid. *AIMS Mathematics*, *5*(3), 1820-1842.

[102] Sharma, V., & Sharma, V. (2020). Love waves in fiber-reinforced layer imperfectly bonded to microstructural couple stress substrate. *Journal of Theoretical and Applied Mechanics*, *58*.

[103] Shin, S. W., Yun, C. B., Popovics, J. S., & Kim, J. H. (2007). Improved Rayleigh wave velocity measurement for nondestructive early-age concrete monitoring. *Research in Nondestructive Evaluation*, *18*(1), 45-68.

[104] Simonetti, F., & Cawley, P. (2004). On the nature of shear horizontal wave propagation in elastic plates coated with viscoelastic materials. *Proceedings of the Royal Society of London. Series A: Mathematical, Physical and Engineering Sciences*, *460*(2048), 2197-2221.

[105] Singh, A. K., Ray, A., & Chattopadhyay, A. (2019). Analytical Study on Propagation of G-Type Waves in a Transversely Isotropic Substrate beneath a Stratum considering Couple Stress. *International Journal of Geomechanics*, *19*(7), 04019071.

[106] Singh, S. S. (2011). Love wave at a layer medium bounded by irregular boundary surfaces. *Journal of Vibration and Control*, *17*(5), 789-795.

[107] Singhal, A., Sahu, S. A., Chaudhary, S., & Baroi, J. (2019). Initial and couple stress influence on the surface waves transmission in material layers with imperfect interface. *Materials Research Express*, *6*(10), 105713.

[108] Smith, M. L., & Dahlen, F. A. (1973). The azimuthal dependence of Love and Rayleigh wave propagation in a slightly anisotropic medium. *Journal of Geophysical Research*, *78*(17), 3321-3333.

[109] Sokolnikoff, I. S., & Specht, R. D. (1956). *Mathematical theory of elasticity*. McGraw-Hill, New York, *83*.

[110] Son, M. S., & Kang, Y. J. (2012). Propagation of shear waves in a poroelastic layer constrained between two elastic layers. *Applied Mathematical Modelling*, *36*(8), 3685-3695.

[111] Sun, J., Chen, X., & Tian, X. (2007). Engineering infrastructure nondestructive testing with Rayleigh waves: case studies in transportation and archaeology. *Journal of Geophysics and Engineering*, *4*(3), 268-275.

[112] Tamarin, O., Comeau, S., Dejous, C., Moynet, D., Rebiere, D., Bezian, J., & Pistre, J. (2003). Real time device for biosensing: design of a bacteriophage model using love acoustic waves. *Biosensors and Bioelectronics*, *18*(5-6), 755-763.

[113] Timoshenko, S. P., & Goodier, J. N. (1951). *Theory of elasticity*. McGraw-Hill.

[114] Tolipov, K. B. (2002). Propagation of Rayleigh waves in an elastic wedge. *Russian journal of nondestructive testing*, *38*(7), 493-497.

[115] Toupin, R. (1962). Elastic materials with couple-stresses. *Archive for rational mechanics and analysis*, *11*(1), 385-414.

[116] Toupin, R. A. (1964). Theories of elasticity with couple-stress. *Archive for Rational Mechanics and Analysis*, *17*, 85-112.

[117] Vardoulakis, I., & Georgiadis, H. (1997). SH surface waves in a homogeneous gradient-elastic half-space with surface energy. *Journal of Elasticity*, *47*(2), 147-165.

[118] Vashishth, A. K., & Dahiya, A. (2013). Shear waves in a piezoceramic layered structure. *Acta Mechanica*, *224*(4), 727-744.

[119] Vashishth, A. K., & Khurana, P. (2005). Rayleigh modes in anisotropic, heterogeneous poroelastic layers. *Journal of seismology*, *9*(4), 431-448.

[120] Vinh, P. C. (2009). Explicit secular equations of Rayleigh waves in elastic media under the influence of gravity and initial stress. *Applied mathematics and computation*, *215*(1), 395-404.

[121] Voigt, W. (1887). *Theoretische Studien über die Elastizitätsverhältnisse der Kristalle (Theoretical studies on the elasticity relationships of crystals)*. Abhandlungen der Gesellschaft der Wissenschaften zu Göttingen, *34*.

[122] Wang, H. M., & Zhao, Z. C. (2013). Love waves in a two-layered piezoelectric/elastic composite plate with an imperfect interface. *Archive of Applied Mechanics*, *83*(1), 43-51.

[123] Wang, Y. S., & Zhang, Z. M. (1998). Propagation of Love waves in a transversely isotropic fluid-saturated porous layered half-space. *The Journal of the Acoustical Society of America*, *103*(2), 695-701.

[124] Weiskopf, W. H. (1945). Stresses in soils under a foundation. *Journal of the Franklin Institute*, *239*(6), 445-465.

[125] Wolf, B. (1970). Propagation of Love waves in layers with irregular boundaries. *Pure and Applied Geophysics*, *78*(1), 48-57.

[126] Xu, L. M., & Fan, H. (2018). Shear horizontal wave in a classical elastic half-space covered by a surface membrane treated by the couple stress theory. *Journal of Applied Physics*, *124*(22), 225303.

[127] Yang, F. A. C. M., Chong, A. C. M., Lam, D. C. C., & Tong, P. (2002). Couple stress based strain gradient theory for elasticity. *International journal of solids and structures*, *39*(10), 2731-2743.

[128] Yu, J., & Zhang, C. (2014). Effects of initial stress on guided waves in orthotropic functionally graded plates. *Applied Mathematical Modelling*, *38*(2), 464-478.

[129] Yuan, S., Song, X., Cai, W., & Hu, Y. (2018). Analysis of attenuation and dispersion of Rayleigh waves in viscoelastic media by finite-difference modeling. *Journal of Applied Geophysics*, *148*, 115-126.

[130] Zagho, M. M., Hussein, E. A., & Elzatahry, A. A. (2018). Recent overviews in functional polymer composites for biomedical applications. *Polymers*, *10*(7), 739.

[131] Zhang, R., Pang, Y., & Feng, W. (2014). Propagation of Rayleigh waves in a magneto-electro-elastic half-space with initial stress. *Mechanics of Advanced Materials and Structures*, *21*(7), 538-543.

[132] Zhu, H., Zhang, L., Han, J., & Zhang, Y. (2014). Love wave in an isotropic homogeneous elastic half-space with a functionally graded cap layer. *Applied Mathematics and Computation*, *231*, 93-99.

LIST OF PUBLISHED/COMMUNICATED PAPERS

1. Love type waves in a dry sandy layer lying over an isotropic elastic half-space with imperfect interface, *Journal of Physics-Conference Series-IOP Science*, 1531, 012069. doi:10.1088/1742-6596/1531/1/012069 (**Scopus, SJR: 0.22**)

2. Love wave propagation in viscoelastic layer sandwiched between fiber-reinforced layer and consistent couple stress substrate, *Iranian Journal of Science and Technology, transactions of mechanical engineering*, 46(1), 225-235, 2022. DOI: 10.1007/s40997-020-00411-3. (**Both SCI and Scopus indexed journal, Impact factor: 1.596, SJR: 0.328**)

3. Analysis of Love waves in pre-stressed layer sandwiched between dry sandy layer and couple stress substrate, *Mechanics of Solids*, 56(5), 807-818, 2021. (**Both SCI and Scopus indexed journal, Impact factor: 0.452, SJR: 0.283**).

4. Dispersion of Love Waves in a Dry Sandy Layer Imperfectly Attached to a Microcontinuum Substrate: An Analysis with Stress-Free and Clamped Top Surface Conditions. (Book Chapter). *Recent Advances in Applied Mechanics.* Part of Lecture notes in Mechanical Engineering, Springer, Singapore, 697-710, 2022. (**Scopus, SJR: 0.15)**.

5. Dispersion of Rayleigh waves in an elastic layer imperfectly attached to a microcontinuum substrate, accepted for publication in *Mechanics of Solids*. (**Both SCI and Scopus indexed journal, Impact factor: 0.452, SJR: 0.283**).

6. An analysis of SH-waves propagation in an inhomogeneous fiber-reinforced layer sandwiched between two microcontinuum substrates. Communicated to SCI indexed journal.

LIST OF CONFERENCES

1. Presented paper and poster in **International Conference on Recent Advances in Fundamental and Applied Sciences** organized by **School of Chemical Engineering and Physical sciences, Lovely Professional University, Punjab** from 05.11.2019 to 06.11.2019.

2. Presented paper in **Virtual Seminar on Applied Mechanics (VSAM-4)** organized by **Indian Society for Applied Mechanics (ISAM), India**, from 30.07.2021 to 31.07.2021.

LIST OF WORKSHOPS

1. Participated in the **Workshop on Scientific Writing using Typesetting Software LATex** organized at **Lovely Professional University, Punjab** from 06.04.2019 to 07.04.2019**.**

2. Participated in the **Workshop on Finite Element Analysis with ANSYS and MATLAB** organized by **National Institute of Technology, Hamirpur** on 03.01.2022 to 07.01.2022.